THE ROLE OF HEME SYNTHESIS IN ENDOTHELIAL MITOCHONDRIAL FUNCTION AND OCULAR ANGIOGENESIS

Trupti Shetty

Submitted to the faculty of the University Graduate School

in partial fulfillment of the requirements

for the degree

Doctor of Philosophy

in the Department of Pharmacology and Toxicology,

Indiana University

August 2020

Accepted by the Graduate Faculty of Indiana University, in partial fulfillment of the requirements for the degree of Doctor of Philosophy.

Doctoral Committee

_____
Timothy W. Corson, Ph.D., Chair

_____
Ashay D. Bhatwadekar, Ph.D.

February 7, 2020

_____
Krista J. Hoffmann-Longtin, Ph.D.

_____
Travis J. Jerde, Ph.D.

_____
Tao Lu, Ph.D.

_____
William J. Sullivan, Ph.D.

DEDICATION

To Bombay, my first home. The city that inspired me to dream.

ACKNOWLEDGMENT

My deepest and sincere thanks to all the members of the Corson Lab. I would like to thank my PhD mentor, Dr. Tim Corson, for trusting me with this project, encouraging my ideas, boosting my confidence, and standing up for me when needed. Tim was patient, gave me the space to make mistakes, and pushed me, when I needed the push. Tim's dedication towards my success, in life and in my career, has been gratifying. I would also like to thank my unofficial mentor, and friend, Kamakshi Sishtla, for helping me out in the lab every day, and offering countless advice on topics ranging from tissue culture to career choices. My sincere thanks to Bomina Park, for inspiring me with her work ethic and passion for science. I would also like to thank former members – Dr. Sheik Pran Babu Sardar Pasha, Dr. Rania Sulaiman, Dr. Halesha Basavarajappa, Khoa Dang, Mehdi Shadmand, Dr. Christian Briggs and all the trainees over the last few years.

I would like to thank my committee members – Dr. Ashay Bhatwadekar, Dr. Krista Hoffmann-Longtin, Dr. Travis Jerde, Dr. Tao Lu, and Dr. William Sullivan, for their feedback and support on my project, and for making me reach my potential. I have enjoyed our discussions and learnt immensely on being an effective communicator. I would also like to take this opportunity to thank all the faculty, staff, and students of the Department of Pharmacology and Toxicology and Department of Ophthalmology, for their support and encouragement. My most sincere gratitude to all the members of the IBMG Graduate Division,

especially Tara Hobson-Prater, Brandy Wood, and Lauren Easterling for career advice and never-ending support.

My research methodology would not have been successful without the technical assistance of Matthew Repass and instrumentation at the Angiogenesis BioCore, IUSM. All the flow cytometry experiments were conducted at Indiana Center for Biomedical Innovation, and I would like to thank Kevin Harvey for all his help and advice.

A huge shout out to all my friends Dr. Nikita Meswani, Tanmaye Nalan, Neha Chandrakant, Harsh Shrimali, James Harris, Allison Moore, April Barnard, Omar ElJordi, Vaishnavi Jadhav, Adnan Gopinadhan, Apoorva Bharthur, Sankalp Srivastava, Arkaprabha Banerjee, and Debjyoti Kundu. I am so grateful to Dr. Lakshmi Prabhu, Dr. Bidisha Mitra, Dr. Sudha Savant, and Dr. Sreeparna Majumdar, for helping me settle in a new city. These amazing individuals were my support system throughout graduate school and I will always be thankful for their friendship.

My final gratitude to my lovely family in India and New Zealand. I thank my brother, Savinay Shetty for his words of wisdom and teaching me to be independent. I thank my Mum and Dad for their faith and support towards a career that was alien to them. They rejected patriarchy way before it was cool. Finally, thanks to my life partner Kedar Shenoy, who has endured my stress, felt my pain, loved me unconditionally, and more importantly, always made me laugh.

Trupti Shetty

THE ROLE OF HEME SYNTHESIS IN ENDOTHELIAL MITOCHONDRIAL FUNCTION AND OCULAR ANGIOGENESIS

Abnormal blood vessel growth from pre-existing blood vessels, termed pathological angiogenesis, is a common characteristic of vascular diseases like proliferative diabetic retinopathy (PDR) and wet age-related macular degeneration (wet AMD). Retinal detachment, hemorrhage, and loss of vision are only some of the debilitating consequences of advanced pathological angiogenesis. Current therapeutics targeting these blood vessels are ineffective in many patients. We previously identified a novel angiogenesis target, ferrochelatase (FECH), from the heme synthesis pathway, and found that FECH inhibition is antiangiogenic in cell and animal models. Heme synthesis occurs in mitochondria, where FECH inserts Fe^{2+} into protoporphyrin IX (PPIX) to produce heme. However, the relationship between heme metabolism and angiogenesis is poorly understood.

I sought to understand the mechanism of how FECH and thus, heme is involved in endothelial cell function. First, I determined the energetic state of retinal and choroidal endothelial cells, previously uncharacterized. I found that mitochondria in endothelial cells had several functional defects after heme inhibition. FECH loss changed the shape of mitochondria and depleted expression of genes maintaining mitochondrial dynamics. FECH blockade elevated oxidative stress and depolarized mitochondrial membrane potential. Heme depletion had negative effects on cellular metabolism, affecting oxidative

phosphorylation and glycolysis. Mitochondrial complex IV of the electron transport chain (cytochrome c oxidase) was decreased in cultured human retinal endothelial cells and in murine retina ex vivo after FECH inhibition. Supplementation with heme partially rescued phenotypes of FECH blockade. Additionally, I discovered that partial loss-of-function *Fech* mutation in mice caused PPIX accumulation with no change in normal vasculature, as assessed by fundoscopy. These findings provide an unexpected link between mitochondrial heme metabolism and angiogenesis. My studies identify a novel role of a heme synthesis enzyme in blood vessel formation and provide an opportunity to exploit these findings therapeutically for patients with PDR and wet AMD.

Timothy W. Corson, Ph.D., Chair

TABLE OF CONTENTS

LIST OF TABLES

CHAPTER 4

LIST OF FIGURES

CHAPTER 1

CHAPTER 3

CHAPTER 4

CHAPTER 6

LIST OF ABBREVIATIONS

2-DG	2-deoxyglucose
AD	Alzheimer’s disease
AGE	advanced glycation end products
ALA	5-aminolevulinic acid
ALAD	aminolevulinic acid dehydratase
ALAS	aminolevulinic acid synthase
AMD	age related macular degeneration
BAEC	bovine aortic endothelial cells
BMEC	brain microvascular endothelial cell
BSA	bovine serum albumin
CNV	choroidal neovascularization
COX IV	complex IV
COX4I1	complex IV subunit 1
COX10	cytochrome c oxidase assembly factor heme *a*
COX15	cytochrome c oxidase assembly homolog
COX2	complex IV subunit 2
COX5	complex IV subunit 5
CPOX	coproporphyrinogen oxidase
CYP450	cytochrome P450
DAG	diacylglycerol
DMSO	dimethyl sulfoxide
DNML1	dynamin-1

DR	diabetic retinopathy
EC	endothelial cell
ECAR	extracellular acidification rate
ECM	extracellular matrix
eNOS	endothelial nitric oxide synthase
EPC	endothelial progenitor cells
EPP	erythropoietic protoporphyria
ERG	electroretinogram
ERK	extracellular signaling-regulated kinases
ETC	electron transport chain
FAK	focal adhesion kinase
FCCP	carbonyl cyanide-4-(trifluoromethoxy)phenylhydrazone
FECH	ferrochelatase
Fech^{m1Pas}	ferrochelatase partial loss-of-function mutation
FLVCR1a	feline leukemia virus subgroup C cellular receptor 1
GA	geographic atrophy
GCL	ganglion cell layer
GFAP	glial fibrillary acidic protein
HEPES	4-(2-hydroxyethyl)-1-piperazineethanesulfonic acid
HIF1α	hypoxia inducible factor 1 alpha
HMB	hydroxymethylbilane
HO-1	heme oxygenase-1
HPRT	hypoxanthine phosphoribosyl transferase 1

HREC	human microvascular retinal endothelial cell
HUVEC	human umbilical vein endothelial cells
IBA-1	ionized calcium binding adaptor molecule 1
IL-8	interleukin-8
INL	inner nuclear layer
IP3	inositol-triphosphate
JC-1	5,5′,6,6′-tetrachloro-1,1′,3,3′-tetraethylbenzimidazolcarbocyanine iodide
L-CNV	laser-induced choroidal neovascularization
LC3	light chain 3
MAPK	mitogen activated protein kinases
MFI	median fluorescence intensity
MFN2	mitofusin 2
mito	mitochondria
MMP-9	matrix metalloproteinase 9
mtDNA	mitochondrial DNA
MTG	MitoTracker green
NaOH	sodium hydroxide
NFL	nerve fiber layer
NMPP	*N*-methyl protoporphyrin
NO	nitric oxide
NOS	nitric oxide synthase
OCR	oxygen consumption rate

OCT	optical coherence tomography
OIR	oxygen-induced retinopathy
ONH	optic nerve head
ONL	outer nuclear layer
OPA1	optic atrophy 1
P3	postnatal day 3
PBG	porphobilinogen
PBGS	porphobilinogen synthase
PDR	proliferative diabetic retinopathy
PDT	photodynamic therapy
PEDF	pigment-derived factor
PGC1α	proliferator-activated receptor gamma coactivator 1 alpha
PI3K	phosphatidyl-inositol-3-kinase
PIGF	placental growth factor
PIP2	phosphatidyl-inositol-4,5-bisphosphate
PKC	protein kinase C
PLC-γ	phospholipase C gamma
PPIX	protoporphyrin IX
ROP	retinopathy of prematurity
ROS	reactive oxygen species
RPE	retinal pigment epithelium
sGC	soluble guanylyl cyclase
SnPPIX	tin protoporphyrin-IX

Succ CoA	succinyl-CoA
TCA	tricarboxylic acid cycle
TGF-β	transforming growth factor beta
UPLC	ultra performance liquid chromatography
UPS	ubiquitin-proteasome system
UROD	uroporphyrinogen decarboxylase
UROS	uroporphyrinogen synthase
VEGF	vascular endothelial growth factor
VEGFR	vascular endothelial growth factor receptor
WT	wild-type
XF	extracellular flux
ΔΨm	membrane potential

CHAPTER 1. INTRODUCTION

1.1 Angiogenesis in Health and Disease

1.1.1 Process of Angiogenesis

The formation of new blood vessels from pre-existing blood vessels is termed as angiogenesis. Endothelial cells (EC) lining the inner walls of these small blood vessels drive the process of angiogenesis (Carmeliet and Jain, 2011; Vandekeere et al., 2015). This is different from vasculogenesis, in which new blood vessel formation arises from endothelial progenitor cells. While the balance of both these processes governs growth of blood vessels for embryogenesis and wound repair, severe dysregulation of angiogenesis contributes to many disorders like malignant tumors, inflammation, neovascular blindness, and ischemia (Timar et al., 2001; Carmeliet, 2003). In some cases, excessive angiogenesis contributes to disorders like arthritis, cancer, and blindness. However, inadequate blood vessel growth has also been recognized as causes of cardiac and brain ischemia, neurodegeneration, and osteoporosis (Krupinski et al., 1994; Martinez et al., 2002; Jefferies et al., 2013).

In healthy adults, ECs performing angiogenesis remain quiescent and exhibit little proliferation, once vessel formation is complete (Engerman et al., 1967). ECs are activated in processes like wound healing, endometrium formation during menstruation and hair follicular growth (Yano et al., 2001). Angiogenesis involves three important features of ECs – proliferation, migration and “sprouting” of new vessels. The process begins with dilation of blood vessels and an increase in vascular permeability. ECs need to migrate and form tubes, which is often accompanied by degradation of surrounding extracellular matrix

proteins. The expression of genes required for this proteolytic activity is induced by various angiogenic growth factors and cytokines, depending on the tissue and vascular network (Figure 1.1). For example, a hypoxic angiogenic stimulus was found to increase expression of a major angiogenic growth factor, vascular endothelial growth factor A (VEGF-A), which in turn caused increased expression of matrix metalloproteinases 9 (MMP-9) (Hollborn et al., 2007). Angiogenesis is, thus, a multifactorial process involving a combined effort of many different positive and negative regulators.

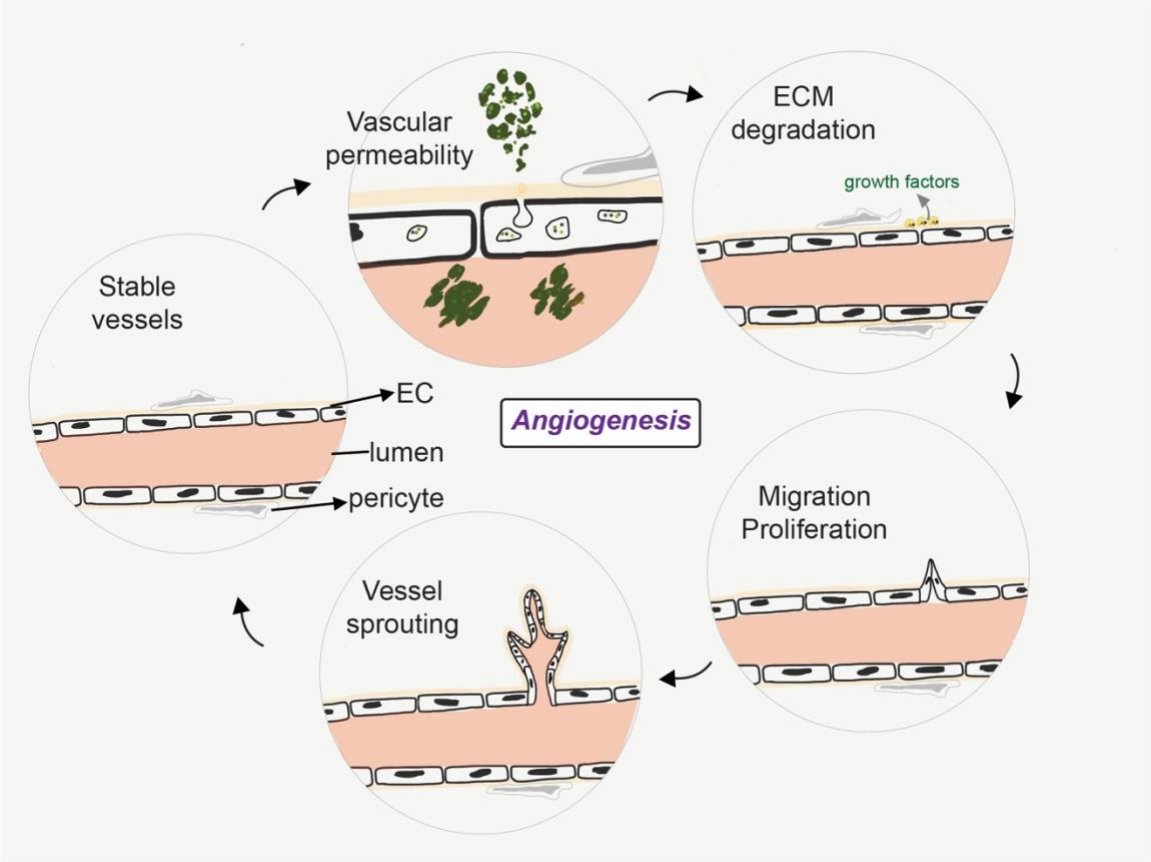

Figure 1.1. Steps in angiogenesis. (Adapted from Bryan BA, D'Amore PA. What tangled webs they weave: Rho-GTPase control of angiogenesis. Cell Mol Life Sci. 2007 Aug;64(16):2053-65)

Some pro-angiogenic factors are VEGF-A, transforming growth factor beta (TGF-β), interleukin-8 (IL-8), among others (Ferrara, 1999). TGF-β promotes VEGF-A induced angiogenesis, by initiating apoptosis of ECs which is critical for this step. Apoptosis in ECs during angiogenesis enables pruning of the growing neovessels and ensures inhibition of abnormal vessels (Ferrari et al., 2009). IL-8 promotes EC proliferation, survival and tube formation, and induces expression of MMPs (Li et al., 2003). Some endogenous anti-angiogenic mediators include

angiostatin, endostatin, and pigment-derived factor (PEDF) (Talks and Harris, 2000). Angiostatin and endostatin inhibit EC proliferation and migration during angiogenesis (Moser et al., 1999; Wickstrom et al., 2005), whereas PEDF inhibits binding of VEGF to VEGFR, preventing angiogenesis (Cai et al., 2006). In order to prevent pathological angiogenesis, a balance is maintained between pro-angiogenic mediators and anti-angiogenic factors. As a result, stable vessels are formed, with a monolayer of ECs lining the lumen, intact junctional proteins, and surrounded by pericytes.

1.1.2 Molecular Mechanisms of Angiogenesis

The vascular endothelial growth factor family includes VEGF-A, VEGF-B, VEGF-C, VEGF-D, VEGF-E and placental growth factor (PIGF) (Olofsson et al., 1998; Persico et al., 1999). Among these, VEGF-A is considered a master regulator, widely studied and commonly found in many different diseases of pathological angiogenesis like diabetic retinopathy and macular degeneration. (Melincovici et al., 2018). VEGF-A has eight exons that have splice variants leading to four isoforms – $VEGF_{121}$, $VEGF_{165}$, $VEGF_{189}$ and $VEGF_{206}$, with $VEGF_{165}$ being the most physiologically relevant isoform (Ferrara et al., 2003). VEGFs carry out signal transduction by binding to one of the three members of the VEGFR tyrosine kinase receptor family, namely, VEGFR-1, VEGFR-2, and VEGFR-3 (Veikkola and Alitalo, 1999; Lohela et al., 2009). During angiogenesis, ECs are classically known to be activated by binding of VEGF-A to VEGFR-2 and initiate a downstream cascade of signaling events (Figure 1.2) (Neufeld et al.,

1999). However, other VEGFs can also bind to VEGFR-2 with some affinity. For example, VEGF-E was found to activate angiogenesis, similar to VEGF-A, after binding to VEGFR-2 (Meyer et al., 1999). During pathological angiogenesis, different types of stimuli can cause induction of VEGF-A production, and this will be discussed in detail below, in the context of specific neovascular disease.

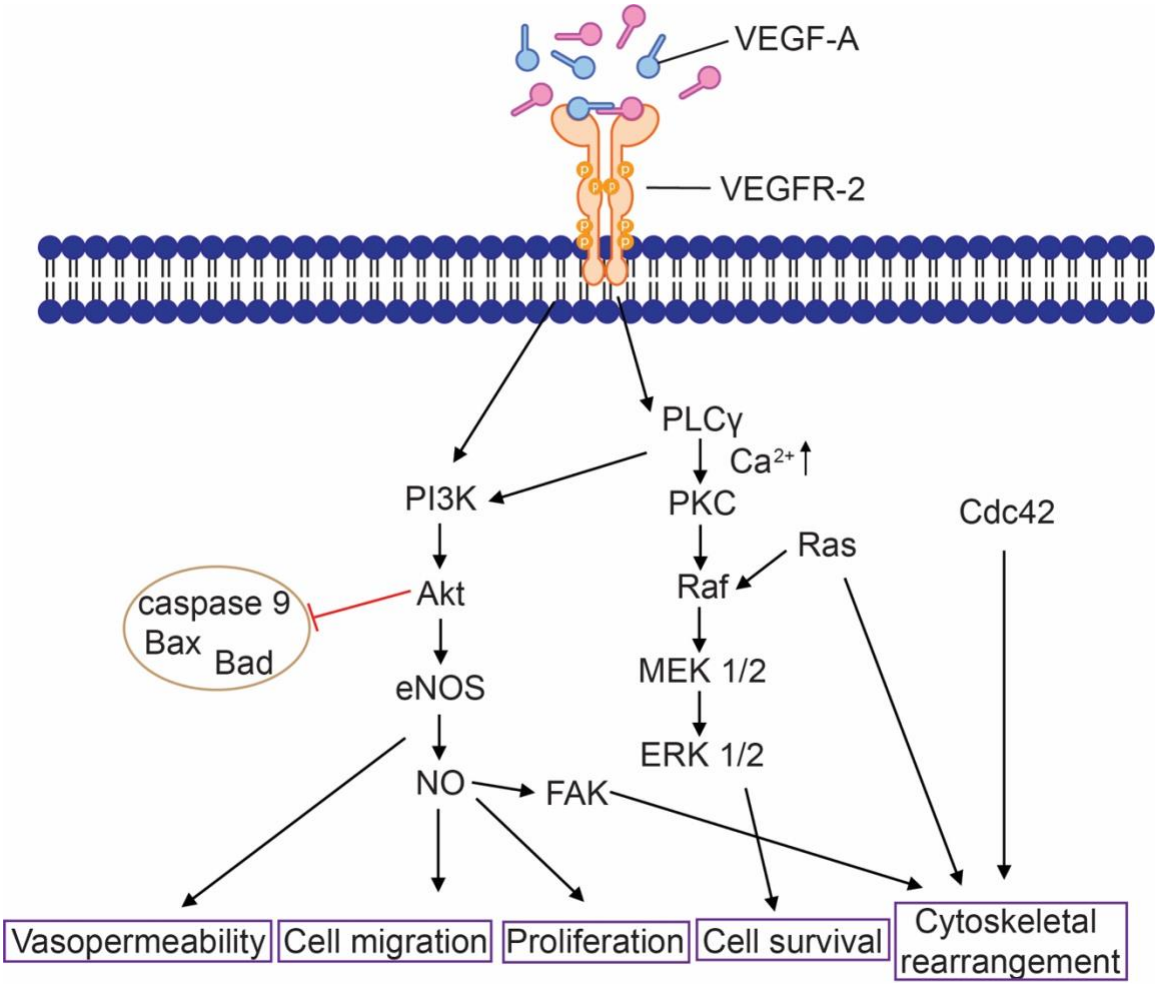

Figure 1.2. VEGF signal transduction. Binding of VEFG-A to a VEGF receptor can result in multiple cellular outcomes. Blocking of heme production via terminal enzyme leads to decrease in activation of VEGFR-2 levels in retinal ECs. Loss of cellular proliferation and migration due to heme loss can be explained through inhibition of signaling cascade downstream of the receptor. Inhibition of heme synthesis leads to decrease in hemoprotein eNOS, also leading to anti-migratory and anti-proliferative effects in retinal ECs.

Signal transduction in angiogenesis leads to downstream cues for multiple cellular processes like proliferation, cell survival, migration, vascular permeability, and ECM degradation, depending on the effectors and mediators of the pathway. I will highlight some pertinent intracellular signaling pathways, however it is important to consider that an angiogenic response is the concerted effort of multiple growth factors, receptors, and signaling pathways in ECs (Ucuzian et al., 2010). Transduction of proliferation signals depend upon the activation signal received by the receptor. The main VEGFR-2 mediated pathway typically begins by extracellular binding of growth factors like VEGF-A. Phosphorylated VEGFR-2 activates phospholipase C-γ (PLC-γ), which further cleaves phosphatidyl-inositol-4,5-bisphosphate (PIP2) to produce diacylglycerol (DAG) and inositol-triphosphate (IP3). DAG and IP3 can induce release of Ca^{2+} from the endoplasmic reticulum and further activate protein kinase C (PKC), and mediators of the extracellular signaling-regulated kinases-mitogen-activated protein kinases (ERK-MAPK) pathway (Cebe-Suarez et al., 2006). Activation of ERK-MAPK concludes with nuclear translocation and activation of transcription factors that mediate cellular proliferation like c-Fos, c-Myc among others (Mavria et al., 2006).

Similarly, VEGFR-2 phosphorylation can initiate signaling cascades that lead to transduction of cell survival signals. Phosphatidyl-inositol-3-kinase (PI3K) is the key effector that is recruited by activated VEGFR-2, which activates Akt (also known as protein kinase B). Akt can further inhibit the activity of pro-apoptotic proteins like caspase-9, Bad, and Bax. Akt can also activate nitric oxide

synthase (NOS), which can cause cytoskeletal rearrangement during EC migration, through the action of nitric oxide (NO) on signaling proteins like focal adhesion kinase (FAK) (Shiojima and Walsh, 2002). The Rho family of GTP binding proteins like Rho, Cdc42, Rac control cytoskeletal dynamics. VEGF has been found primarily to be an activator of Ras-ERK-MAPK pathway. Rac and Cdc42 enable polymerization of actin fibers, and lamellipodia formation by activating p21-activated Pak. Pak can activate ERK-MAPK cascade and mediate cell shape and motility, required for migration. Crosstalk between effector proteins is commonly seen in ECs, and thus, angiogenic response is a result of a complex network of intracellular signaling molecules (Apte et al., 2019).

1.2 Diseases of Angiogenesis

1.2.1 Retinal and Choroidal Angiogenesis

The retina has two major sources of vasculature for blood supply. The inner layers of the retina are fed by a network of retinal vessels. The retinal neurons consist of bipolar, horizontal, amacrine and ganglion cells, interspersed between the inner retinal layers and the photoreceptor cells, aiding in image processing (Masland, 2012). The outer retina gets its nutrient supply from the choroidal circulation made up by the choriocapillaris (Figure 1.3). The photoreceptor cells (rods and cones) are devoid of any vessels and receive nutrient supply from the choroidal blood vessels. This is an important feature for visual processing – light is transduced by the avascular photoreceptors, without interference from biomolecules present in blood, to produce a clear visual image.

In case of a neovascular pathology, fluid and contents from blood vessels often leak into the sub-retinal space and thus, can impair vision. One major difference between the retinal vessels and choriocapillaris is the barrier function. Retinal ECs have tight junctions that maintain a tightly regulated blood-retina barrier, while the latter has no barrier function and relies on the retinal pigment epithelium (RPE) to maintain a blood-retinal barrier in the outer layers of the retina (Sun and Smith, 2018).

Neovascularization is the process of blood vessel formation in avascular regions (areas devoid of any vasculature), and can involve both angiogenic and vasculogenic mechanisms. In the posterior section of the eye, there is scope of neovascularization in two areas of the vasculature – the retinal or the choroidal blood vessels. Neovascular vessels can be prematurely developed, due to a hyperproliferative state of ECs, and can leak fluid and blood in the surrounding subretinal space (Campochiaro, 2000). I will further elaborate on retinal and choroidal angiogenesis in the context of three common neovascular eye diseases – proliferative diabetic retinopathy (PDR), wet age-related macular degeneration (AMD), and retinopathy of prematurity (ROP).

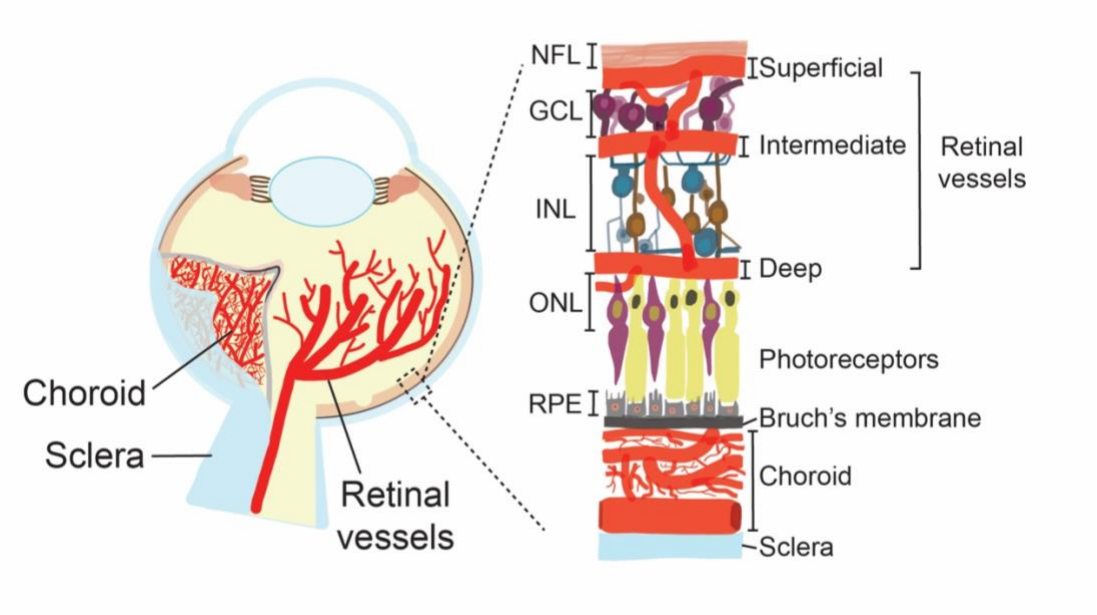

Figure 1.3. Anatomy of the posterior section of the eye and a magnified illustration of the retinal layers and vasculature. NFL, nerve fiber layer; GCL, ganglion cell layer; INL, inner nuclear layer; ONL, outer nuclear layer; RPE, retinal pigment epithelium. (Adapted from Chen J, Liu CH, Sapieha P. Retinal Vascular Development. In: Anti-Angiogenic Therapy in Ophthalmology, edited by Cham SA. New York, NY: Springer, 2016, p. 1–19.)

1.2.2 Proliferative Diabetic Retinopathy (PDR)

Diabetic Retinopathy (DR) is the leading cause of blindness in the United States among the working population (Fong et al., 2004). Nearly 98% of individuals with type-1 and 78% individuals with type-2 diabetes developed DR within the first 15 years of diagnosis (Varma, 2008). In the same 15 years of diagnosis, 33% of type-1 patients and 17% of type-2 patients develop PDR. With the increase in the prevalence of type-2 diabetes, this epidemiological burden has been projected to triple by 2050 (Saaddine et al., 2008). Central vision loss,

blindness, maculopathy, and macular edema are some of the symptoms of PDR patient population (Tong et al., 2001). High levels of intravitreal VEGF, induced due to an ischemic retina, cause PDR. Abnormally grown neo-vessels are leaky, and often result in vitreous hemorrhaging, and ultimately, retinal detachment.

PDR is the advanced form of retinal neovascularization caused due to hyperglycemic levels, and an imbalance between pro-angiogenic and anti-angiogenic factors in the retina. Retinal cells fail to use insulin for glucose uptake, like that for other tissues, and depend on the activity of glucose transporters like GLUT-1 for uptake of glucose into cells (Sone et al., 2000). Hyperglycemia underlies the development of early stages of DR, where increased glucose levels lead to loss of pericytes, increase in vascular permeability, damage to blood-retinal barrier, and formation of microaneurysms. This is followed by increased formation of free radicals and advanced glycation end products (AGEs), both leading to pronounced buildup of oxidative stress in the diabetic retina (Williamson et al., 1993; Stitt et al., 2005). During this stage, an intracellular “pseudohypoxic” environment is a common occurrence, and compounds the effects of increased oxidative stress, inducing the production of VEGF-A from retinal ECs (Aiello et al., 1994; Shinoda et al., 2000). Increased levels of VEGF-A in the ischemic retina further induces enhanced proliferation of ECs and results in retinal neovascularization (Smith et al., 1997).

1.2.3 Wet Age-Related Macular Degeneration (wet AMD)

AMD remains the leading cause of central vision impairment in older adults of developed countries (Jager et al., 2008). In the United States alone, more than 8 million cases have been reported with intermediate AMD and approximately 2 million have progressed to the more advanced form of AMD (National Eye Institute, 2019). This number has been predicted to explode by 2020, raising serious concerns over management of the disease. Although the patients with wet AMD sustain peripheral vision, the loss of central acuity severely burdens quality of life with an added risk of depression and visual hallucinations to the affected individual. Additionally, development of AMD in one eye also considerably increases the risk of affecting the second eye, increasing complications (Campochiaro, 1999).

Early stages of AMD include accumulation of lipid and protein deposits, referred to as “drusen”, between the RPE and Bruch’s membrane. Drusen deposits in the retina is indicative as dry AMD, this can progress to geographic atrophy (GA), which is characterized by degeneration of the RPE and the photoreceptor cells. The advanced form of AMD, more commonly known as “wet” AMD or the exudative form of AMD is caused due to abnormal neovascularization in the choroidal vessels. Neovascular choroidal vessels invade the RPE, by rupturing the Bruch’s membrane, and release their contents in the outer retina and subretinal space (Campochiaro et al., 1999, Al-Zamil and Yassin, 2017). The exact trigger of how choroidal neovascularization is initiated is unclear, however several mechanisms have been postulated in the literature.

Multiple stressors can stimulate the production of pro-angiogenic factors like VEGF-A, predominantly secreted by the RPE. Drusen deposits can trigger inflammation and recruit components of the complement pathway like C3a and C5a. Oxidative stress is another stressor, known to induce CNV, and can be a result of genetic factors or poor lifestyle choices. Both of these stressors individually, or in combination, can induce RPE to secrete VEGF-A, thus initiating CNV. Another possible mechanism postulated is age-related thickening of the Bruch's membrane, that can result in a hypoxic environment in the outer retina, by decreasing the supply of oxygen from the choroid to the RPE (Holz et al., 1994). This may result in stimulation of VEGF-A production, and lead to angiogenesis in the choroid. It is clear that RPE is largely involved in the pathogenesis of AMD, and like in several aging neurodegenerative diseases, accumulation of damaged mitochondria in the RPE have also been reported (Lin and Beal, 2006).

1.2.4 Retinopathy of Prematurity (ROP)

ROP is a major cause of blindness affecting children, with nearly 16,000 cases reported each year in the United States alone (National Eye Institute, 2019). Approximately 60% of preterm births develop some degree of ROP annually, and require medical treatment for their condition. Out of these, nearly 35% infants lose their vision, with permanent blindness (Lad et al., 2009). ROP does not manifest early symptoms, while some late symptoms of ROP include unusual eye movements, white pupils and vision loss, often diagnosed through eye exam and retinal fundoscopy.

The pathogenesis of ROP is biphasic, with phase I being characterized by hyperoxia, and followed by phase II, hypoxia-driven neovascularization (Hellstrom et al., 2013). Preterm babies are, often, housed in a closed incubator with high oxygen, to improve respiration and survival. However, a detrimental side effect of this treatment is obliteration of the developing retinal vessels, as hyperoxia has been found to suppress the production of VEGF-A (Stone et al., 1996). Subsequent transfer of neonates to normal atmospheric conditions creates a relative hypoxic environment in the developing retina and contributes to conditions conducive to abnormal neovascularization. Low birthweight, hyperglycemia, and low serum insulin-like growth factor, can increase the risk of ROP in preterm infants, and exacerbate the symptoms. Studies mimicking these physiological manifestations, in vitro and in animal studies, have reported hypoxia to be the major driver of neovascularization during phase II. The imbalance in oxygen concentrations in the developing retina, results in pockets of avascular zones, due to hyperoxia-driven obliterated vessels, and neovascular areas induced by hypoxia-VEGF-A-driven angiogenesis (Heidary et al., 2009).

1.3 Therapy for Neovascular Eye Diseases

Clinically, therapeutic strategies include destruction of abnormal vessels, restriction of abnormal vessels mediated by blockade of growth factors, and in some extreme cases, surgical intervention is required. Due to the common prevalence of VEGF-A in the underlying pathogenesis of both retinal and

choroidal neovascularization, anti-VEGF biologics have revolutionized neovascular therapy.

In early PDR, laser photocoagulation therapy has been traditionally used, where laser is used to target neovessels directly in the retina. However, laser itself can have damaging side effects like destruction of healthy cells, retinal detachment, and relapse of neovascularization (Evans et al., 2014). Laser therapy has been proven effective in targeting peripheral vessels for ROP. Cryotherapy is the standard of care, used by clinicians to slow down abnormally growing vessels, however most severe cases of ROP remain beyond the reach of current treatment strategies (Cryotherapy for Retinopathy of Prematurity Cooperative, 2001). Intravitreal administration of anti-VEGF-A biologics are now included in the standard of care for wet AMD and PDR, with clinical trials underway for ROP. However, it is important to consider the invasive route of administeration of anti-VEGFs can present with complications like blurred vision, discomfort and/or elevated intraocular pressure.

Humanized monoclonal antibodies like ranibizumab and bevacizumab are effective in binding to all isoforms of VEGF-A (Ellis, 2006; Lowe et al., 2007). Human recombinant protein called VEGF trap or Aflibercept consists of VEGFR binding domains and acts like a neutralizing antibody, capturing all VEGF-A isoforms (Semeraro et al., 2013). Apart from these proteins, a 28-nucleotide chemically synthesized RNA aptamer, called pegaptanib has also been approved, for its high selectivity in binding $VEGF_{165}$ isoform of VEGF-A (Ruckman et al., 1998; Eyetech Study, 2002). Even with the success of anti-

VEGFs, some patients still remain unresponsive to these treatments, owing to multifactorial pathways involved in the pathogenesis of neovascular diseases (Yang et al., 2016). In addition, some cases of anti-VEGF therapy show loss of efficacy after repeated administeration and patients are reported to develop tolerance to ranibizumab and bevacizumab (Keane et al., 2008;Schaal et al., 2008) and in certain cases, these treatment regimens are limited owing to financial and ethical reasons. Bevacizumab was developed for treating colon cancer, and its use for AMD is off-label. The CATT research trial found the efficacy of bevacizumab equivalent to ranibizumab in improving visual acuity (The CATT Research Group, 2011). Additionally, FDA approved ranibizumab costs nearly 23,000 USD per patient annually compared to the 600 USD cost of administering bevacizumab (Schmucker et al., 2009; Nepomuceno et al., 2013; Silver, 2014).

Thus, there is a rising need to develop novel, better therapeutic strategies, one that does not rely solely on the action of VEGF-A, and less invasive routes of administration for treatment. Detailed characterization of the mechanism of these pathologies is the first step towards designing different therapeutic strategies against these diseases. For example, without the information on growth factors like VEGF, anti-VEGF biologics would never have come into the picture. More importantly, studies on the basic cellular mechanisms in the pathogenesis of neovascularization, would result in better therapeutic avenues, reducing toxic side effects, and an improved understanding of the disease itself.

1.4 Heme Synthesis Proteins as Angiogenesis Mediators

To find new angiogenesis mediators, in a reverse chemical genetics approach, the Corson laboratory screened an anti-angiogenic compound cremastranone, and identified an enzyme ferrochelatase as the cellular target (Basavarajappa et al., 2017). The terminal heme synthesis enzyme, ferrochelatase, encoded by FECH, was the first heme pathway component to be identified as a druggable target in pathological angiogenesis. FECH blockade (both genetically and pharmacologically) reduced proliferation, migration and endothelial tube formation in retinal and choroidal microvascular ECs. This effect was specific to ECs; FECH inhibition had a negligible effect on non-endothelial ocular cell proliferation. FECH blockade was cytostatic, with no resulting activation of apoptosis proteins observed in ECs. This anti-angiogenic effect was also seen in vivo: mice with a partial loss-of-function *Fech*$_{m1Pas}$ point mutation formed reduced neovascular lesions in the eye in the laser-induced choroidal neovascularization (L-CNV) model with features of wet AMD, as did mice with ocular *Fech* knockdown. In addition, FECH was overexpressed in and around these lesions, and in human wet AMD eyes (Basavarajappa et al., 2017). Moreover, FECH was upregulated, particularly in neovascular tufts, in the oxygen-induced retinopathy (OIR) mouse model of ROP (Sardar Pasha and Corson, 2019). FECH blockade resulted in reduced expression of angiogenesis signaling proteins like eNOS, VEGFR-2, activated VEGFR-2, and HIF1α. The mechanisms of how heme contributes to EC physiology and drives angiogenesis are now beginning to be understood.

1.5 Synthesis and Functions of Heme

Mitochondrial function in ECs is interconnected by a mesh of signaling molecules that cross pathways often (Kluge et al., 2013). One such versatile biomolecule is heme. Heme is important for respiration, curbing oxidative stress, drug metabolism, and oxygen transport (Dailey and Meissner, 2013). The heme synthesis pathway and intermediates have been studied in detail over decades, with crystal structures and cloned genes available (Poulos, 2014). Intriguingly, heme is an important prosthetic moiety of key proteins in ECs (Chiabrando et al., 2014b).

In mammalian cells, heme synthesis is accomplished in the mitochondria and cytosol over a series of eight enzymatic reactions, followed by modification of heme in a couple of sub-hemylation steps (Nilsson et al., 2009; Hamza and Dailey, 2012; Dailey et al., 2017). Heme biosynthesis in cells other than erythrocytes is initiated by the rate-limiting enzyme aminolevulinic acid synthase (ALAS1) that catalyzes formation of 5-aminolevulinic acid (ALA) from succinyl-CoA and glycine (Figure 1.4). ALA is exported out into the cytosol, where two molecules of ALA are condensed to form porphobilinogen (PBG) by porphobilinogen synthase (PBGS), the first pyrrole structure of the heme pathway. Four monopyrrole PBG are linearized to form tetrapyrrole hydroxymethylbilane (HMB) by HMB synthase. HMB is converted to uroporphyrinogen III by uroporphyrinogen synthase (UROS). The final cytoplasmic intermediate synthesized next is coproporphyrinogen III by

uroporphyrinogen decarboxylase (UROD). This coproporphyrinogen III is shuttled into the mitochondrial intermembrane space, where coproporphyrinogen oxidase (CPOX) produces protoporphyrinogen IX. The second last step is catalyzed by protoporphyrinogen IX oxidase to produce protoporphyrin IX (PPIX). In the final step, ferrochelatase (FECH) incorporates ferrous iron into protoporphyrin IX (PPIX), synthesizing protoheme. Heme is then available to enable cellular processes by combining with enzyme subunits as a prosthetic group. For example, heme-iron is part of the catalytically active form of eNOS (Raman et al., 1998). Similarly, different forms of heme are incorporated into mitochondrial respiratory complexes II-IV of the electron transport chain (ETC) (Kim et al., 2012). Of course, the majority of heme is used for incorporation into hemoglobin during erythropoiesis (Korolnek and Hamza, 2014) and some (primarily in the liver) for the synthesis of cytochrome P450s, responsible for xenobiotic metabolism (Correia et al., 2011).

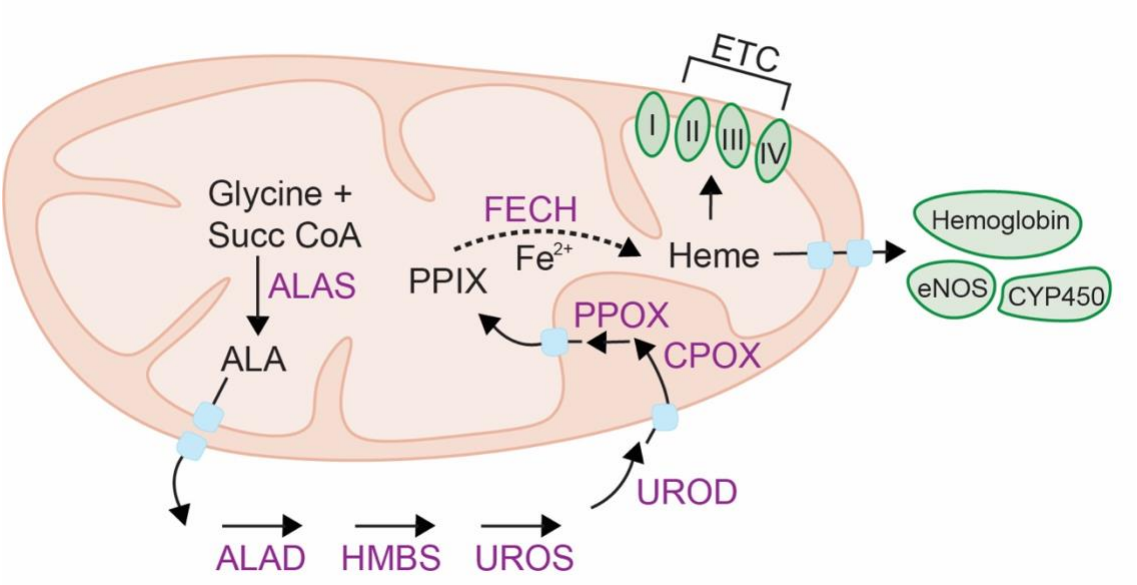

Figure 1.4. Schematic diagram of the heme synthesis pathway in the mitochondrion. Eight sequential steps in the heme synthesis pathway are depicted, along with some heme-containing proteins. Red dotted lines indicate blockade. Succ CoA, succinyl-CoA, ALA, 5-aminolevulinic acid; ALAS, ALA synthase; ALAD, ALA dehydratase; HMBS, hydroxymethylbilane synthase; UROS, uroporphyrinogen synthase; UROD, uroporphyrinogen decarboxylase; CPOX, coproporphyrinogen oxidase; PPOX, protoporphyrinogen oxidase; FECH, ferrochelatase; PPIX, protoporphyrin IX; eNOS, endothelial nitric oxide synthase; CYP450, cytochrome P450; ETC, electron transport chain.

Apart from being a prosthetic cofactor for enzymes, heme's regulated production ensures that active iron is sequestered before it can promote formation of reactive oxygen species (ROS) (Ryter and Tyrrell, 2000). Hence, heme plays a crucial role in ROS homeostasis in the mitochondria, without which many mitochondrial processes would be damaged (Alonso et al., 2003). One key

regulator involved in detoxification of ROS and stimulating mitochondrial biogenesis is proliferator-activated receptor gamma coactivator 1α (PGC1α) (Austin and St-Pierre, 2012). PGC1α regulates ALAS1 expression in the liver, linking heme synthesis directly to the nutritional state of cells (Handschin et al., 2005). Fasting-induced PGC1α was found to be essential for vascular growth and pathological angiogenesis (Saint-Geniez et al., 2013). In the following sections, I will review recent studies that have identified an unexpected link between angiogenesis and heme synthesis, offering exciting therapeutic relevance to neovascular diseases like PDR, wet AMD and ROP discussed previously.

1.6 Mechanisms of Heme Regulation of Angiogenesis

1.6.1 Mitochondrial Function

Inhibition of heme synthesis has varying impact on the hemoproteins (heme-binding proteins) of the ETC (Vijayasarathy et al., 1999; Atamna et al., 2001). Heme *b* and *c* are present in complexes II and III, whereas complex IV has two groups of heme *a*, made after two consecutive modifications to protoheme (Kim et al., 2012). Heme biosynthesis inhibition in vivo was found to decrease expression of key mitochondrial subunit proteins of complex IV like COX1, COX2 and COX5 in liver, brain and kidney tissues (Vijayasarathy et al., 1999). Chemical inhibition of FECH showed similar effects on complex IV in other cell types like IMR90 fibroblast, neuroblastoma and astrocyte cells (Atamna et al., 2001; Atamna et al., 2002). There is increasing evidence of the involvement

of COX and mitochondrial reactive oxygen species (ROS) activity in VEGF induced pro-angiogenic stimuli in umbilical vein ECs (Wang et al., 2011). COX muscle-specific knockout exhibits reduced capillaries in skeletal muscle, indicating an important role for complex IV in angiogenesis (Lee et al., 2012). However, the direct effect on ETC activity after heme depletion in the retina has not been studied before.

1.6.2 Cytosolic Effects

Lack of heme synthesis also leads to incomplete formation of eNOS and reduced activity (Feng, 2012). Heme depletion via FECH inhibition led to decreased expression, hemylation, and activity of eNOS in retinal microvascular ECs (Basavarajappa et al., 2017). Heme inhibition by chemically blocking the second synthesis enzyme aminolevulinic acid dehydratase (ALAD) in rats led to reduced eNOS and downstream mediator soluble guanylyl cyclase (sGC), both important in maintaining regular cardiovascular function. These effects did not affect vascular tension and resulted in no change to arterial blood pressure (Bourque et al., 2010). But heme depletion-driven eNOS dysfunction led to impaired NO mediated vascular relaxation in bovine coronary arteries (Zhang et al., 2018). NO, a potent vasodilator, is pro-angiogenic and NO itself is known to inhibit hemylation of extramitochondrial apo-hemoproteins (Waheed et al., 2010). Heme oxygenase-1 (HO-1) is a heme degradation enzyme and a stress protein induced by hypoxic conditions which causes release of NO in ECs (Motterlini et

al., 2000). HO-1 inhibition by tin protoporphyrin-IX (SnPPIX) reduced VEGF-induced angiogenesis in ECs (Jozkowicz et al., 2003).

It is important to note that heme overload in ECs also leads to abnormal angiogenesis. Silencing of the heme transporter FLVCR1a led to intracellular heme accumulation in microvascular ECs, but not in macrovascular ECs. This heme accumulation in microvascular ECs led to impaired angiogenesis, damaged vessel formation and embryonic lethality in vivo (Petrillo et al., 2018). Heme toxicity has been investigated previously in hemolytic diseases like sickle cell disease and thalassemia, where heme scavengers are helpful in reducing heme-induced ROS accumulation (Vinchi et al., 2013). In non-small cell lung cancer, tumor cells had elevated heme synthesis activity, increasing respiratory function of the ETC and enhancing tumorigenic properties like migration and invasiveness (Sohoni et al., 2019). This suggests in addition to heme loss being anti-angiogenic, heme synthesis overdrive can increase mitochondrial function, but this remains to be validated in ECs.

1.7 Summary, Hypothesis, and Aims

Angiogenesis is a double-edged sword that can work both therapeutically for some diseases as well as being damaging in others. Abnormal angiogenesis underlies many pathologies like neovascular eye diseases, tumors, and inflammatory diseases whereas angiogenesis is favorable for revascularization in case of stroke, myocardial infarction, neurodegeneration and ischemia (Chung and Ferrara, 2011). ECs that line newly sprouting vasculature drive the process

of angiogenesis. ECs of microvascular origin are predominant in these neovessels (Jackson and Nguyen, 1997). VEGF-driven angiogenesis signal transduction is considered a common downstream pathway.

We previously demonstrated that inhibition of FECH was sufficient to block angiogenic function of these microvascular ECs (Basavarajappa et al., 2017). FECH overexpression is seen in human patient samples of wet AMD as well as in an animal model of neovascularization. Inhibition of FECH reduces neovascularization in vivo without toxicity. Loss of FECH directly affects heme biosynthesis by reducing heme production and causes accumulation of precursor PPIX levels. Depletion of heme will eventually affect heme containing proteins and hemoprotein-regulated pathways, for example proteins of the ETC, which will be discussed in subsequent chapters in this thesis. However, the detailed function of FECH in angiogenesis has not been described previously. I **hypothesized that FECH is a mediator of pathological angiogenesis via altering mitochondrial function of endothelial cells.** To test my central hypothesis, I proposed the following aims –

Aim I: Determine the bioenergetic profile of retinal and choroidal ECs. To address this aim, I determined optimized parameters essential for determining basal energetics of retinal and choroidal ECs. I determined optimal cell seeding density that provides maximal oxygen consumption rates and extracellular acidification rates. I distinguished ATP production from mitochondrial respiration and glycolysis and recorded basal and stressed energy outputs. These studies

characterized the physiologic energetic state of ECs and helped in designing experiments under FECH inhibition conditions.

Aim II: Elucidate mitochondrial function of ECs under FECH blockade.

I addressed this by examining mitochondrial parameters like morphology, mass, dynamics, membrane potential and oxidative stress after FECH inhibition. I studied the cellular bioenergetics of retinal and choroidal ECs and retina in vivo after FECH inhibition, using Seahorse extracellular flux measurements. Expression, function and activity of complexes of the ETC was examined under conditions of FECH blockade. These experiments identified the role of FECH and thus, heme synthesis in maintaining mitochondrial function of ECs.

Aim III Characterize the retinal phenotype of partial loss-of-function *Fech* mutation in vivo.

Here, I characterized the retinal structural and physiological phenotype after loss of *Fech* activity in a mouse model of *Fech* partial loss-of-function mutation (*Fech*$_{m1Pas}$). I documented retinal fundus appearance, vessel integrity and PPIX levels in *Fech*$_{m1Pas}$ mice of wild-type (WT), heterozygous and homozygous genotypes. To assess retinal function, I recorded visual activity using electroretinography. I characterized the retinal bioenergetic function using Seahorse extracellular flux analyzer. To determine aberrations in developing as well as fully developed pre-existing retinal vessels, I assessed retinas from juvenile and adult *Fech*$_{m1Pas}$ mice. These experiments provided the first study of retinal physiology of the *Fech*$_{m1Pas}$ mouse model and together, my results provided a comprehensive study of heme deficiency in the eye.

1.8 Dissertation Overview

This dissertation will describe experiments performed towards testing the above-mentioned hypothesis by addressing the specific aims outlined in this chapter. Chapter II will detail the materials and methods used in designing the experiments in subsequent chapters. Chapter III will cover experiments addressing Aim I and will provide optimized parameters for using the Seahorse extracellular flux analyzer, which will be used in Chapters IV and V for studying bioenergetics of ECs and retina. The Seahorse technology will be detailed in this chapter, with the importance and limitations of its use in vitro and in vivo. Chapter IV will address Aim II and provide results for mitochondrial function of ECs after FECH loss. This chapter will outline findings in vitro in retinal and choroidal ECs, and go on to document the effect seen in vivo after FECH inhibition. In order to understand retinal physiology under an inherent point mutation in *Fech* in vivo, Chapter V will elaborate on results from retinal characterization of *Fech*^{m1Pas} mouse model, specified in Aim III. Together, all results will be discussed in Chapter VI, while addressing limitations and potential future studies that can be explored as an outcome of this dissertation project.

CHAPTER 2. METHODOLOGY

2.1 In Vitro Experiments

2.1.1 Cell Culture

HRECs and Attachment Factor were purchased from Cell Systems (Kirkland, WA, USA). HRECs were grown in endothelial growth medium (EGM-2) and used between passages 4 and 8. EGM-2 was prepared by combining components of EGM-2 “bullet kit” (Cat no. CC-4176) and endothelial basal medium (EBM, Lonza, Walkersville, MD, USA; Cat No. CC-3156). RF/6A cells were obtained from ATCC (Manassas, VA, USA) and grown in Eagle’s Minimum Essential Medium (EMEM, ATCC Cat No. 30-2003) supplemented with 10% fetal bovine serum (FBS, PAA Laboratories, Etobicoke, ON, Canada; Cat No. A15-751). Since short tandem repeat profiles are not available for Rhesus, these cells were not authenticated after receipt from the supplier, and sex was not reported. Glucose, sodium pyruvate and L-glutamine were purchased from Sigma-Aldrich (St. Louis, MO, USA). XF Base Dulbecco’s Minimum Essential Medium (Cat No. 102353-100) and XFp FluxPak (Cat No. 103022-100) were purchased from Seahorse Biosciences (Billerica, MA, USA). Cells were reordered from the suppliers at least annually, and grown at 37°C in a 5% CO_2 incubator. Cultures were routinely tested for mycoplasma contamination. *N*-methyl protoporphyrin (NMPP) was purchased from Frontier Scientific (Logan, Utah, USA) and prepared in DMSO. HRECs were treated with 10 µM and RF/6A at 100 µM NMPP for 48 hours. FECH siRNA (SASI_Hs01_00052189 and SASI_Hs01_00052190) was purchased from Sigma and MISSION® siRNA Universal from Sigma was used as a negative siRNA

control. HRECs were transfected with 30 pmol of either control or FECH siRNA for 48 hours using 7.5 µl of Lipofectamine RNAiMAX reagent (Life Technologies).

2.1.2 FCCP Titration and Cell Seeding Density

OCR was measured using the Seahorse Extracellular XFp Analyzer (Agilent, Santa Clara, CA, USA) at the Indiana University School of Medicine Angio BioCore. The Seahorse XFp Analyzer makes use of sensor probes that measure changes in oxygen and pH, to assess energy consumption from a monolayer of cells, in real time. The sensor probes contain embedded fluorophores that measures changes in O_2 and H^+ in the cellular microenvironment, in response to specific mitochondrial inhibitors (for example FCCP, oligomycin etc.), injected transiently into the microplate containing cells. This method allows determination of a kinetic measurement of oxygen consumption directly correlating with oxidative phosphorylation by the ETC, indicating mitochondrial function of ECs.

Cells (2×10^4 per well) were seeded overnight in XFp miniplates. Sensor cartridges were hydrated overnight in XF calibrant in a room air incubator. Next day, XF Base assay medium was prepared by addition of 5.5 mM glucose and 0.61 mM sodium pyruvate. For HRECs, 3.2 mM L-glutamine was used, while for RF/6A cells 1.6 mM concentration was used as per their respective routine culture medium compositions. The unbuffered base medium was filter sterilized followed by pH adjustment to 7.4 using 0.2 N NaOH solution. Cells were rinsed

with base medium twice to remove overnight culture medium and this was replaced with base assay medium. Cells were incubated for a minimum of 1 hour in a room air incubator before proceeding with the assay. For determining optimal FCCP concentration, two ranges of FCCP were used. Low range concentrations of 0.125, 0.25 and 0.5 µM and high range concentrations of 0.5, 1 and 2 µM were used for titration. Cells were first treated with oligomycin at 1 µM concentration followed by three serial injections of FCCP low and high range concentrations. For the cell seeding density experiment, cells at $5\times10_3$, $2\times10_4$ and $4\times10_4$ cells per well were plated overnight, photographed using an EVOS fl digital microscope, and then subjected to OCR and ECAR measurements to determine optimal cell number for assay conditions.

2.1.3 Cell Energy Phenotype

Cells were grown, as indicated, overnight followed by assessment of metabolic phenotype using the Seahorse XFp Cell Energy Phenotype test kit (Cat. No. 103275-100). Stressor mix was prepared by combining 1 µM oligomycin and 0.125 or 1 µM FCCP. Cells were incubated in base medium for 1 hour in a room air incubator prior to measurements. Five cycles of readings were taken after the injection of stressor mix on the cells and kinetic traces indicating OCR and ECAR were produced in tandem.

2.1.4 Mitochondrial Energetics

For measuring mitochondrial function, Seahorse XFp Cell Mito Stress test kit (Cat No. 103010-100) was used (Dranka et al., 2011). Mitochondrial inhibitors at final well concentrations of 1 µM oligomycin, 0.125 µM (for RF/6A cells) or 1 µM FCCP (for HRECs) and 0.5 µM rotenone/antimycin A were prepared using freshly buffered base medium. After incubating cells in a room air incubator, oxygen consumption rate (OCR) readings were determined using the XFp analyzer. The assay program was set up to measure three cycles of oligomycin followed by FCCP and a final injection of rotenone/antimycin A.

2.1.5 Glycolytic Function

Glycolytic parameters were measured using the Seahorse XF Glycolysis Stress test kit (Cat No. 103020-100). Cells ($2\times10_4$ per well) were grown overnight followed by glucose starvation in assay medium containing sodium pyruvate and glutamine for 1 hour in a room air incubator. Compounds modulating glycolysis were prepared using the same assay medium. Glucose at a final well concentration of 10 mM, oligomycin at 1 µM and 2-deoxyglucose at 50 mM were loaded onto ports of the hydrated sensor cartridge followed by measurement of extracellular acidification rate (ECAR) using the XFp analyzer.

2.1.6 ATP Production Rate Assay

Cells ($2\times10_4$ per well) were seeded and grown overnight in a miniplate followed by replacement of culture medium with Seahorse XF DMEM Medium

pH 7.4 supplemented with glucose, pyruvate and glutamine and incubation in a room air incubator for an hour. Working stocks of oligomycin and antimycin A/rotenone mixture were prepared fresh prior to assay and loaded into sensor cartridges at 1.5 µM and 0.5 µM final well concentrations respectively. The assay was run using the XFp analyzer according to the manufacturer's instructions and kinetic traces for OCR and ECAR were generated.

2.1.7 mRNA Quantification Using qPCR

RNA was isolated using Trizol reagent, 1 µg RNA was used for cDNA synthesis, made using iScript cDNA synthesis kit from Bio Rad (Cat no. 1708897, Hercules, CA, USA). TaqMan probes for *MFN2* (Hs00208382_m1), *DNM1L* (Hs01552605_m1), *OPA1* (Hs01047013_m1), and *FECH* (Hs01555261_m1) were purchased from Thermo Fisher Scientific (Pittsburgh, PA, USA). qPCR was performed using Fast Advanced Master Mix, TaqMan probes, and a ViiA7 thermal cycler (Applied Biosystems). Gene expression was determined using $\Delta\Delta C_t$ method and HPRT (Hs02800695_m1) as housekeeping control and normalized to individual sample controls.

2.1.8 Immunoblotting

Cells were lysed in RIPA buffer (Sigma-Aldrich, St. Louis, MO, USA, Cat no. R0278) and processed for protein quantification followed by SDS-PAGE. For ETC proteins, total OXPHOS Rodent WB Antibody Cocktail (Abcam, ab110413, Cambridge, MA, USA) at 1:250 dilution was used. COX IV-1 antibody was

purchased from Thermo Fisher Scientific (Cat no. PA5-19471, Pittsburgh, PA, USA) and used at 1:1000 dilution. β-actin antibody was purchased from Sigma (Cat no. A5441) and used at 1:2000 dilution. FECH antibody was purchased from LifeSpan BioSciences (Seattle, WA, USA, Cat no LS C409953) and used at 1:500 dilution prepared in 5% BSA solution. Chemiluminescent reagent ECL Prime was purchased from GE Healthcare (Buckinghamshire, UK, Cat no. RPN2232).

2.1.9 Protoporphyrin IX Quantification

PPIX analysis was performed at the Iron and Heme Core facility at the University of Utah. Briefly, cells were washed with PBS, pelleted, and stored frozen at -80°C. The cells were homogenized and extraction solvent (EtOAc:HOAc, 4:1) was slowly added to 50 µL concentration-adjusted sample and shaken. The mixture was centrifuged, supernatant was collected and the supernatant solution was injected into a Waters Acquity ultra performance liquid chromatography (UPLC) system with an Acquity UPLC BEH C18, 1.7 µm, 2.1 x 100 mm column. PPIX was detected at 404 nm excitation and 630 nm emission. Solvent A was 0.2% aqueous formic acid while Solvent B was 0.2% formic acid in methanol. The flow rate was kept at 0.40 mL per minute and the column maintained at 60˚C for the total run time of 7 min. The following successive linear gradient settings for run time in minutes versus Solvent A were as follows: 0.0, 80%; 2.5, 1%; 4.5, 1%; 5.0, 80%.

2.1.10 Mitochondrial Morphology

Cells were plated on 35 mm coverslip bottom dishes. HRECs were stained using MitoTracker Green (Thermo Fisher, Cat no M7514) at 200 nM for 10 minutes in the dark at 37°C. Imaging was performed immediately following staining using an LSM700 confocal microscope (Zeiss, Thornwood, NY, USA) under a 63× oil immersion lens and acquired Z-stacked images were analyzed using ImageJ software (Trudeau et al., 2010). Briefly, individual cells were selected and particle analysis was performed to determine form factor ($perimeter^2/4\pi*area$) and aspect ratio (length of major and minor axes). Mitochondria of 12 cells per condition were analyzed and the mean per cell was considered for further statistical tests.

2.1.11 Mitochondrial Membrane Potential Assessment

Membrane potential ($\Delta\Psi m$) was measured with 5,5′,6,6′-tetrachloro-1,1′,3,3′-tetraethylbenzimidazolcarbo cyanine iodide (JC-1) (Santa Cruz, Santa Cruz, CA, USA) dye (Perelman et al., 2012). JC-1 is a polychromatic cationic dye that on excitation accumulates in the membrane bound mitochondria as red aggregates and green monomers depending on the energized or deenergized state of the mitochondria. High mitochondrial membrane potential (or negative interior potential of mitochondria compared to cytosol) leads to accumulation of high concentrations of JC-1 aggregates that emit red fluorescence. In case of low interior potential, JC-1 dye forms monomers that fluoresce green. Cells were stained with JC-1 dye at 5 µg/mL final concentration for 10 minutes in the dark at

37°C. Cells were washed with 1× HBSS and prepared for flow cytometry (FACSCalibur, BD Biosciences, San Jose, CA) in Fluorobrite DMEM. JC-1 dye after accumulation in mitochondria forms red aggregates and green monomers that emit fluorescence at 590 nm and 510 nm respectively. For live imaging, cells grown in coverslip bottom 35mm dishes were stained and imaged using the Zeiss confocal microscope under a 63× oil immersion objective.

2.1.12 Mitochondrial ROS Measurement

Cells were labeled with MitoSox ROS (Thermo Fisher Scientific) dye at 5 µM final concentration for 10 minutes in the dark at 37°C using phenol red-free Fluorobrite DMEM. Cells were washed and stained with Hoechst 33342 stain for 10 minutes at room temperature. Flow cytometric analysis was performed at Indiana Center for Biomedical Innovation. For flow cytometry, cells were labeled with dye at 1 µM final concentration, incubated in the dark at 37°C and immediately loaded for ROS fluorescence detection in the FL-2 channel using BD FACSCalibur flow cytometer (Kauffman et al., 2016).

2.1.13 Complex IV Activity

ELISA was performed on cell lysates treated using COX IV ELISA kit (Abcam, Cambridge, MA, USA, Cat no. ab109909) following manufacturer's instructions. Briefly, 10 µg protein was loaded into plates coated with COX IV antibody and cytochrome c reduction by the immunocaptured COX IV from the sample was measured, using absorbance at 550 nm. Kinetic reads were

obtained and slopes directly correlating to enzyme activity were determined. Total amount of COX IV was also assessed on the same samples.

2.1.14 Hemin Rescue

For hemin rescue experiments, hemin (Sigma-Aldrich, Cat no H9039) 10 µM (final well concentration) was freshly prepared in DMSO. Cells pretreated with NMPP were supplemented with hemin in EBM2 containing 0.2% FBS for 6 hrs, followed by harvesting and processing for immunoblotting or ELISA.

2.2 In Vivo Experiments

2.2.1 Animals

Animal studies were approved by the Indiana University School of Medicine Institutional Animal Care and Use Committee, and were consistent with the Association for Research in Vision and Ophthalmology Statement for the Use of Animals in Ophthalmic and Visual Research. C57BL/6J wild-type, healthy female mice, 8 weeks of age were purchased from Jackson Laboratories and group housed under standard conditions (Wenzel et al., 2015). For technical ease of housing conditions, males were excluded from this study. NMPP at 10 µM final vitreous concentration was injected intravitreally into naïve mice under ketamine/xylazine anesthesia as described (Sulaiman et al., 2016), and 24 hrs post-injection, animals were euthanized, and retinas were immediately isolated from the animals and processed for the energetics experiment.

2.2.2 PPIX Fundus Imaging

Mice were anesthetized and eyes were topically administered with 1% tropicamide solution and hypromellose ophthalmic demulcent solution (Gonak, Akorn, Lake Forest, IL). PPIX fluorescence (excitation at 403 nm, emission at 628 nm) was measured under a bandpass filter using the Micron IV system (Phoenix Research Labs, Pleasanton, CA). Fundus images were captured for each individual eye and images were further processed for qualitative analysis.

2.2.3 Retinal Vasculature Staining

Eyes were harvested from postnatal day 3 and 2-month old adult mice. Individual retina was dissected from the posterior chamber of the eye and fixed in 4% paraformaldehyde overnight at 4°C. The following day, retina was washed with 1X PBS, permeabilized in blocking buffer containing 0.5% Triton X-100 in 5% BSA solution for 2 hours at room temperature and incubated in GS-IB4 isolectin (Biotin, 1:250 dilution, Invitrogen, Cat no., 121414) for 48 hours under static conditions at 4°C. Retinal flatmounts were then incubated in secondary antibody overnight at 4°C. This was followed by mounting retinal tissues on glass slides using Fluoromount-G (Southern Biotech, Birmingham, AL) and imaged using confocal microscopy.

2.2.4 Retinal Structure and Integrity Using Optical Coherence Tomography and Histological Sections

Retinal layers were assessed by optical coherence tomography (OCT) imaging, using rodent Micron IV system (Phoenix Research Labs, Pleasanton, CA). Mice were anesthetized by intraperitoneal injections of 80 mg/kg ketamine hydrochloride and 10 mg/kg xylazine. Eyes were dilated with 1% tropicamide solution and lubricated with hypromellose ophthalmic demulcent solution (Gonak, Akorn, Lake Forest, IL). Mice were placed on a heated stage and the anterior part of the eye was positioned appropriately for acquiring OCT images.

For examining histological sections of the posterior section of individual eyes, mice were euthanized and eyes were enucleated for overnight fixation in 4% paraformaldehyde solution. Eyes were processed embedded in paraffin and sectioned at 5 µM thickness by the Indiana University School of Medicine Histology Core. Hematoxylin and eosin staining was performed, and retinal structure and morphology was assessed. The thickness of retinal layers was determined by calculating the distance between ganglion cell layer to inner nuclear layer and to outer nuclear layer and by counting DAPI stained nuclei in the three respective nuclear layers (Park et al., 2014).

2.2.5 Retinal Mitochondrial Bioenergetics

For retinal ex vivo OCR measurements, protocols were adapted as previously described (Joyal et al., 2016; Kooragayala et al., 2015). Briefly, eyes were enucleated and retina was isolated from the posterior cup. Retinal punches (1 mm diameter) were dissected from an area adjacent to optic nerve to minimize variability in retinal thickness. Retinal punches were incubated in Seahorse XF

DMEM Medium pH 7.4 containing 5 mM HEPES supplemented with 12 mM glucose and 2 mM L-glutamine for 1 hour in a room air incubator at 37°C. For OCR measurement, 0.5 µM FCCP and 0.5 µM rotenone/antimycin A were injected and OCR readings were determined.

2.2.6 Electroretinogram for Assessing Visual Activity

Mice were anesthetized by intraperitoneal injections of 80 mg/kg ketamine hydrochloride and 10 mg/kg xylazine. Eyes were dilated with 1% tropicamide solution and lubricated with hypromellose ophthalmic demulcent solution (Gonak, Akorn, Lake Forest, IL). Electroretinogram (ERG) was measured using an electrodiagnostic LKC system (UTAS-E 2000, LKC Technologies, Gaithersburg, MD) to assess the function of the retina. Mice were dark adapted overnight before taking measurements for scotopic a-wave and b-wave responses (Benchorin et al., 2017). Scotopic rod measurements were recorded following white light flashes of increasing intensities of 0.025, 0.25 and 2.5 log cd·s/m_2, at time intervals of 10, 20 and 30 seconds. For measurement of photopic cone responses, mice were light adapted to a white background for 10 minutes, followed by flashes of light stimulation at 0, 5, 10 and 25 log cd·s/m_2 intensities. The trace amplitude between time 0 and the lowest point on the trace was considered as a-wave and the amplitude between the lowest trace and the highest peak following oscillatory potentials, was considered as b-wave.

2.3 Software and Statistical Analysis

All Seahorse kinetic traces were analyzed using Wave 2.4 software (Agilent) and GraphPad Prism v. 8.0. FCS files for flow cytometry were analyzed using FlowJo v10. Image quantification for mitochondrial morphology and immunoblotting was done using ImageJ v1.52. Comparisons between groups were performed using GraphPad Prism v8 with either unpaired, two-tailed Student's t-test or one-way ANOVA with Tukey's post-hoc tests as indicated. p values < 0.05 were considered statistically significant. Mean±SEM shown for all graphs unless indicated otherwise; n is listed in figure legends.

CHAPTER 3. ASSESSMENT OF CELLULAR BIOENERGETICS OF OCULAR ENDOTHELIAL CELLS

3.1 Summary

Metabolic dysfunction in endothelial cells underlies many ocular diseases characterized by pathological angiogenesis. Here, I sought to determine the metabolic phenotype of HRECs and RF/6A cell line by measuring changes in their oxygen consumption rate and extracellular acidification rate due to various stressor cues. I aimed to develop a standardized protocol for assessment of these parameters in these widely used ocular cell models. I used a Seahorse extracellular flux analyzer to measure changes in O_2 and pH after injecting inhibitors of the electron transport chain and glycolysis. I also measured ATP production rate to distinguish between pathway specific sources of cellular energy. I determined optimized cell seeding density and doses of potential-gradient uncoupler, and measured oxygen consumption as well as acidification rate of the medium.

Under these optimized assay conditions, I observed a difference in energy phenotype as well as ATP production between these two cell types, with HRECs relying on oxidative phosphorylation to meet energy needs and RF/6A preferring glycolysis under stress. I also determined oxidative phosphorylation and glycolysis parameters essential for their cellular metabolism. Knowledge of the baseline bioenergetic phenotype of ocular endothelial cells will be crucial for studying defects in complexes of the electron transport chain as well as dysregulated glycolysis behavior in different disease models.

3.2 Background and Rationale

Mitochondrial function is responsible for maintaining important cellular processes like oxidative phosphorylation, programmed cell death, oxidative stress, heme biosynthesis, mitophagy and calcium signaling (Kluge et al., 2013; Tang et al., 2014). These basic functions work in consortium, and damage to these mitochondrial dynamics can cause endothelial dysfunction and development of vascular diseases. As detailed in Chapter 1, such diseases of the posterior eye vasculature include ROP, PDR and wet AMD, are all characterized by neovascularization, driven by either retinal or choroidal microvascular ECs (Bharadwaj et al., 2013).

Mitochondrial dysfunction is associated with many retinal diseases (Barot et al., 2011; Lefevere et al., 2017). Formation of DNA base mismatches and mitochondrial DNA damage have been implicated in the pathobiology of diabetic retinopathy (Mishra and Kowluru, 2018). Post-translational modifications of mitochondrial transcription factors can impair biogenesis of mitochondria (Santos et al., 2014). Relevant to PDR, high glucose has been shown to disrupt mitochondrial morphology, membrane potential and respiratory functions in rat retinal endothelial cells and bovine retinal pericytes (Trudeau et al., 2011; Tien et al., 2017). High glucose also triggered increased mitochondrial DNA methylation (Mishra and Kowluru, 2015), mitochondrial DNA damage, increased reactive oxygen species levels and reduced mitochondrial membrane potential (Xie et al., 2008). Tigecycline, an FDA approved antibiotic, was recently shown to reduce mitochondrial respiration in Y79 retinoblastoma cells and HRECs and was

effective in suppressing retinoblastoma and angiogenesis pre-clinically (Xiong et al., 2018). Anti-VEGF agents like aflibercept used clinically for anti-angiogenic therapy provide a protective function to RPE by restoring mitochondrial membrane potential (De Cilla et al., 2017), indicating the importance of mitochondrial function directly in therapy.

Given the significance of mitochondrial function in the mechanisms of retinal diseases, understanding the bioenergetic profile of posterior eye microvascular ECs is crucial. However, this profile remains undocumented for the primate endothelial cell line RF/6A, established from rhesus retina-choroid tissue (Lou and Hu, 1987) and widely used as a model of choroidal endothelial cells (Rusovici et al., 2013; Cabrera et al., 2016; Basavarajappa et al., 2017). Moreover, the bioenergetic profile has not been explored in detail in primary human retinal microvascular endothelial cells (HRECs), another widely-used in vitro angiogenesis model (Liu et al., 2017; Xiong et al., 2018).

Before we can understand the role of mitochondrial deregulation in cellular disease models, the metabolic characteristics of mitochondria in these cells under normal conditions need to be established. In this chapter, I aimed to characterize the cellular bioenergetics of these ocular endothelial cells from the retina and choroid. I investigated the basal energy phenotype of HREC and RF/6A cells and measured their ability to meet energy demands under metabolic stress. I used the Seahorse extracellular flux (XF) analyzer, which detects changes in O_2 and protons from cells in real time by making use of fluorescent sensors (Divakaruni et al., 2014). This system has been used previously for

assessing metabolism of other ocular cell types, including Müller glial cells (Tien et al., 2017), retinoblastoma (Xiong et al., 2018), pericytes (Trudeau et al., 2011), RPE (Iacovelli et al., 2016; Kurihara et al., 2016), and even whole retina (Kooragayala et al., 2015), however, not in microvascular ECs.

The results in this chapter provide optimal key parameters ideal for these assays in ocular endothelial cells. Mitochondrial stress was induced using a serial injection of inhibitors oligomycin, carbonyl cyanide-4-(trifluoromethoxy)phenylhydrazone (FCCP), rotenone, and antimycin A. Oligomycin inhibits ATP synthase allowing measurement of ATP related to mitochondrial respiration, while FCCP is an ETC uncoupler. Antimycin A and rotenone, complex I and III inhibitors respectively, shut down ETC function to reveal oxygen consumption rate (OCR) from non-mitochondrial sources. I also measured the extracellular acidification rate (ECAR) of cells by inducing stress by brief glucose starvation. This was followed by stimulation of glycolysis with a saturating dose of glucose and blockade of mitochondrial ATP production by oligomycin. I confirmed glycolytic function using deoxyglucose (2-DG) and measured glycolytic capacity. 2-DG competitively binds to hexokinase, blocking the glycolysis pathway and revealing ECAR unrelated to glycolysis. Finally, in this chapter, I also report, for the first time in endothelial cells, a real-time ATP production rate assay that allows ATP measurement from both mitochondrial respiration and glycolysis.

3.3 Results

3.3.1 Optimization of Uncoupler FCCP Concentration Produces Maximal Respiration at 1 μm and 0.125 μm Concentrations

Uncoupler FCCP induces uninhibited flow of electrons across the ETC, causing the enzymes of the respiratory chain to use metabolic substrates at full potential and in turn, revealing the maximal cellular capacity that can meet energy demands under metabolically stressed conditions. To determine the FCCP dose that produces the highest maximal respiration, I chose to perform titrations of increasing concentrations of FCCP. Cells were injected with concentrations of FCCP ranging from 0.125 μM to 2 μM and their maximal OCR was measured. HRECs produced maximal respiration at 1 μM FCCP concentration (Figure 3.1A). RF/6A needed 0.125 μM FCCP to produce maximal respiration (Figure 3.1B). I proceeded to use these FCCP concentrations for all experiments in this thesis, in order to compare the FCCP-induced maximal respiration to the respective cell type's basal respiration parameter.

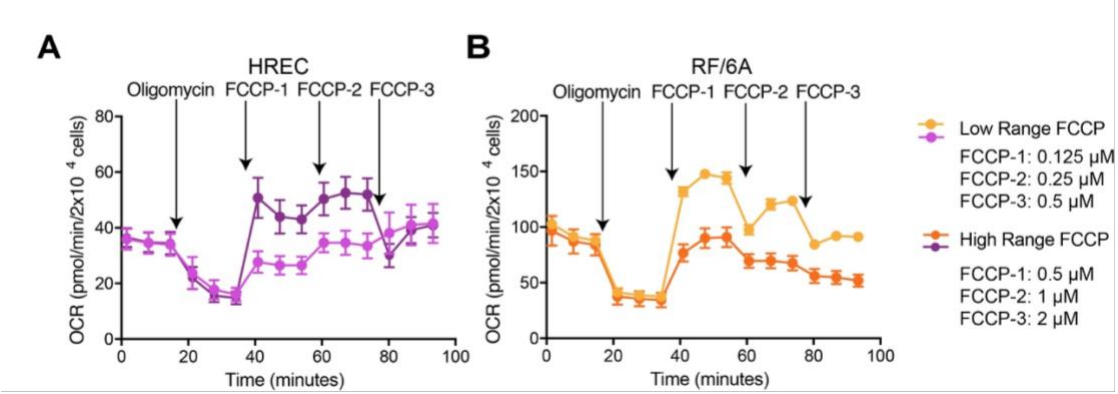

Figure 3.1. Optimization of uncoupler FCCP concentration that produces maximal respiration in ocular endothelial cells. Oxygen consumption rate (OCR) traces of (A) HRECs and (B) RF/6A cells. $2\times10_4$ cells seeded. Mean ± SEM, n=3.

3.3.2 Cellular Energetic Behavior of HRECs and RF/6A Differ Under Metabolic Stress

To determine the energy phenotype of HRECs and RF/6A cells, I tested ATP synthase inhibitor oligomycin and mitochondrial uncoupler FCCP. Induced stress caused HRECs to use both oxidative phosphorylation as well as glycolysis to meet energy demands with equal propensity (Figures 3.2A, 3.2B). RF/6A cells behaved differently under stress. Their cellular metabolic needs were met by enhanced glycolysis, with an increase in ECAR of roughly 50% over baseline (Figures 3.2C, 3.2D), without any change in OCR. On comparing OCR versus ECAR, HRECs moved to a more energetic phenotype (Figure 3.2A) under stressed conditions. Meanwhile, RF/6A cells became more glycolytic on being stressed (Figure 3.2C).

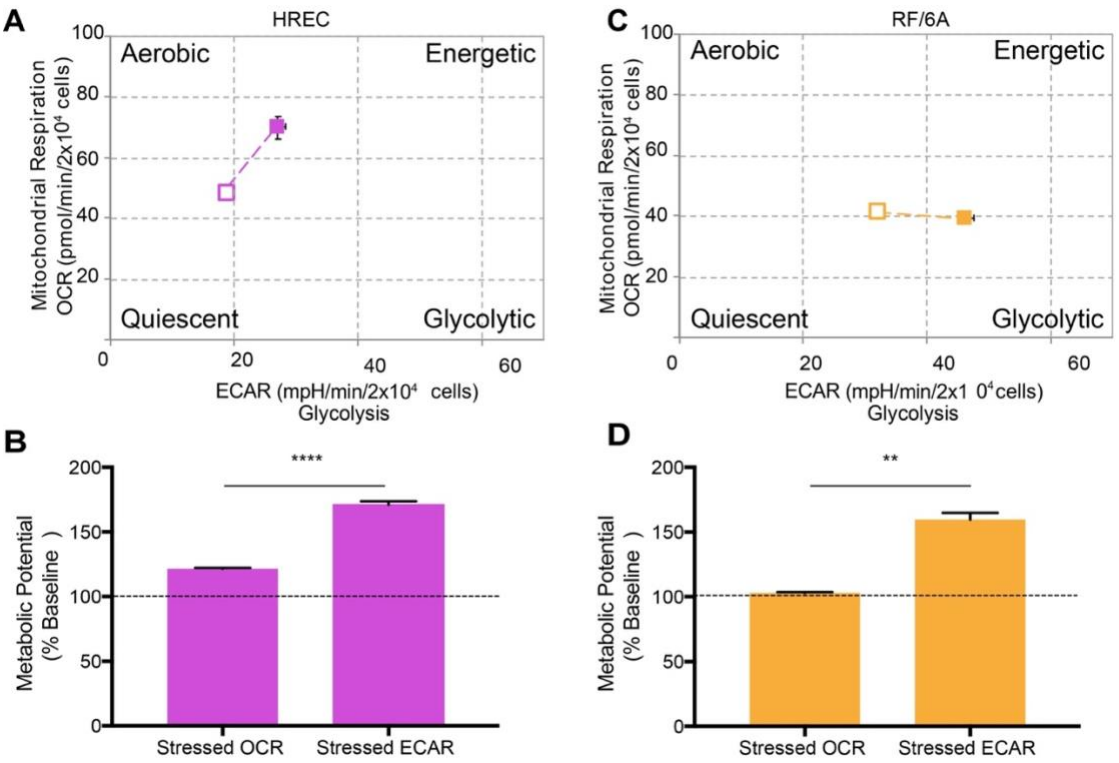

Figure 3.2. Cellular energetic behavior of endothelial cells under metabolic stress. Cell energy phenotype profiles of (A) HRECs and (C) RF/6A cells. Open box indicates baseline phenotype, filled box indicates stressed phenotype. Representative plots of three independent experiments. Some error bars are too small to be seen. (B, D) % stressed OCR and ECAR produced over 100 % baseline OCR and ECAR. Mean ± SEM, n=3; **p<0.01, ****p<0.0001, two-tailed unpaired Student's t-test.

3.3.3 The majority of intracellular ATP is produced from mitochondrial respiration

In order to understand the source of ATP during OCR and ECAR measurements, I performed an assay that would distinguish between ATP generated by mitochondrial oxidative phosphorylation and glycolysis (Figure 3.3A, 3.3B). Total cellular ATP generation was higher in RF/6A cells (Figure 3.3C) with nearly 70% of ATP generation from mitochondria and the remainder from glycolysis. For HRECs, mitochondrial ATP generation was higher than that in RF/6A cells at 75% (Figure 3.3C). I also assessed the ATP rate index for both cell types, with HRECs showing higher ATP production from mitochondrial respiration compared to RF/6As, even though both cell types had an index >1, indicating cellular energy mostly to be mitochondrial (Figure 3.3D).

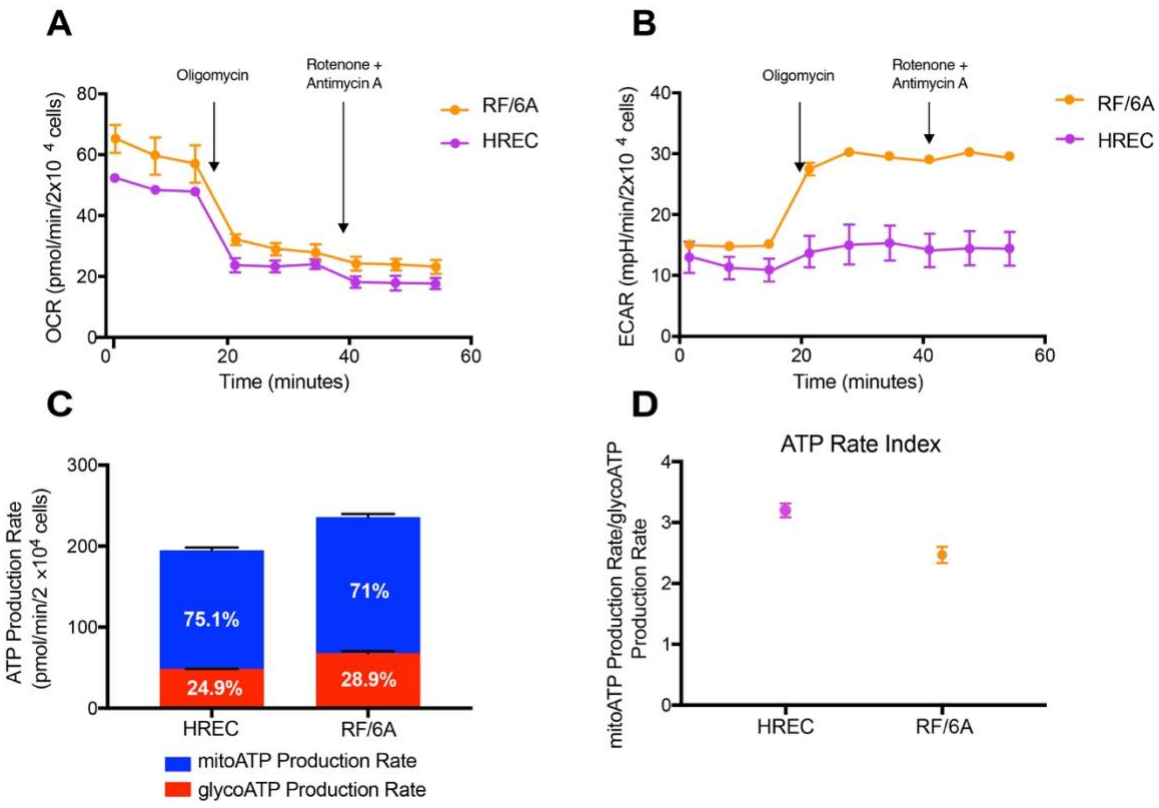

Figure 3.3. Total intracellular ATP generation. (A) OCR and (B) ECAR kinetic traces for RF/6A and HRECs with respective modulators injected at indicated time points during assay run. Representative plots from three independent experiments. (C) Total ATP generation measured with demarcations indicating mitochondrial and glycolytic ATP in the stacked columns. (D) Ratio of mitochondrial ATP to glycolysis ATP production rates for each cell type. Mean ± SEM, n=3.

3.3.4 Optimal Cell Seeding Density Ranged Between 2×10^4 Cells and 4×10^4 Cells

To understand the mitochondrial response to variable cell number, I tested three different densities of cells to identify the optimal working range of cells for assays (Figures 3.4A, 3.5A). Basal respiration signal increased in proportion to increase in cell number (Figures 3,4B, 3.5B). For both cell types, 4×10^4 cells (100% confluent) had the highest reportable FCCP-induced maximal respiration (Figures 3.4C, 3.5C), with no significant change in coupling efficiency (Figures 3.4G, 3.5G). Significant changes in proton leak were observed in 2×10^4 and 4×10^4 HRECs and 4×10^4 RF/6A cells respectively (Figures 3.4D, 3.5D). OCR-linked ATP for HREC and RF/6A was significantly higher at 4×10^4 seeding density than at lower densities (Figures 3.4E, 3.5E). Spare respiratory capacity remained unchanged for HRECs (Figure 3.4F), whereas for RF/6A, 4×10^4 cells increased the potential of cells to meet their spare respiratory capacity (Figure 3.5F). Based on these findings, I opted to work with 2×10^4 cells and 4×10^4 cells for all further assays.

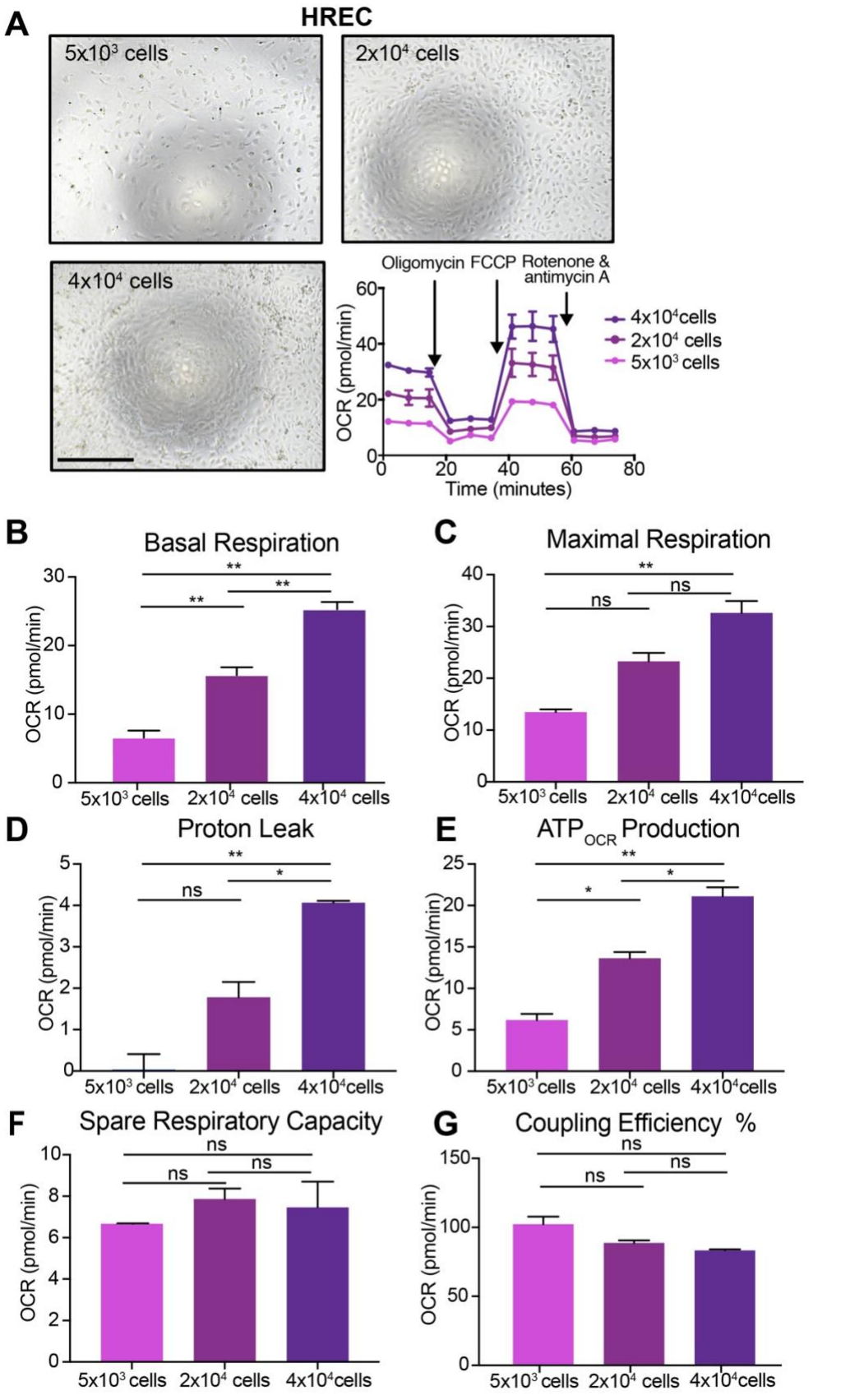
A
HREC
5x10³ cells
2x10⁴ cells
4x10⁴ cells
Oligomycin
FCCP
Rotenone & antimycin A
OCR (pmol/min)
Time (minutes)
4x10⁴cells
2x10⁴ cells
5x10³ cells
B
Basal Respiration
C
Maximal Respiration
D
Proton Leak
E
ATP OCR Production
F
Spare Respiratory Capacity
G
Coupling Efficiency %
ns

Figure 3.4. Optimizing cell seeding density for HRECs. (A) representative images from three independent experiments of HRECs along with their OCR traces. Scale bar = 500 µm. (B) basal respiration, (C) maximal respiration, (D) proton leak, (E) OCR-linked ATP, (F) spare respiratory capacity and (G) coupling efficiency. Mean ± SEM, n=3; ns – not significant, *p<0.05, **p<0.01, ANOVA with Tukey's post-hoc tests.

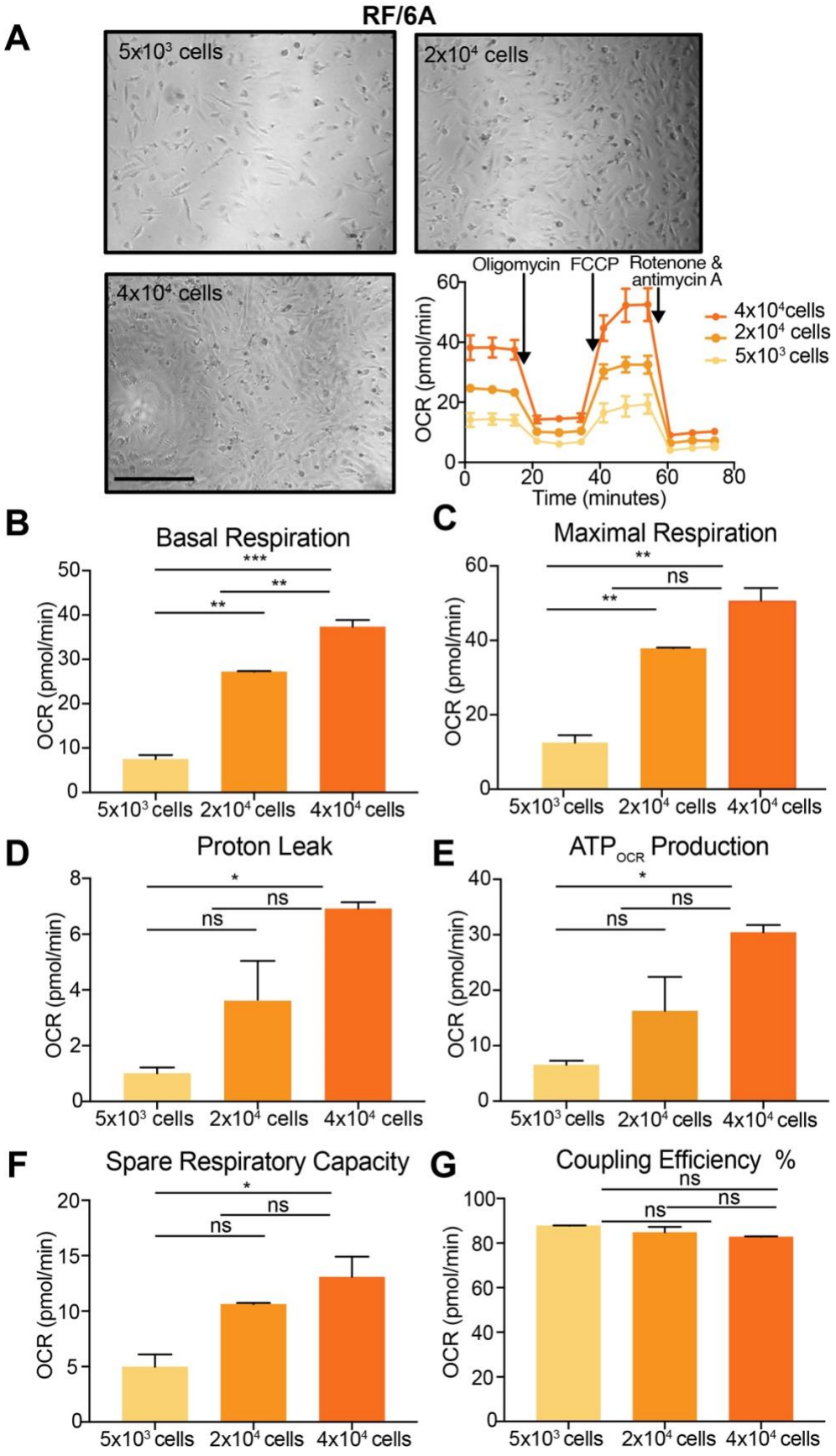
RF/6A
A
5x10³ cells
2x10⁴ cells
4x10⁴ cells
Oligomycin
FCCP
Rotenone & antimycin A
OCR (pmol/min)
Time (minutes)
4x10⁴cells
2x10⁴ cells
5x10³ cells
B
Basal Respiration
C
Maximal Respiration
D
Proton Leak
E
ATP OCR Production
F
Spare Respiratory Capacity
G
Coupling Efficiency %
ns

Figure 3.5. Optimizing cell seeding density for RF/6A cells. (A) representative images from three independent experiments of RF/6A cells along with their OCR traces. Scale bar = 500 µm. (B) basal respiration, (C) maximal respiration, (D) proton leak, (E) OCR-linked ATP, (F) spare respiratory capacity and (G) coupling efficiency. Mean ± SEM, n=3; ns – not significant, *p<0.05, **p<0.01, ***p<0.001, ANOVA with Tukey's post-hoc tests.

3.3.5 HREC and RF/6A cells Show Comparable FCCP-Induced Maximal Respiration

To assess parameters that regulate oxidative phosphorylation, I performed serial injection of oligomycin, FCCP and complex I and III inhibitors rotenone and antimycin and measured cellular oxygen consumption (Figures 3.6A, 3.6B). Basal respiration and ATP_{OCR} was slightly higher for RF/6A cells compared to HRECs (Figures 3.6C, 3.6D). I observed similar OCR for maximal and non-mitochondrial respiration as well as spare respiratory capacity (Figures 3.6E, 3.6G, 3.6H). Similarly, there was a difference in proton leak, with OCR measurement higher for RF/6A compared to HRECs (Figure 3.6F). Both HREC and RF/6A cells showed comparable coupling efficiency (Figure 3.6I). Coupling efficiency indicates how well the protons are utilized during ATP generation and also estimates proton leak during oxidative phosphorylation-coupled reactions.

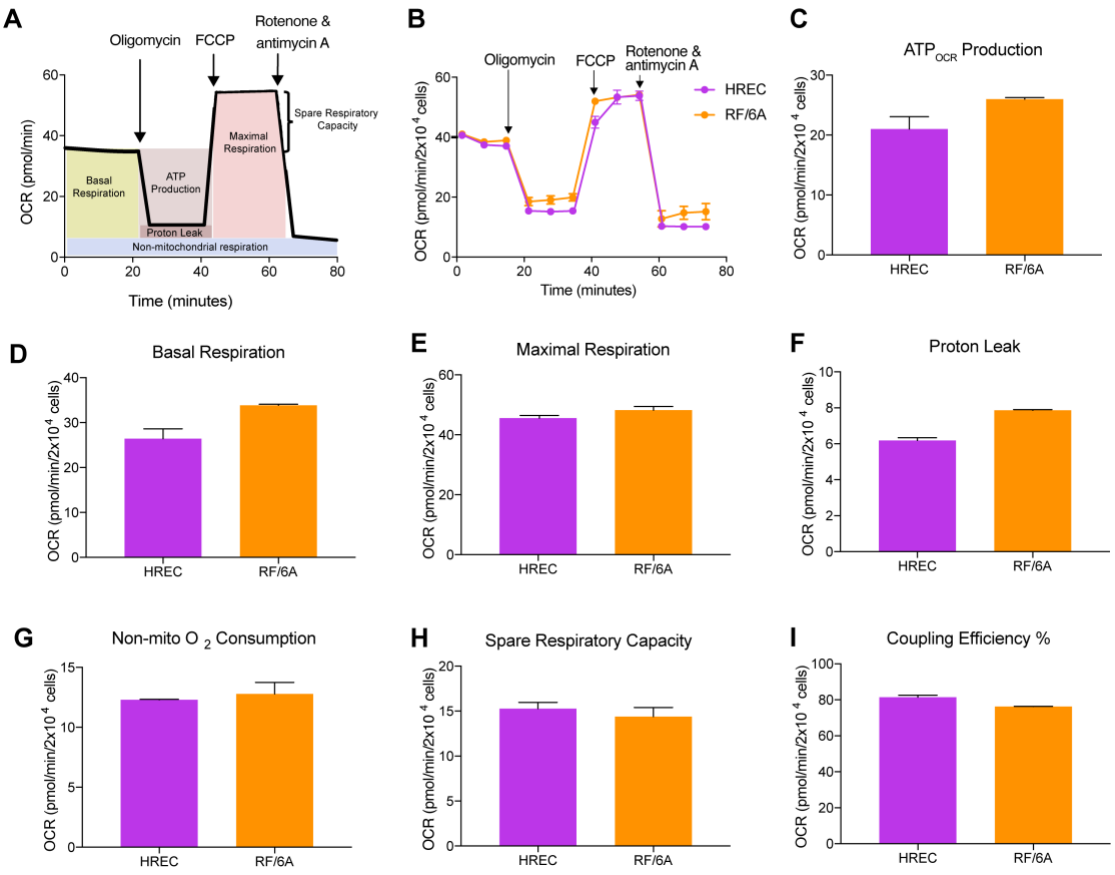

Figure 3.6. Characterizing FCCP-induced maximal respiration and key mitochondrial parameters. (A) Schematic of data generated in the mitochondrial stress experiment. (B) OCR kinetic traces for RF/6A and HRECs. Representative plots from three independent experiments. (C-I) Comparison of cell types for the parameters: (C) OCR-linked ATP production, (D) basal respiration, (E) maximal respiration, (F) proton leak, (G) non-mitochondrial oxygen consumption, (H) spare respiratory capacity, and (I) % coupling efficiency. Mean ± SEM, n=3.

3.3.6 Modulators of Glycolysis Allow for Assessing Glycolytic Capacity of Cells

In order to document cellular glycolysis and glycolytic parameters, I measured ECAR in glucose starved cells that were injected with oligomycin and glucose analog 2-deoxyglucose (Figure 3.7A) that inhibits the action of hexokinase (Figure 3.7B). Glycolysis ECAR measurement was higher in HRECs compared to RF/6A (Figure 3.7C), indicating a reduced baseline glycolysis in RF/6A cells. As seen previously in Figures 2 and 3, I observed higher glycolytic capacity in RF/6A cells compared to HRECs (Figure 3.7D) as well as glycolytic reserve (Figure 3.7E) and acidification due to non-glycolytic reactions (Figure 3.7F).

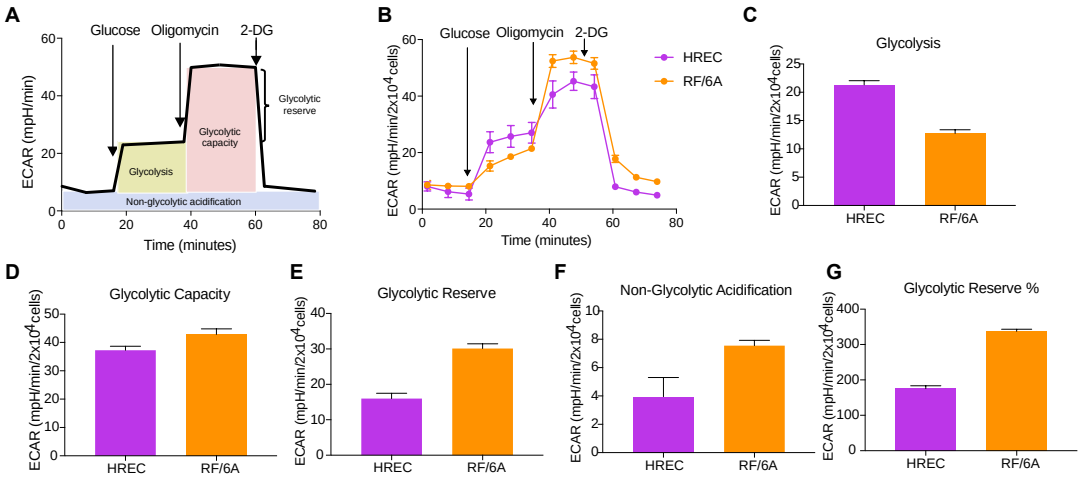

Figure 3.7. Modulators of glycolysis allow for assessing glycolytic capacity of cells. (A) Schematic of data generated in the glycolysis stress experiment. (B) ECAR kinetic traces for HRECs and RF/6A. Representative plots of three independent experiments. (C-G) Comparison of cell types for the parameters: (C) glycolysis, (D) glycolytic capacity, (E) glycolytic reserve, (F) non-glycolytic acidification and (G) % glycolytic reserve (% of glycolytic capacity rate over glycolysis rate). Mean ± SEM, n=3.

3.4 Discussion

Mitochondrial dysfunction is an area of growing interest in ocular endothelial cell biology (Kluge et al., 2013). It has become increasingly evident from recent studies that components of the ETC like complexes III and IV mediate endothelial function during angiogenesis (Vandekeere et al., 2018, Diebold et al., 2019). Blocking heme production diminishes glycolytic capacity of retinal ECs, as discussed in Chapter 4 (Shetty et al., 2019). Recent taxonomical analysis of murine choroidal ECs from neovascularization revealed potential metabolic candidates not found in healthy cells, suggesting targeting endothelial metabolism could be the way forward in vascular therapeutics (Rohlenova et al., 2020). To provide a baseline for future studies, I set out to characterize the cellular energetic phenotype of endothelial cells that form important cellular models for neovascular diseases (Alizadeh et al., 2018). Traditionally, closed oxygen sensors like Clark electrodes were employed on isolated mitochondria, to assess oxygen consumption and rate of respiration (Wolfbeis 2015). However, this technique can often be technically cumbersome and severely restrictive for use in intact cells. I made use of a real-time flux analyzer Seahorse, developed in the late 2000s, that senses O_2 from a monolayer of cells and measures respiration as a function of mitochondria. I provide a detailed optimization method that can be employed before working with these or other cell types, identifying the optimum FCCP dosage and cell seeding density. I detailed the metabolic parameters of two of the most widely-used posterior eye endothelial cell models, primary HRECs and the RF/6A cell line.

FCCP titration was critical as a first step, as the assay measures FCCP-induced maximal respiration compared to basal respiration of cells (Dranka et al., 2011). The FCCP concentration that gave the maximal OCR changed significantly from one cell type to another, highlighting the importance of characterizing the phenotype of each cell type under various experimental conditions. Selection of appropriate cell seeding density is important to minimize variability in metabolic parameters owing to clumping of cells (over-seeding) or changes in morphology due to low confluency (low seeding) (Lange et al., 2012). I recommend working with cell number ranges of $2\times10_4$ and $4\times10_4$ as lower cell numbers were unable to generate accurate maximal respiration, proton leak and spare respiratory capacity.

In cell energy phenotype assays, I observed a difference between HRECs and RF/6A cells in their response to metabolic stress. In parallel with these results, I saw similar results with the ATP index ratio that signifies the differences in energy behavior between retinal and choroidal endothelial cells. This could be due to differences in their culture phenotype, one being primary cells isolated from humans and the other being an immortalized cell line. Transformed cells rely on glutamine metabolism to replenish TCA cycle intermediates in case of anaplerosis (DeBerardinis et al., 2007). However, it might also reflect a fundamental difference between microvascular cells of retinal versus choroidal origin, as already documented for gene expression profiles (Smith et al., 2007).

My findings were comparable to the metabolic phenotype of other endothelial cell systems. HRECs showed similar maximal respiration to bovine

aortic endothelial cells (BAEC) (Dranka et al., 2011). Another study observed human umbilical vein endothelial cells (HUVEC) with OCR_{ATP} between 4-15 pmol/min (Gupta et al., 2016), compared to nearly 20 pmol/min in our cell models, HRECS and RF/6A cells. Similarly, in a glycolysis stress test, HUVECs showed basal ECAR of roughly 3 mpH/min and glycolytic capacity of nearly 40 mpH/min, analogous to HRECs and RF/6A (Doddaballapur et al., 2015; Balogh et al., 2018).

Extracellular flux assays have some limitations. Fluorophore sensors can be sensitive to quenching; care must be taken while testing compounds that may interfere with fluorescence, namely inclusion of controls without cells and basal medium, and calibration of these wells with treated cells (Koopman et al., 2016). If treatment leads to loss of cell viability, normalization with protein content would be appropriate. Cell viability markers can be used at the end of the assay to count the number of viable cells. Basal medium components like glutamine and glucose vary between different culture media. Thus, I recommend using concentrations during assay basal medium preparation similar to cell culture medium concentrations.

Making use of different mitochondrial inhibitors as well as glycolytic modulators not only allows for assessment of metabolic function due to different stress cues, but also lets one examine different components directly involved in the metabolic pathway. Detecting changes in spare respiratory capacity can indicate early signs of stress (Perron et al., 2013). The effects of small molecules on cellular metabolism, especially in the case of disease models like

hyperglycemia or hypoxia can be compared with the baseline phenotype of these endothelial cells as described here. Genetic and pharmacological manipulations in endothelial cells and their effect on pathway specific changes in metabolism can be examined using the ATP production assay, which has not been a part of previous metabolic analyses in ocular or other endothelial cells (Liu et al., 2017; Al-Shabrawey, 2017; Xiong et al., 2018). Recent studies of non-ocular tissues also indicate endothelial cell specific metabolic changes in pathological angiogenesis conditions that can be exploited in a novel approach to therapeutic target discovery (Goveia et al., 2014; Schoors et al., 2014; Schoors et al., 2015; Eelen et al., 2018).

Together, my findings in this chapter have built a metabolic profile of key ocular endothelial cell types, elucidating their energy phenotype and assessing parameters governing both oxidative phosphorylation and glycolytic capacity. I have also reported an ATP production rate assay that determines the sources of ATP generated in the cell and allows for identifying metabolic switching in response to different modulators, compounds, genetic modifications or other interventions. These results serve as a reference point for testing various experimental conditions and metabolic parameters in the two endothelial cell types used here. Moreover, this approach provides a framework for characterizing the cellular energetics of different cell types prior to further manipulations in Chapter 4, and aid in designing experiments addressing Aim II and Aim III.

CHAPTER 4. HEME SYNTHESIS INHIBITION BLOCKS ANGIOGENESIS BY CAUSING MITOCHONDRIAL DYSFUNCTION

4.1 Summary

The relationship between heme metabolism and angiogenesis is poorly understood. The final synthesis of heme occurs in mitochondria, where FECH inserts Fe^{2+} into protoporphyrin IX to produce proto-heme IX. We previously showed that FECH inhibition is antiangiogenic in HRECs and in animal models of ocular neovascularization. In the present chapter, I sought to understand the mechanism of how FECH and thus heme is involved in maintaining endothelial cell function. Heme synthesis inhibition changed mitochondrial morphology in endothelial cells. Loss of heme causes a buildup of mitochondrial ROS and depolarized membrane potential ($\Delta\Psi m$). Oxidative phosphorylation and mitochondrial complex IV were decreased in HRECs and in mice retina ex vivo after heme depletion (Figure 4.1). Exogenous supplementation with heme partially restored phenotypes of FECH blockade. The findings presented in this chapter provide a previously unknown link between mitochondrial heme metabolism and angiogenesis.

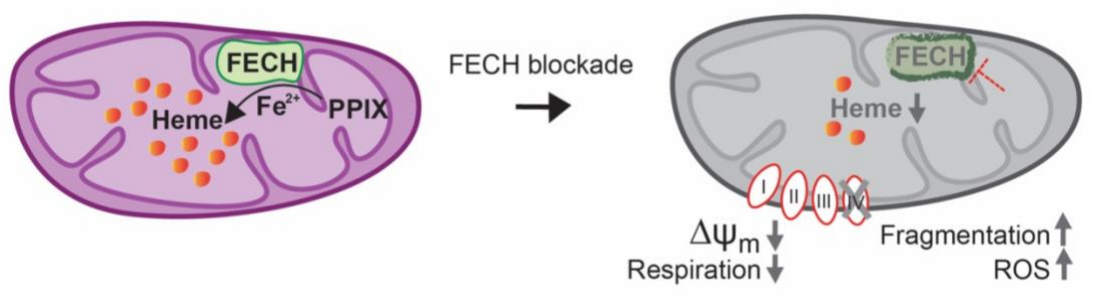

Figure 4.1. Graphical summary of chapter 4. Heme depletion via FECH blockade disrupts key mitochondrial functions like respiration, membrane potential, morphology and elimination of reactive oxygen radicals. ETC components like complex IV are directly affected due to insufficient incorporation of heme in the enzyme catalytic core for complex formation. $\Delta\Psi_m$ = membrane potential, ROS, reactive oxygen species; I, II, III, IV, ETC complexes.

4.2 Background and Rationale

An imbalance in mitochondrial metabolism has been implicated in the development of neovascular diseases catalyzed by aberrant angiogenesis. However, the role of heme synthesis in the development of mitochondrial dysfunction in neovascular diseases is unclear. As discussed above, neovascularization is a common phenomenon seen in vascular diseases like cancer, type 2 diabetes mellitus, PDR, ROP, and wet AMD (Friedman et al., 2004; Hellstrom et al., 2013; Kempen et al., 2004; Kizhakekuttu et al., 2012). We previously reported that heme synthesis inhibition is anti-angiogenic in retinal ECs in vitro and in animal models of ocular neovascularization. Blocking heme production in HRECs decreased proliferation, migration, and endothelial tube formation and caused reduced protein expression of total and phosphorylated VEGFR-2 (Basavarajappa et al., 2017). This antiangiogenic effect was only seen in ocular ECs, while ocular non-endothelial cells were not similarly affected. Heme synthesis inhibition was associated with smaller ocular neovascular lesions in a choroidal neovascularization mouse model. However, the mechanism underlying this effect remains unknown. The final synthesis of heme takes place in the mitochondria, when FECH inserts ferrous ion into a precursor PPIX to form protoheme (iron-protoporphyrin IX) (Dailey et al., 2017; Nilsson et al., 2009; Poulos, 2014). By directly targeting FECH, cells can be depleted of heme and heme-containing proteins, with a concomitant build-up of PPIX (Atamna et al., 2001; Vijayasarathy et al., 1999). Apart from the role of heme in oxygen transport and storage, heme acts as a prosthetic group in many

hemoprotein enzymes involved in oxidative phosphorylation, plus cytochrome P450s, catalases, and nitric oxide synthase (Chiabrando et al., 2014).

In the present chapter, I aimed to assess the relationship between mitochondrial physiology in human ECs and heme inhibition. I hypothesized that heme inhibition would lead to defects in heme-containing enzymes of the mitochondrial ETC, and thus affect mitochondrial function of ECs. I show that loss of heme altered mitochondrial morphology and dynamics, causing increased ROS levels and depolarized membrane potential. These studies reveal that heme synthesis is required for EC respiration and COX IV function specifically, and can negatively impact glycolytic capacity of ECs. Thus, I characterized a previously unknown role of heme in cellular metabolism that facilitates EC function in angiogenesis.

4.3 Results

4.3.1 Heme Inhibition Caused Changes to Mitochondrial Morphology and Increased Oxidative Stress

To block heme production, I used a competitive inhibitor of FECH called *N*-methylprotoporphyrin (NMPP) (Shi and Ferreira, 2006). Blockade of FECH with active site inhibitor NMPP (K_i ~ 10 nM) causes accumulation of precursor PPIX, as NMPP competes with FECH substrate PPIX for the binding site of the enzyme (Table 4.1). We have previously shown that HRECs exposed to NMPP showed remarkably reduced proliferation, migration and tube forming ability. NMPP was shown to produce a GI_{50} value of 30 µM in HRECs and 126 µM in RF/6A cells. This effect was specific to ECs, with brain microvascular ECs showing GI_{50} value of 39 µM and non-EC ocular cell types having negligible anti-proliferative effects (Basavarajappa et al., 2017). While NMPP has been used widely as chemical inhibitor of FECH, NMPP could have off-target effects in the cells.

HRECs treated with NMPP showed changes in mitochondrial fragmentation and shape (Figure 4.2A). NMPP treated cells had decreased form factor values, indicating reduced mitochondrial branching (Figure 4.2B; Figure 4.3A-F), owing to more highly fragmented mitochondria (Figure 4.2B, inset image). Mitochondria appeared less elongated and elliptical in NMPP treated HRECs as seen by lower aspect ratio values (Figure 4.2C). To determine mitochondrial mass, I used flow cytometry and quantified median fluorescence intensity (MFI) of NMPP treated HRECs (Doherty and Perl, 2017). NMPP

treatment led to reduced MFI, indicating decreased mass in mitochondria (Figure 4.2D).

Treatment	PPIX
	(pmol/mg)
DMSO	4.058
NMPP	97.244

Table 4.1. PPIX levels in HRECs treated with NMPP. PPIX levels quantified by ultra-performance liquid chromatography in HRECs treated with DMSO control and NMPP. This analysis was performed by the Iron and Heme Core, University of Utah.

Changes in mitochondrial morphology are commonly accompanied by transcriptional changes in genes regulating mitochondrial dynamics like the fusion-fission proteins (Westermann 2010, Duriaswamy et al., 2019). Metabolically active mitochondria undergo fusion events to form large interconnected mitochondria, whereas cells under low energy demands consists of smaller spherical mitochondria (Collins et al., 2002). Hence, I tested mRNA levels of key mitochondrial fusion proteins involved in mitochondrial dynamics, MFN2 and OPA1, and found significantly lower levels under FECH blockade conditions (Figures 4.2E and 4.2F). Fission regulator *DNM1L* (encoding Drp1) showed no change. I measured mitochondrial specific ROS using MitoSox ROS and cells treated with NMPP showed a marked increase in ROS levels (Figure 4.4A). I quantified this increase using flow cytometry and found a significant increase in MitoSox ROS labeled HRECs treated with NMPP (Figures 4.4B-C). This effect of elevated ROS levels was also seen in RF/6A cells treated with NMPP (Figures 4.4D and 4.4E). This primate cell line has properties of chorioretinal ECs (Lou and Hu, 1987), and thus provides corroboration of the primary HREC data.

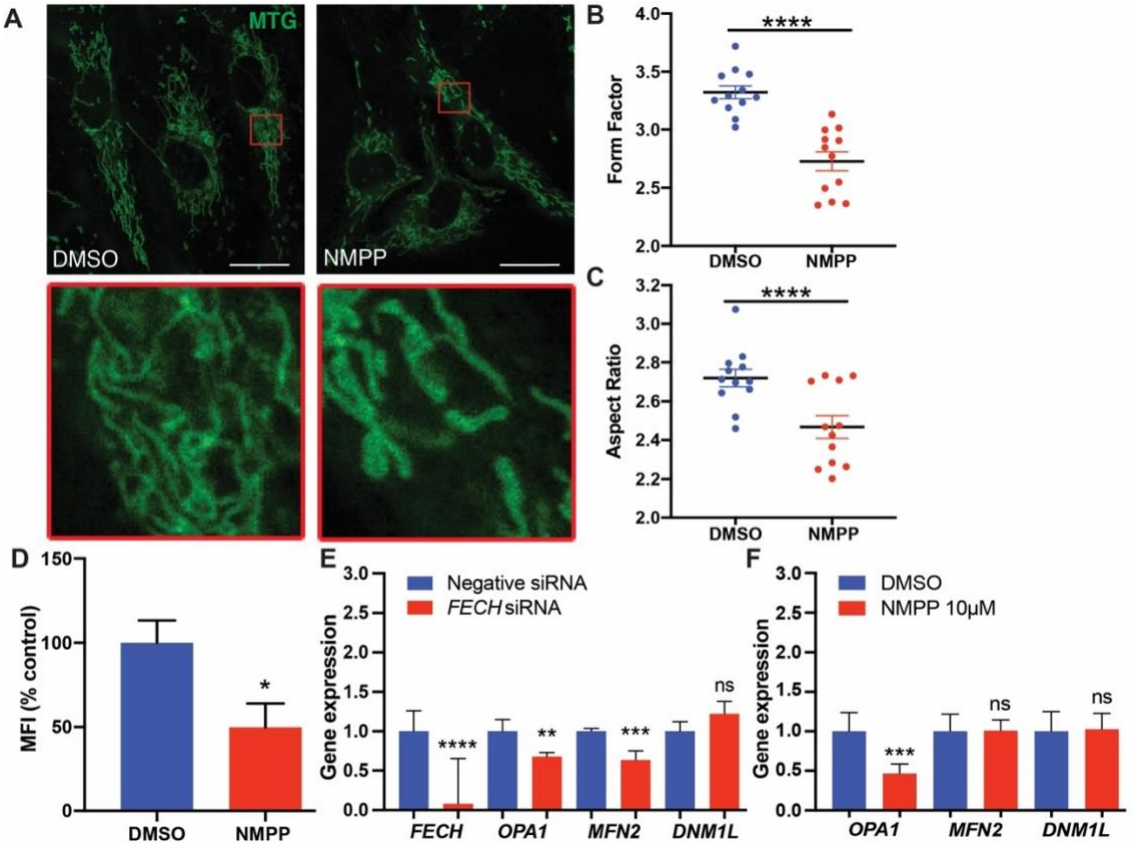

Figure 4.2. FECH blockade alters mitochondrial morphology and increases oxidative stress. (A) HRECs treated with DMSO or FECH inhibitor NMPP stained with MitoTracker green (MTG). Inset images indicate magnified region marked in red boxes. Form factor (B) and aspect ratio (C) as quantified using ImageJ. Individual data points indicate mean of mitochondria analyzed from each of 12 individual cells per treatment group. (D) Quantification of MTG fluorescence using flow cytometry and calculated Median Fluorescence intensity (MFI). qPCR analysis of mRNA expression under FECH knockdown (E) or NMPP treatment (F). Bar graphs indicate mean ± SEM, n=3. Representative results from three independent experiments. ns, non-significant, *p<0.05,

**p<0.01, ***p<0.001, ****p<0.0001, two-tailed unpaired Student’s t-test. Scale bars = 20 µm.

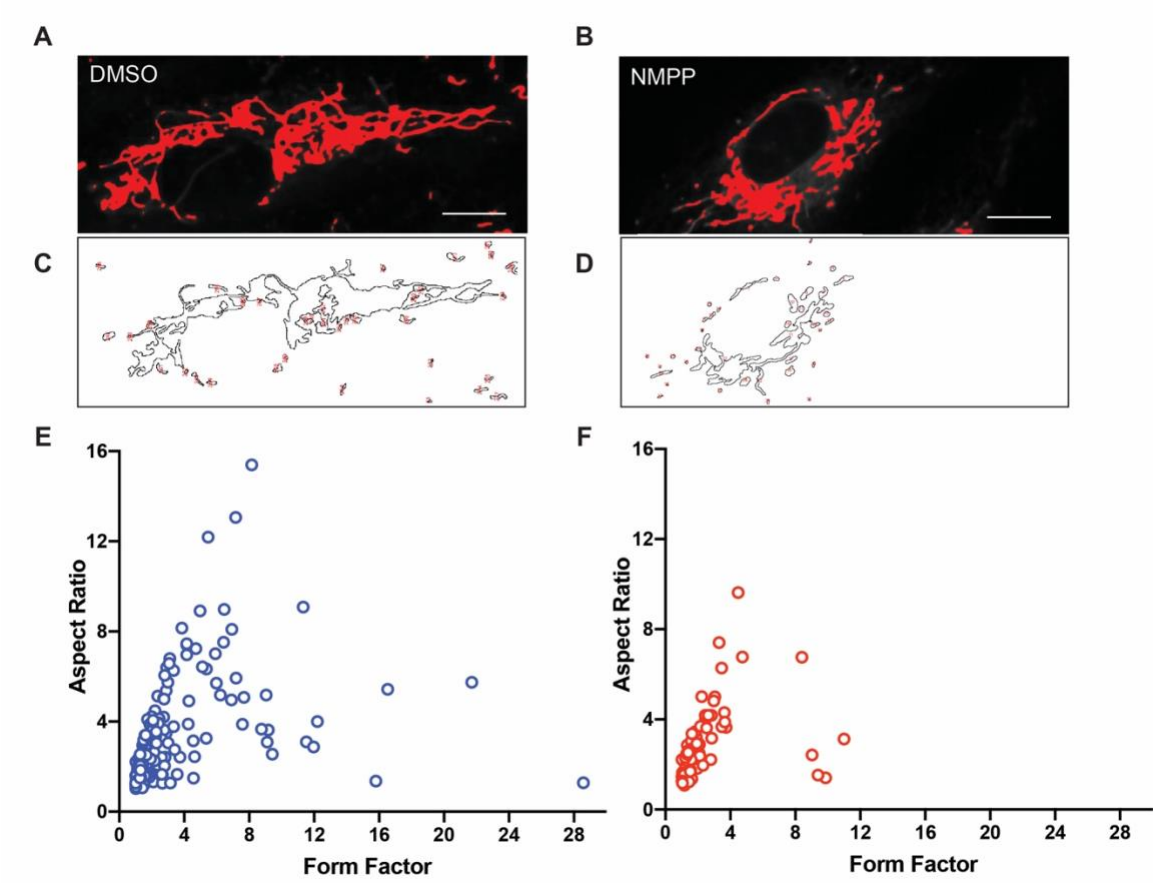

Figure 4.3. Morphometric analysis of mitochondria in HRECs (A-D) Representative HRECs depicting particle analysis for measuring mitochondria. (A, B) Representative slice from Z-stack images showing threshold intensity set for DMSO and NMPP treated HRECs. (C, D) Representative slice from Z-stack images showing outlines of assessed mitochondria. (E, F) Correlation of form factor versus aspect ratio under DMSO and NMPP treatments for the representative cells shown above. Scale bars = 10 µm.

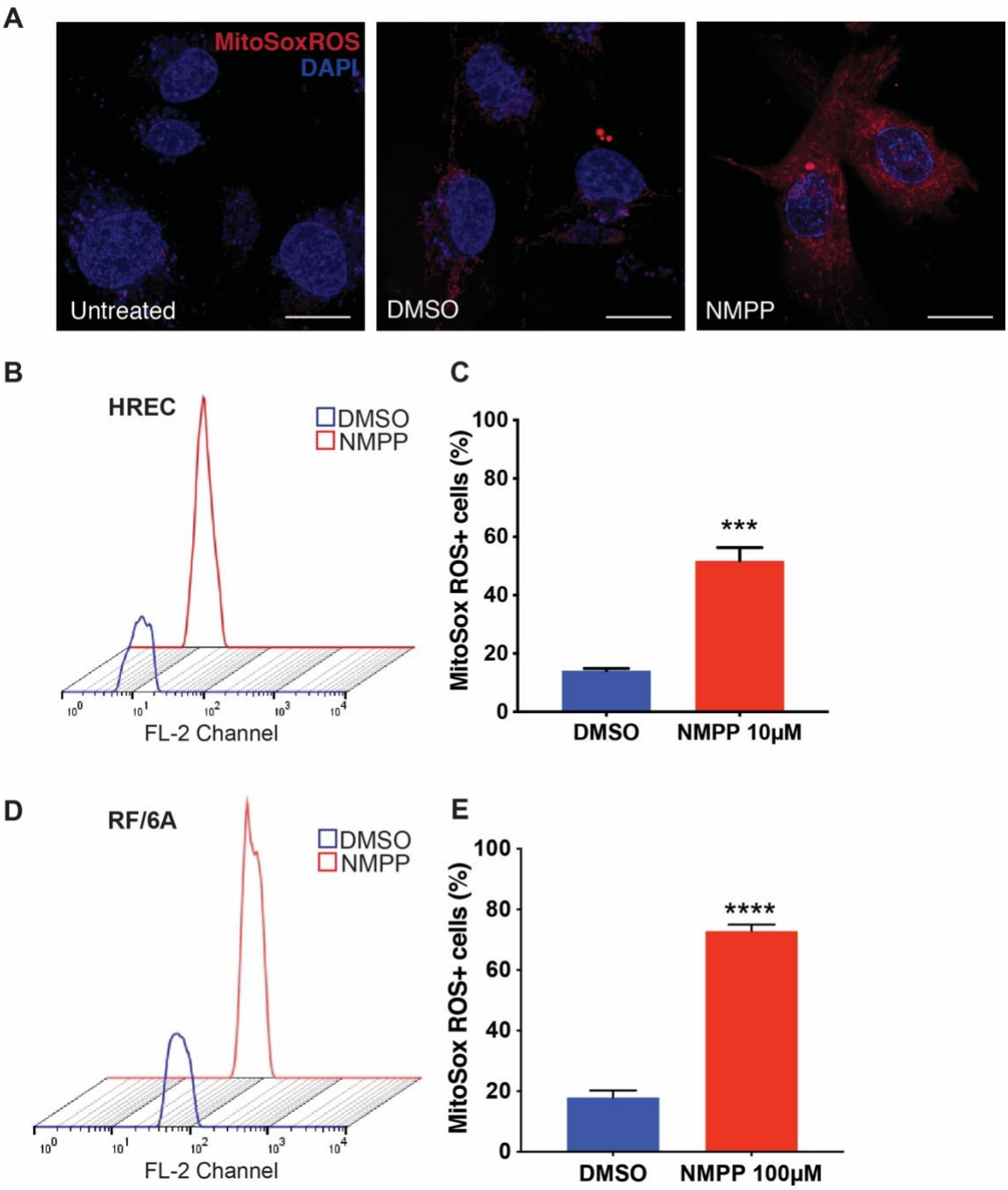

Figure 4.4. FECH inhibition elevated ROS levels in HRECs and RF/6A cells. (A) HRECs stained with mitoSox ROS in red and Hoechst staining in blue. (B) Representative fluorescence peaks as measured by flow cytometry followed by

(C) quantification of cells positive for red fluorescence. (D) RF/6A cells labeled with mitoSox ROS were assessed using flow cytometry. Representative fluorescence peaks. (E) Quantification of cells positive for red fluorescence. Bar graphs indicate mean ± SEM, n=3. Representative results from three independent experiments. ***p<0.001, ****p<0.0001, two-tailed unpaired Student's t-test. Scale bars = 20 μm.

4.3.2 Loss of FECH Depolarized Mitochondrial Membrane Potential

To assess mitochondrial health, I next measured membrane potential using JC-1, a polychromatic dye that on excitation forms red aggregates and green monomers depending on the energized or deenergized state of the mitochondria. Both siRNA mediated knockdown of FECH and chemical inhibition using NMPP induced loss of healthy red aggregates and an increase in monomers as seen by the green fluorescence (Figures 4.5A and 4.5D). This JC-1 excitation was quantified using flow cytometry on HRECs labeled with JC-1 dye, and showed reduced red to green fluorescence ratio, indicative of mitochondrial depolarization (Figures 4.5B, 4.5C, 4.5E and 4.5F). RF/6A cells also showed depolarized membrane potential after NMPP treatment (Figures 4.6A-C).

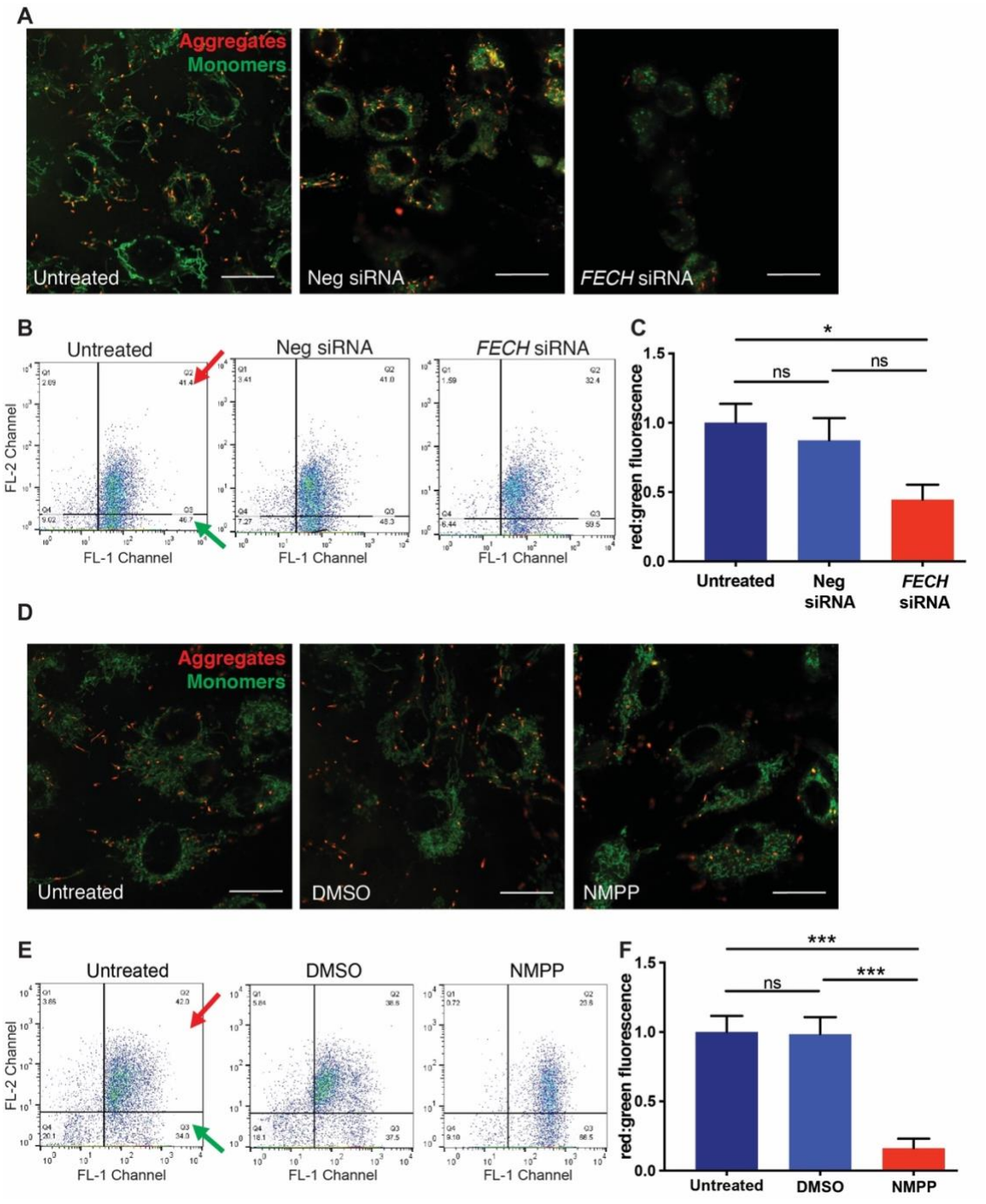

Figure 4.5. Loss of FECH reduced mitochondrial membrane potential in HRECs. (A) HRECs stained with JC-1 dye showing green monomers and red aggregates under FECH knockdown condition and (D) NMPP treatment. (B) Representative dot plots of FL1 versus FL2 channel from three individual experiments,

measuring red and green fluorescence using flow cytometry after FECH knockdown and (E) NMPP treatment. Red and green arrows indicate quadrants expressing FL1-red and FL2-green fluorescent cells. (C, F) Quantification of red:green fluorescence from flow experiment. *$p<0.05$ vs. untreated, one-way ANOVA with Tukey's post hoc tests. Bar graphs indicate mean ± SEM, n=3; Scale bars = 20 μm.

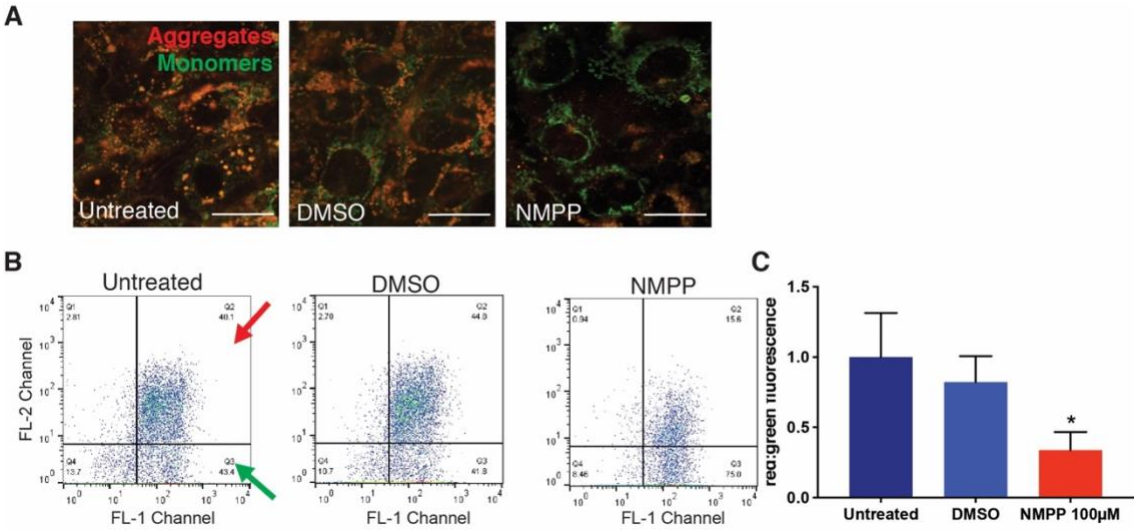

Figure 4.6. FECH blockade depolarized mitochondria in RF/6A cells. (A) RF/6A cells stained with JC-1 dye showing green monomers and red aggregates under NMPP treatment. (B) Representative dot plots of FL1 versus FL2 channel measuring red and green fluorescence using flow cytometry after NMPP treatment. Red and green arrows indicate quadrants expressing FL1-red and FL2-green fluorescent cells. (C) Quantification of red:green fluorescence from flow experiment. *$p<0.05$ vs. untreated, one-way ANOVA with Tukey's post hoc tests. Bar graphs indicate mean ± SEM, n=3; Scale bars = 20 μm.

4.3.3 Reduced COX IV Protein Expression and Activity Rescued by Hemin

To determine where heme depletion was influencing mitochondrial function, I evaluated protein complexes of the ETC after heme inhibition, as complexes II, III and IV contain heme in their prosthetic groups (Kim et al., 2012). FECH knockdown resulted in a significant decrease of only Complex IV protein levels (Figures 4.7A and 4.7B). NMPP treated cells showed a similar decrease in COX IV, and I also found increased expression in COXV ATP synthase upon treatment with this small molecule (Figures 4.7A and 4.7C). I then examined the heme containing subunit 1 of COX IV and found a significant decrease under both knockdown and NMPP treatment (Figures 4.7D-G). Enzyme activity of COX IV was also reduced, and total levels of the complex were significantly reduced after FECH blockade (Figures 4.7H-K). To confirm if these results were dependent on heme, I sought to rescue the phenotype of COX IV reduction by external supplementation of heme to the cells. Hemin, a stable form of heme, was able to alleviate COX IV protein expression and partially rescue COX IV enzyme activity (Figures 4.7L-N). RF/6A cells showed a similar rescue phenotype of COX IV enzyme after heme addition (Figures 4.8A-D).

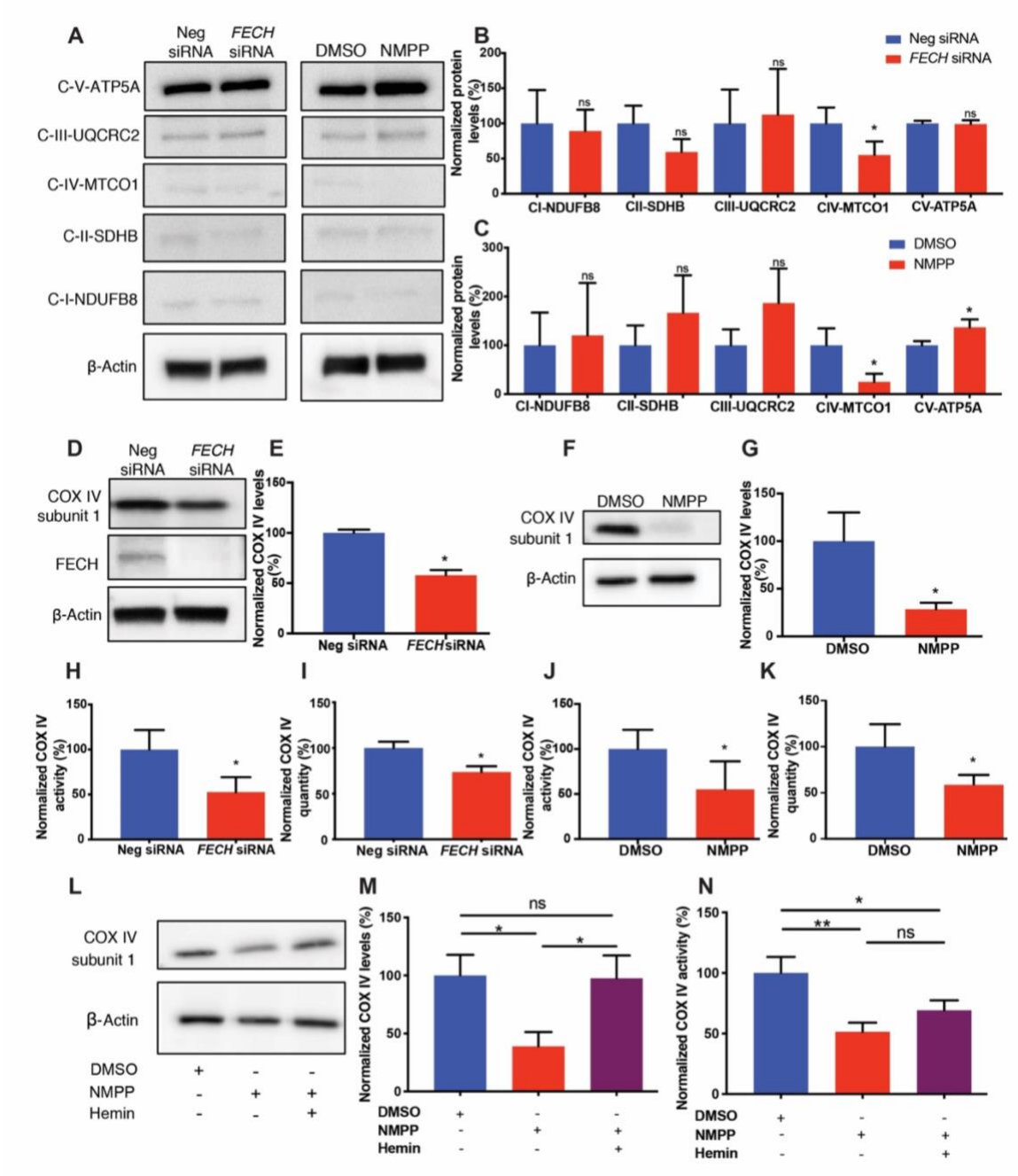

Figure 4.7. FECH inhibition caused reduced COX IV expression, rescued by hemin. (A) HRECs under FECH siRNA or NMPP treated conditions were immunoblotted for Complexes I-V as indicated. (B, C) Quantification of the blots was graphed as shown relative to appropriate control. (D) FECH siRNA treated HRECs were probed for COX IV subunit 1 and FECH along with housekeeping

control and (E) quantified. Similarly, HRECs treated with NMPP were blotted for COX IV subunit 1 (F) with (G) quantification as shown. COX IV enzyme activity was measured under FECH knockdown condition (H) and NMPP treatment (J) and total COX IV levels were quantified by ELISA for both the conditions (I, K). (L, M) COX IV protein expression and quantification under defined conditions. (N) COX IV enzyme activity was partially rescued in NMPP treated cells exposed to hemin. Immunoblot images representative from three independent experiments. Bar graphs indicate mean ± SEM, n=3-4; ns, non-significant, *$p<0.05$, **$p<0.01$. (B, C, E, G, H-K) unpaired Student's t-test (M, N) one-way ANOVA with Tukey's post hoc tests.

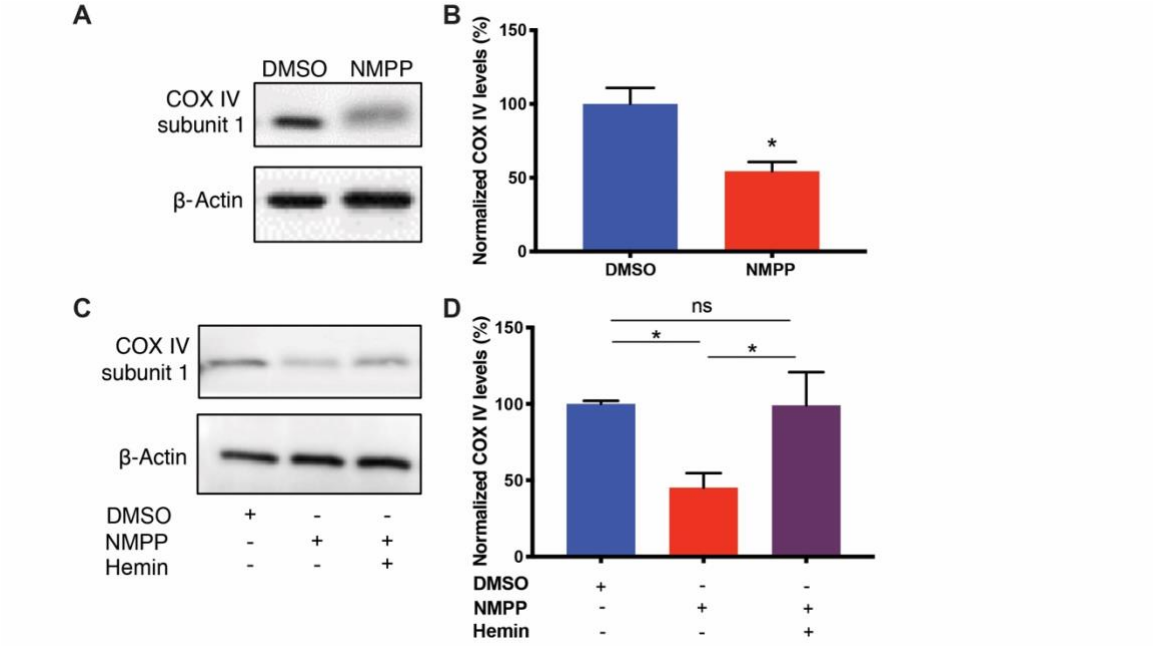

Figure 4.8. FECH inhibition decreases mitochondrial respiration and COX IV expression, which is rescued by hemin in RF/6A cells. (A) RF/6A cells treated with NMPP were blotted for COX IV subunit 1 with (B) quantification as shown. (C, D) RF/6A cells treated with 100 µM NMPP show rescue of COX IV protein levels after hemin supplementation. Bar graphs indicate mean ± SEM, n=3; *p<0.05, (B) unpaired Student's t-test; (D) one-way ANOVA with Tukey's post hoc tests.

4.3.4 FECH Blockade Reduced Mitochondrial Function of Retinal ECs

Based on the optimized parameters for bioenergetics of HRECs and RF/6A cells described in Chapter 3, I sought to understand whether loss of function of an important complex in the ETC resulted in defects in mitochondrial respiration. I measured OCR of HRECs after FECH knockdown and observed reduced basal respiration (Figures 4.9A, 4.9B). Uncoupler-induced maximal respiration was significantly decreased, with a marked reduction also found in OCR-linked ATP production and spare respiratory capacity (Figures 4.9C-E). Similarly, NMPP treated cells showed a dose dependent decrease in basal (Figure 4.9F and 4.9G) and maximal respiration (Figure 4.9H) along with a decline in OCR-linked ATP production and spare respiratory capacity (Figures 4.9I and 4.9J). I saw a similar decrease in mitochondrial respiratory activity in RF/6A cells (Figures 4.10A-E).

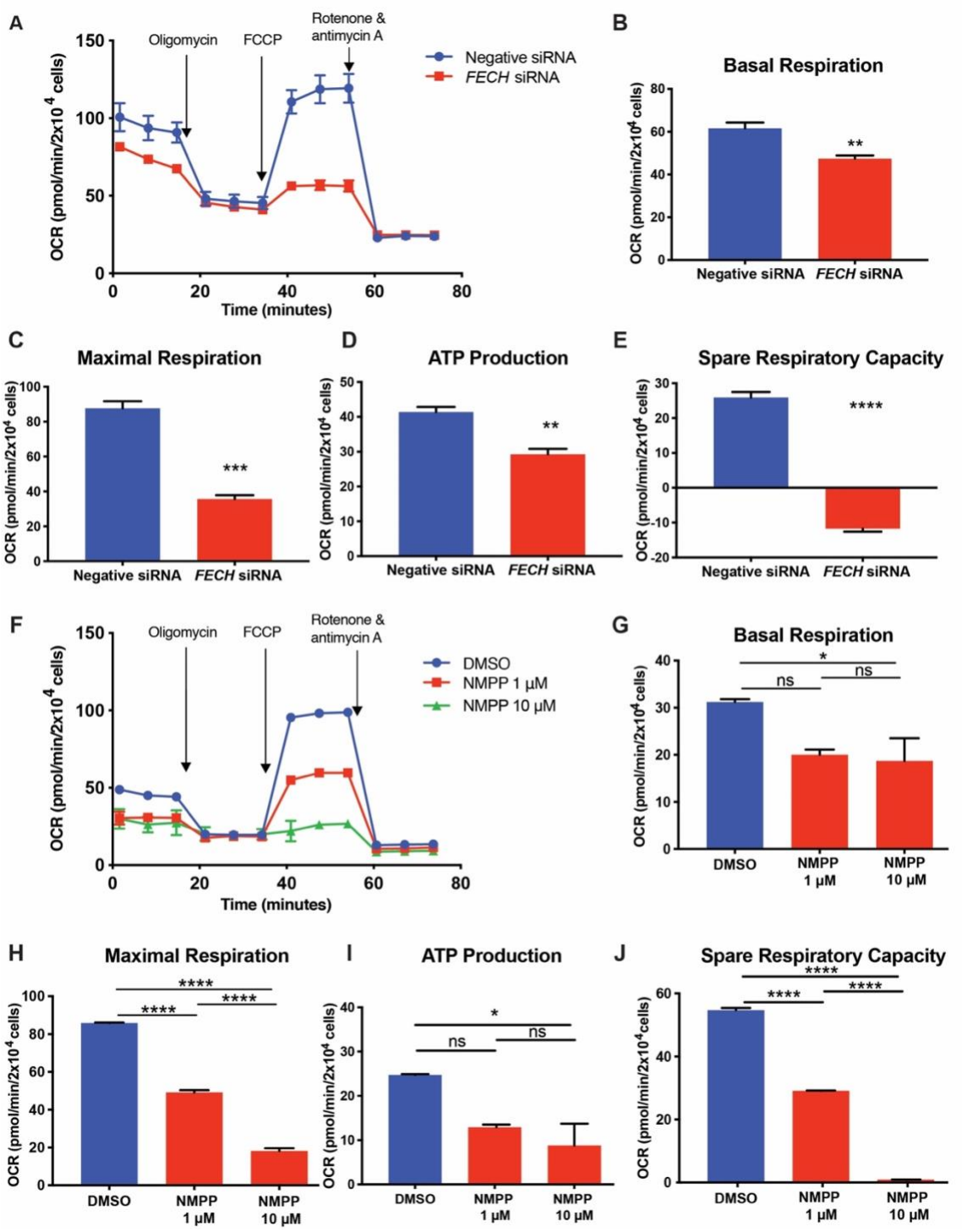

Figure 4.9. Loss of FECH reduced mitochondrial respiration in HRECs. (A, F) OCR kinetic traces for HRECs under FECH knockdown or NMPP chemical inhibition. (B, G) Basal respiration, (C, H) maximal respiration, (D, I) OCR-linked

ATP production, and (E, J) spare respiratory capacity were calculated based on OCR curves for the respective treatment group. (A, F) Representative OCR curve of three individual experiments. Bar graphs indicate mean ± SEM, n=3; *p<0.05, **p<0.01, ***p<0.001, ****p<0.0001 (B, C, D, E) unpaired Student's t-test (G, H, I, J) one-way ANOVA with Tukey's post hoc tests.

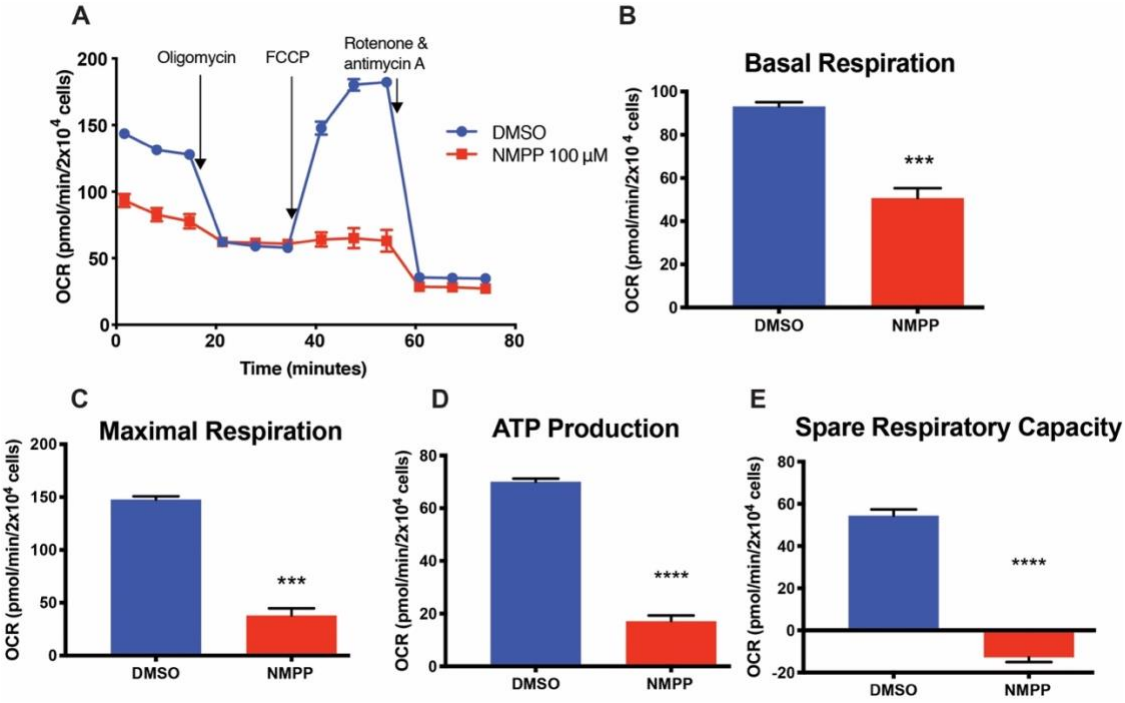

Figure 4.10. Reduced mitochondrial respiration in RF/6A after FECH inhibition. (A) Representative OCR kinetic traces for RF/6As under NMPP chemical inhibition. (B) Basal respiration, (C) maximal respiration, (D) OCR-linked ATP production, and (E) spare respiratory capacity were calculated based on OCR curves for the respective treatment group. Bar graphs indicate mean ± SEM, n=3; ***p<0.001, ****p<0.0001, unpaired Student's t-test.

4.3.5 Inhibition of FECH Led to Decreased Glycolytic Function

Microvascular ECs are highly glycolytic compared to other cell types (De Bock et al., 2013). As determined in Chapter 3, under mitochondrial stress, both HREC and RF/6A cells had increased glycolysis over mitochondrial respiration in our system (Figure 3.2, Chapter 3). Hence, I next investigated this key cellular energetic pathway in HRECs, by measuring changes in the pH of the extracellular medium. Cells were briefly starved in glucose deficient medium, followed by induction of glycolysis using a saturating dose of glucose. Interestingly, HRECs under siRNA mediated FECH knockdown and NMPP treatment each had decreased glycolytic capacity and glycolysis (Figures 4.11A-C, 4.11E-G). Both conditions depleted glycolytic reserve, as seen by a marked decrease in ECAR after 2-DG injection (Figures 4.11D, 4.11H).

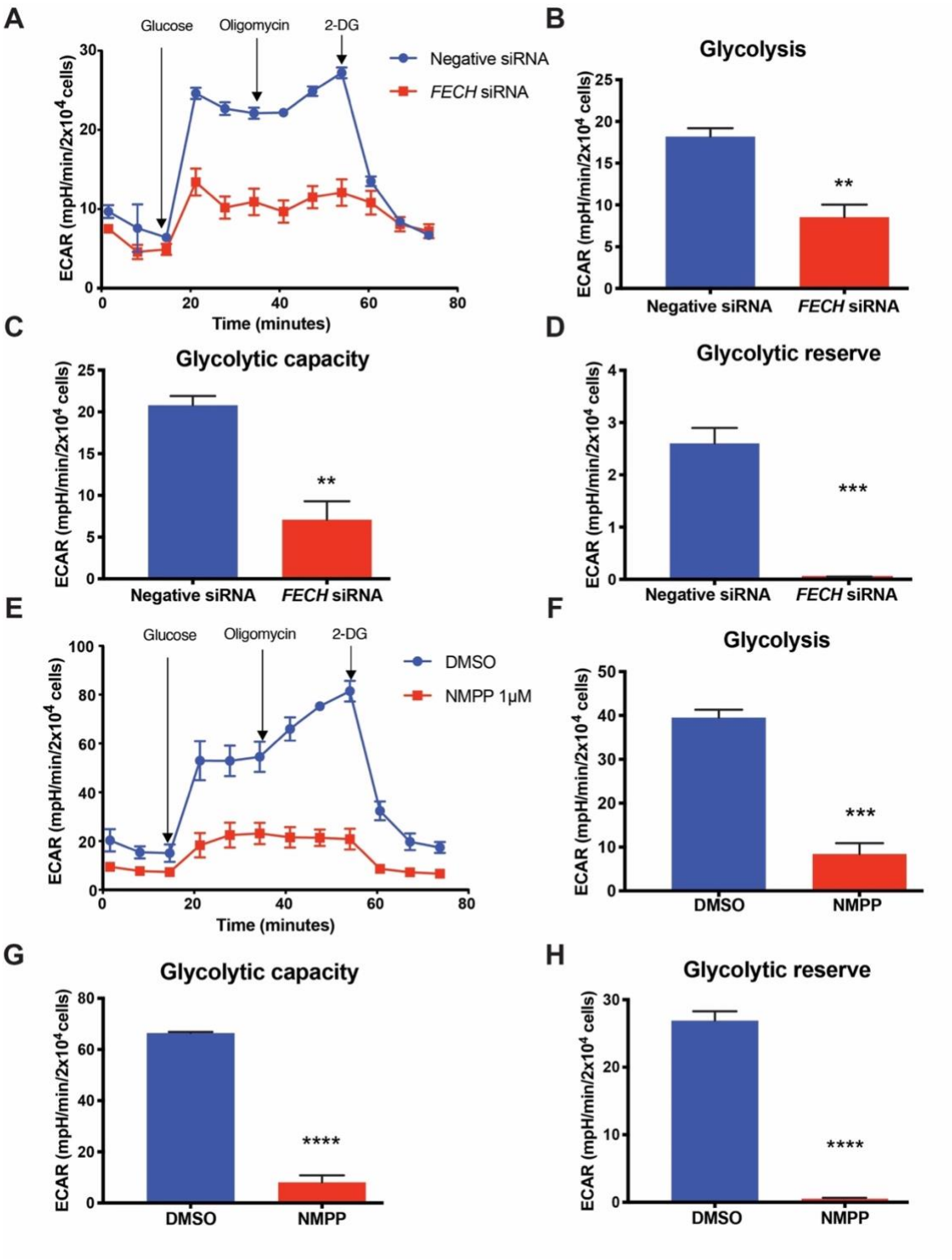

Figure 4.11. FECH inhibition caused a decrease in glycolytic function. (A, E) ECAR kinetic traces for HRECs under FECH knockdown or NMPP chemical inhibition. (B, F) Glycolysis, (C, G) glycolytic capacity, and (D, H) glycolytic

reserve were calculated based on ECAR curves for the respective treatment group. (A, E) Representative ECAR curve of three individual experiments. Bar graphs indicate mean ± SEM, n=3; **p<0.01, ***p<0.001, ****p<0.0001, unpaired Student’s t-test. 2-DG, 2-deoxyglucose.

4.3.6 FECH Inhibition In Vivo Caused Impaired Mitochondrial Energetics in Retina

I further determined if the effect of NMPP had the same phenotype in vivo in an intact eye. For this, we administered NMPP intravitreally to mice and measured OCR of retina in an ex vivo assay (Figure 4.12A). I found that retinas treated with NMPP had a significant decrease in basal respiration and a similar decline in maximal respiration (Figures 4.12B and 4.12C). Spare respiratory capacity was severely reduced in the retinas of NMPP treated animals compared to their vehicle treated counterparts (Figure 4.12D). I also observed about a 30% reduction in protein expression of COX IV in the NMPP-treated retinas (Figures 4.12E and 4.12F).

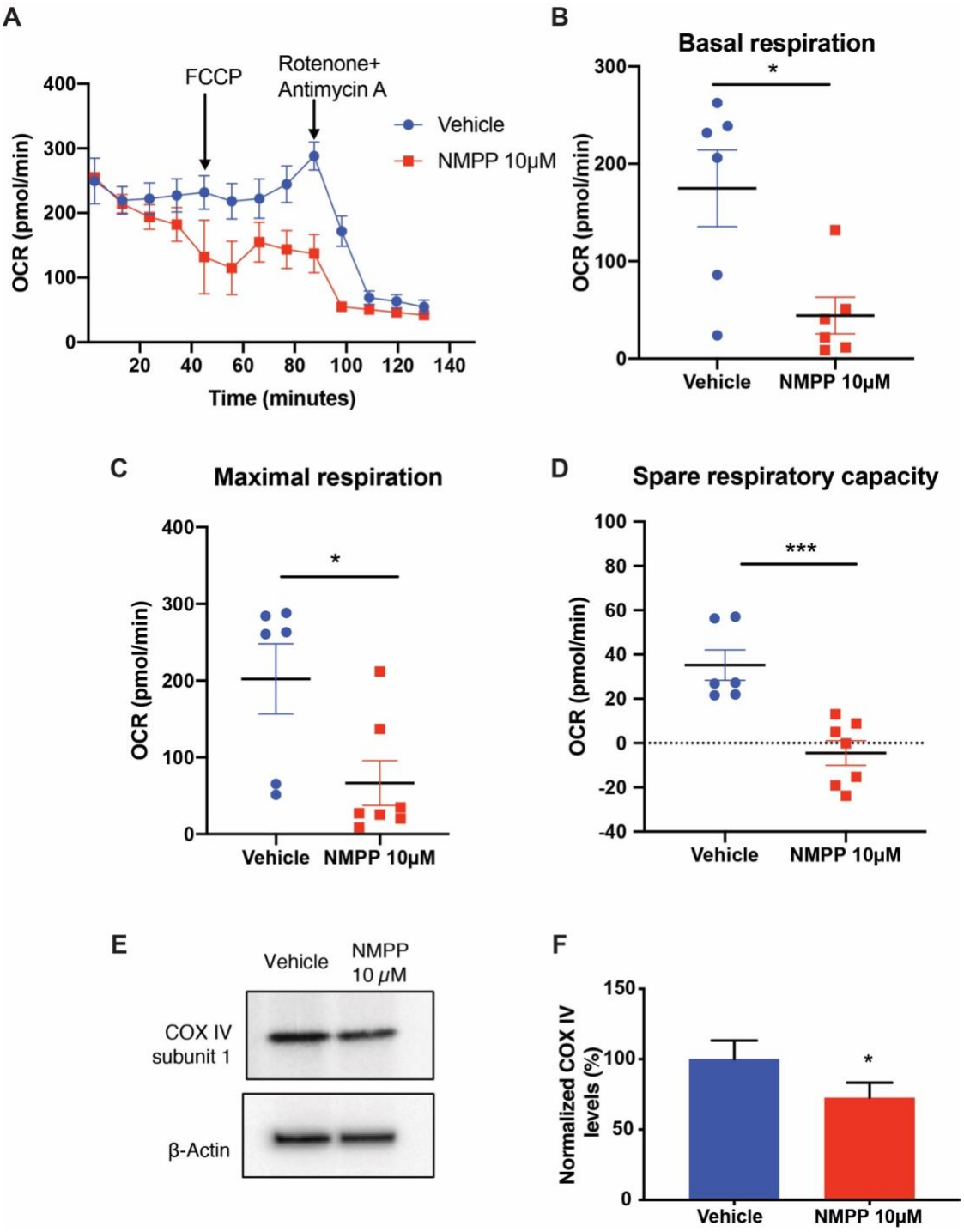

Figure 4.12. FECH inhibition in vivo decreased mitochondrial respiration in retina. (A) Representative OCR kinetic traces for retina from animals treated

with NMPP. (B) Basal respiration, (C) maximal respiration, and (D) spare respiratory capacity were calculated based on OCR curves for the respective treatment groups. (E, F) Immunoblot showing COX IV-1 protein expression from three pooled retinal tissue lysates from NMPP treated eyes and quantification. Graphs indicate mean ± SEM for two tissue punches from each retina per treatment group, n=6-7 per treatment condition. *$p<0.05$, ***$p<0.001$, unpaired Student's t-test.

4.4 Discussion

Heme synthesis blockade suppresses pathological angiogenesis by poorly understood mechanisms. In the present chapter, I sought to investigate the effects of heme inhibition on the mitochondrial function of retinal ECs, by directly studying heme-containing complexes of the ETC and documenting mitochondrial physiology under heme depletion.

The mitochondrial ETC is a major source of ROS induced by VEGF in hyperglycemic and hypoxic cellular environments (Cheng et al., 2011; Pearlstein et al., 2002; Wang et al., 2018). In PDR, increased mitochondrial ROS and impaired Ca^{2+} signaling can cause an increase in oxidative stress (Kowluru and Mishra, 2015; Pangare and Makino, 2012; Tang et al., 2014; Wang et al., 2018). Complex III of the ETC was recently shown to be important for umbilical vein EC respiration and thus proliferation during angiogenesis (Diebold et al., 2019). Mitochondrial dysfunction in the retinal pigment epithelium and photoreceptors have been reported for wet AMD (Barot et al., 2011; Lefevere et al., 2017), but evidence in retinal ECs is lacking. Metabolic factors like succinate and adenosine, generated from the Krebs cycle and ATP metabolism respectively, are proangiogenic for hypoxia-driven neovascularization (Sapieha et al., 2010). However, the exact mechanism of how metabolites disrupt mitochondrial energetics in ischemic retinal ECs remains unclear (Grant et al., 1999; Sapieha et al., 2008).

Mitochondrial dysfunction in ECs is, potentially, involved in pathological angiogenesis. Heme and heme-containing enzymes play a significant role in this

process, but the linkage between these phenomena has not been extensively explored. Serine synthesis deficiency induced heme depletion in ECs and caused decreased mitochondrial respiration and multiorgan angiogenic defects in animals (Vandekeere et al., 2018), while heme accumulation in ECs due to an altered heme exporter affects angiogenesis and causes endoplasmic reticulum stress (Petrillo et al., 2018). Apart from ECs, non-small cell lung carcinoma cells with elevated heme synthesis levels had increases in enzyme activities of the ETC. Increased production of heme was associated with increased migratory and invasive properties of these cells and xenograft tumors in mice (Sohoni et al., 2019). Here, I demonstrated that heme depletion by blockade of the terminal synthesis enzyme FECH led to defects in COX IV and ETC disruption (Figure 4.7). Retinal and choroidal ECs alike have increased mitochondrial specific oxidative stress, dysfunctional mitochondrial physiology and disruption of glycolysis as a result of these defects.

Changes to mitochondrial morphology can indicate alterations in mitochondrial dynamics and cellular function. My findings of reduced form factor and aspect ratio after FECH blockade indicate greater fragmentation and decreased length (Duraisamy et al., 2019; Picard et al., 2013). Further, reduced mitochondrial mass was evident by our flow cytometric analysis. The core components of the mitochondrial fusion proteins include MFN2 (outer membrane) and OPA1 (inner membrane) (Youle and Bliek 2012). FECH knockdown in HRECs reduced *MFN2* and *OPA1* transcript levels. Reduction of these mitochondrial fusion protein marker genes confirms a change in

mitochondrial dynamics. An increase in fragmented mitochondria also leads to increased ROS levels (Jezek et al., 2018), as confirmed by our results. Moreover, disruption of fusion proteins can also lead to an increase in ROS levels (Kim et al., 2018), as also evident in our cell model. Loss of membrane potential can lead to selective blockade of inner membrane fusion, while the fusion of outer membrane can still proceed even without the fusion of inner membrane (Westermann 2010). This could explain why I did not observe any change in fission gene *OPA1* expression in NMPP treated HRECs, but there was a decrease in *MFN2.* This effect is consistent with the smaller, fragmented mitochondria we observed, similar to those seen in diabetic mouse coronary ECs (Makino et al., 2010). It is possible that FECH knockdown, which causes a direct decrease in *FECH* transcription, is more deleterious to cells than a chemical inhibitor like NMPP that only blocks FECH activity while keeping gene expression intact. FECH constitutes the iron-sulfur cluster that functions independent of the FECH catalytic activity, however, the actual cluster function remains unclear (Dailey at al., 2000). While reduced heme biosynthesis can itself cause iron-sulfur cluster deficiency (Crooks et al., 2010), identifying a structural role to FECH could be interesting to explore in future studies. This would potentially explain the differential effect on inner membrane fusion gene *OPA1* between FECH knockdown versus NMPP treated cells.

Mitochondrial fission machinery includes DNML1 among other proteins, however, for a successful fission event, recruitment of DNML1 and subsequent phosphorylation is critical for the fission process (Youle and Bliek 2012).

Blockade of fusion and fission proteins often leads to fragmented mitochondria and have been implicated in several neurodegenerative and metabolic disorders (Liu et al., 2020). I did not observe any change in gene expression of *DNML1*, suggesting that heme deficiency selectively disrupts mitochondrial fusion, while fission remains unperturbed. Another important mitochondrial function is mitochondrial DNA (mtDNA) transcription of genes encoding complexes of the ETC. While it is clear that nuclear encoded genes like those involved in fusion are affected after heme depletion, effect on other genes was not investigated in the present study. FECH inhibition possibly leads to a compensatory overexpression of *COX4I1* (COX IV subunit 1) mRNA levels (data not shown), however a more thorough investigation to compare transcriptional alterations between mtDNA versus nuclear genome should be considered in future.

Inner mitochondrial membrane potential ($\Delta\Psi m$) was considerably decreased after FECH knockdown or NMPP treatment. This finding was explained by my result of reduced COX IV protein expression and activity, which might have collapsed the potential gradient and caused a reduced membrane potential. My mitochondrial energetics findings further support this result. A significant reduction in FCCP-induced maximal respiration indicates defective COX IV, which is unable to perform the role of electron transfer. Uncoupling brought on by FCCP causes the ETC to rely on COX IV to carry out oxidative phosphorylation by the free-flowing electrons (Dranka et al., 2011). Under FECH inhibition conditions, FCCP-induced maximal respiration was affected, indicating COX IV dysfunction due to heme loss.

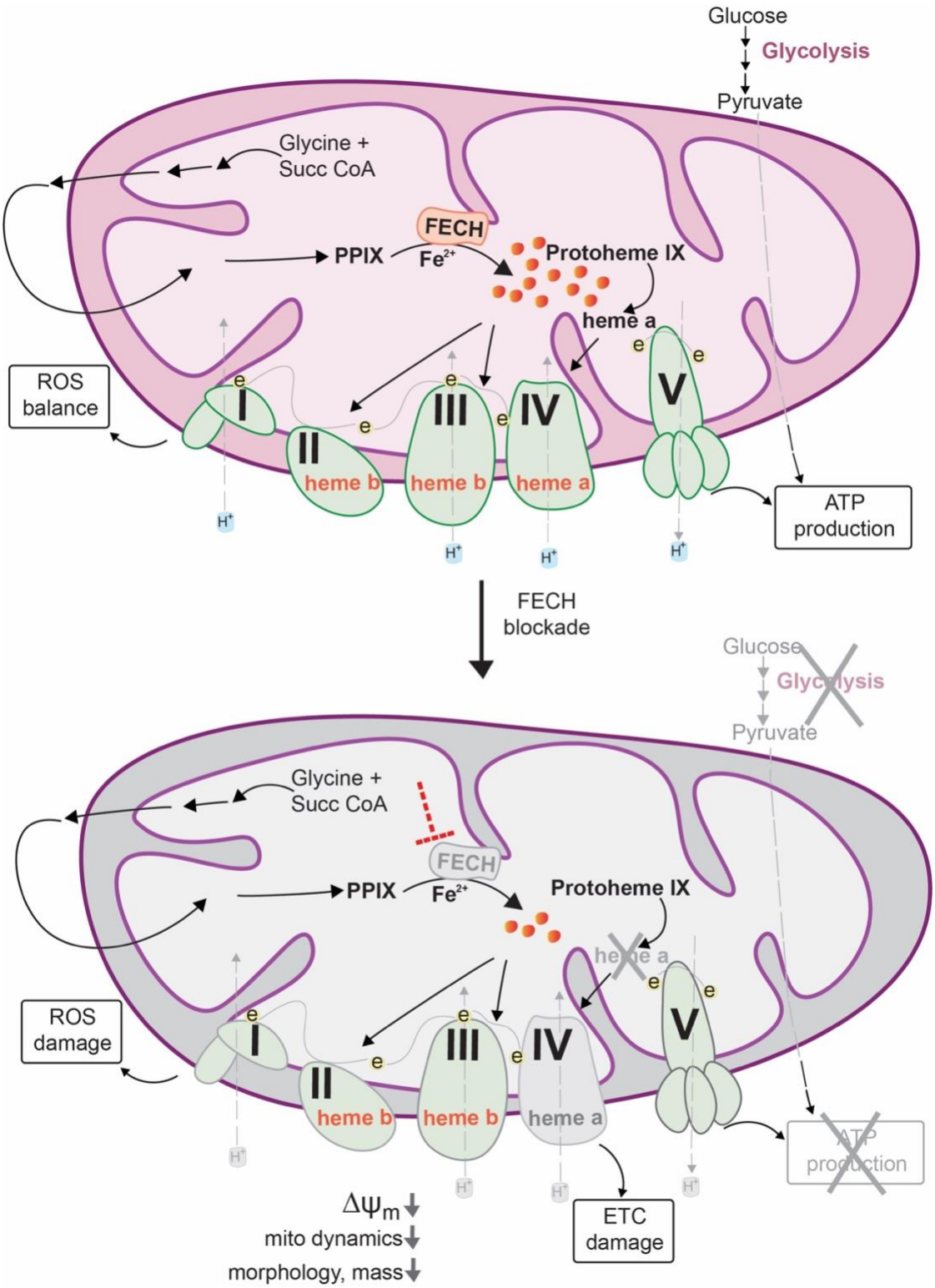
Glucose
Glycolysis
Pyruvate
Glycine +
Succ CoA
FECH
PPIX
Fe2+
Protoheme IX
heme a
ROS
balance
I
II
III
IV
V
heme b
heme b
heme a
ATP
production
FECH
blockade
Glucose
Glycolysis
Pyruvate
Glycine +
Succ CoA
FECH
PPIX
Fe2+
Protoheme IX
heme a
ROS
damage
I
II
III
IV
V
heme b
heme b
heme a
ATP
production
ETC
damage
Δψm
mito dynamics
morphology, mass

Figure 4.13. Schematic model of mitochondrial dysfunction on heme loss. Heme synthesis begins with the condensation of glycine and succinyl CoA in the mitochondrial matrix. The final step is the insertion of ferrous ion into protoporphyrin IX (PPIX) – catalyzed by ferrochelatase (FECH) to produce protoheme (also known as heme *b*). Protoheme and its derivatives are available for different cellular enzymes, including complexes of the electron transport chain (ETC, e = electrons). Heme *a* is synthesized by sub-hemylation steps, and utilized by COX IV for composition of the holoenzyme. Heme synthesis blockade by inhibiting the terminal synthesis enzyme FECH leads to COX IV defects and disrupts cellular energetics. Mitochondrial dynamics is altered with reduced fusion and mass, depolarized membrane potential ($\Delta\Psi m$) and elevated reactive oxygen species (ROS).

Heme depletion by directly blocking FECH primarily affected COX IV of all the other heme containing complexes of the ETC in ECs of the retina and choroid. COX IV subunit 1 contains heme *a* and *a3* (not found in complexes I-III and V). Heme *a* is made in a series of sub-synthesis hemylation steps carried out by heme *a* synthase and is essential for proper folding and stability of COX IV (Kim et al., 2012) (Figure 4.13). COX IV is particularly sensitive to FECH inhibition-induced heme depletion, possibly affecting the hemylation process downstream of protoheme synthesis, leading to a smaller pool of heme *a* (Atamna et al., 2001; Sinkler et al., 2017).

Recently, it was shown that complex III is essential for EC proliferation (but not migration) in macrovascular ECs. Conditional knockout of EC-specific complex III led to reduced retinal, lung and tumor neovascular blood vessels (Diebold et al., 2019). While it is possible that disruption of COX IV could in turn cause functional alterations in other complexes of the ETC, in our system I did not observe a significant change in protein expression of other complexes, including complex III. For this reason, I did not study individual enzymatic activities of complexes I-III and V. Although, it would be interesting to investigate whether heme depletion through FECH inhibition could result in loss of enzyme function of complexes I-III or V, even in the absence of protein level changes.

COX10 and COX15, proteins responsible for conversion of heme *b* (synthesized by FECH) to heme *a* were among the top-scoring genes that caused ETC disruption after heme depletion in acute myeloid leukemia cells (Lin et al., 2019), further suggesting the significance of heme *a* supply as a mediator

of mitochondrial function, since it is a prosthetic group specifically in COX IV holoenzyme. Furthermore, blocking the skeletal muscle specific COX 7a subunit of COX IV decreased mitochondrial ATP production in mouse hindlimb muscles. Interestingly, this was associated with reduced muscle angiogenesis and decreased capillarity (Lee et al., 2012), further supporting a link between COX IV and EC function.

Loss of functional COX IV was restored at least partially by extracellular heme supplementation. This suggests that the EC phenotype after FECH inhibition is heme dependent and not due to an off-target effect of NMPP or due to PPIX buildup/toxicity (Wyld et al., 1997). NMPP caused significant overexpression of complex V (not seen under FECH knockdown), which could be a secondary effect of damage to COX IV, causing compensatory upregulation of ATP synthase (Havlickova-Karbanova et al., 2012; Rolland et al., 2013). Our studies previously indicated effects of NMPP and FECH knockdown specific to ECs of retina, choroid, brain and umbilical vein, and we did not observe a similar anti-proliferative phenotype on FECH blockade in other ocular cell types of non-endothelial origin (Basavarajappa et al., 2017). However, the phenotype of FECH deficiency on ETC complexes in other cell types beyond ECs would be an interesting aspect for future exploration.

CHAPTER 5. OCULAR PHENOTYPE OF PARTIAL LOSS-OF-FUNCTION FECH MUTANT MICE

5.1 Summary

Heme depletion, through inhibition of terminal synthesis enzyme FECH, blocks pathological angiogenesis by causing mitochondrial damage. We previously assessed ocular neovascularization in animal models of *Fech* loss. In vivo genetic and pharmacological inhibition of *Fech* intraocularly led to smaller neovascular lesions in the posterior mouse eye. We also confirmed this finding in mice with a partial loss-of-function *Fech* mutation (*Fech*^{m1Pas}). Biochemical and clinical features of *Fech*^{m1Pas} mice have been documented, where liver, bone marrow and spleen were examined. However, the ocular physiology of *Fech*^{m1Pas} mice, under normal conditions, have not been characterized. In the present chapter, I aimed to characterize the retinal phenotype of *Fech*^{m1Pas} mice.

We studied retinal vasculature of postnatal and adult mice. We assessed retinal parameters like mitochondrial bioenergetics, PPIX levels, visual activity and histology. We found that homozygous *Fech*^{m1Pas} mice had pronounced buildup of PPIX in the posterior eye with no damage to visual function and integrity of retinal layers. These findings provide a baseline retinal phenotype of *Fech* deficient mice and help characterize ocular abnormalities.

5.2 Background and Rationale

FECH catalyzes heme production in the mitochondria in the terminal step of the heme synthesis pathway (Dailey and Meissner, 2013). FECH inserts

reduced ferrous iron into PPIX to produce proto-heme IX. Loss of FECH activity, thus, leads to reduced heme production, accompanied by accumulation of substrate PPIX. Many intermediates of heme synthesis are porphyrins, known for diseases of porphyria caused due to defects in the synthesis pathway (Bonkovsky et al., 2013). In humans, diminished FECH activity is associated with erythropoietic protoporphyria (EPP), caused due to build-up of PPIX in erythrocytes. The main symptom of EPP includes photosensitization of skin due to PPIX phototoxicity, and in certain cases, mild anemia and liver damage (Rufenacht et al., 1998).

Fech$_{m1Pas}$ mice have a point mutation in the *Fech* gene, causing loss of *Fech* activity and PPIX accumulation. This autosomal recessive inherited defect in FECH is due to a T to A transversion mutation at nucleotide 293, resulting in a methionine to lysine substitution at position 98 of the Fech protein. This leads to reduced enzyme activity in heterozygous and homozygous mutant backgrounds, compared to wild-type mice. The mutation in the gene was first identified following a chemical mutagenesis experiment using ethylnitrosourea (ENU) during in-breeding of mice. ENU was injected into the male mice and following subsequent mating among littermates for a few generations, the mutation was determined to be transmitted as a Mendelian recessive trait. Heterozygous mutants are phenotypically normal and exhibit close to 65-70% *Fech* activity without any pathological abnormalities (Tutois et al., 1991). *Fech*$_{m1Pas}$ homozygotes, however, have less than 6-7% *Fech* activity. Often used as a mouse model for EPP, *Fech*$_{m1Pas}$ homozygous mice have been reported to

show photosensitivity and jaundiced liver (Abitbol et al., 2005). Mice with complete loss of *Fech* are embryonically lethal (Magness et al., 2002).

I previously described how FECH and thus heme is involved in neovascularization (Chapter 4). *Fech*^{m1Pas} mice, in the laser-induced choroidal neovascularization model, had angiogenic defects. *Fech*^{m1Pas} homozygous and heterozygous mice developed smaller neovascular lesions compared to WT group (Basavarajappa et al., 2017). Acute inhibition of FECH using a chemical analog of PPIX, NMPP, showed that this anti-angiogenic effect was due to mitochondrial dysfunction, as discussed in chapter 4.

The molecular mechanism studies underlying some of the pathological characteristics of FECH-deficient mice have been heavily focused towards EPP, liver diseases, and now pathological angiogenesis. However, the normal ocular phenotype of these mutant mice remains uncharacterized. While it is clear that *Fech* deficiency in mice produces smaller neovascular lesions, the normal retinal physiology of *Fech* mutants under non-angiogenic stimulus remains unclassified.

The objective of this chapter is to perform a thorough characterization of the ocular features of FECH-deficient mice and document any ocular abnormalities that are phenotypically distinct for the strain. We bred BALB/cJ *Fech*^{m1Pas} backcrossed with wild-type C57Bl/6 mice for five generations. We assessed retinal structure, PPIX, vasculature, visual activity and bioenergetic phenotypes of *Fech*^{m1Pas} homozygous, heterozygous and wild-type (WT) littermates. These parameters will provide a baseline phenotype, useful for manipulations in angiogenesis models. This will also enable differentiating

future experimental results under angiogenic pathology from inherent phenotype, that is distinct for the *Fech*$_{m1Pas}$ strain.

5.3 Results

5.3.1 *Fech*$_{m1Pas}$ Homozygotes Have Pronounced PPIX Buildup in The Retina

I evaluated retinal structure in vivo using optical coherence tomography and captured composite images of retinal layers from anesthetized mice. No abnormalities were found in the retinal structure (Figure 5.1A, 1B). Additionally, we assessed vascular leakage and performed fluorescein angiography. Retinal vessels showed no pathological signs of leakage (Figure 5.1C). In order to assess the presence of FECH substrate PPIX in the retinal vasculature, I evaluated fundi of littermates from WT, heterozygous and homozygous *Fech*$_{m1Pas}$ mice. PPIX fluorescence was detected in the retinal vasculature of adult *Fech*$_{m1Pas}$ homozygotes, with no PPIX buildup observed in WT and heterozygous animals (Figure 5.1D).

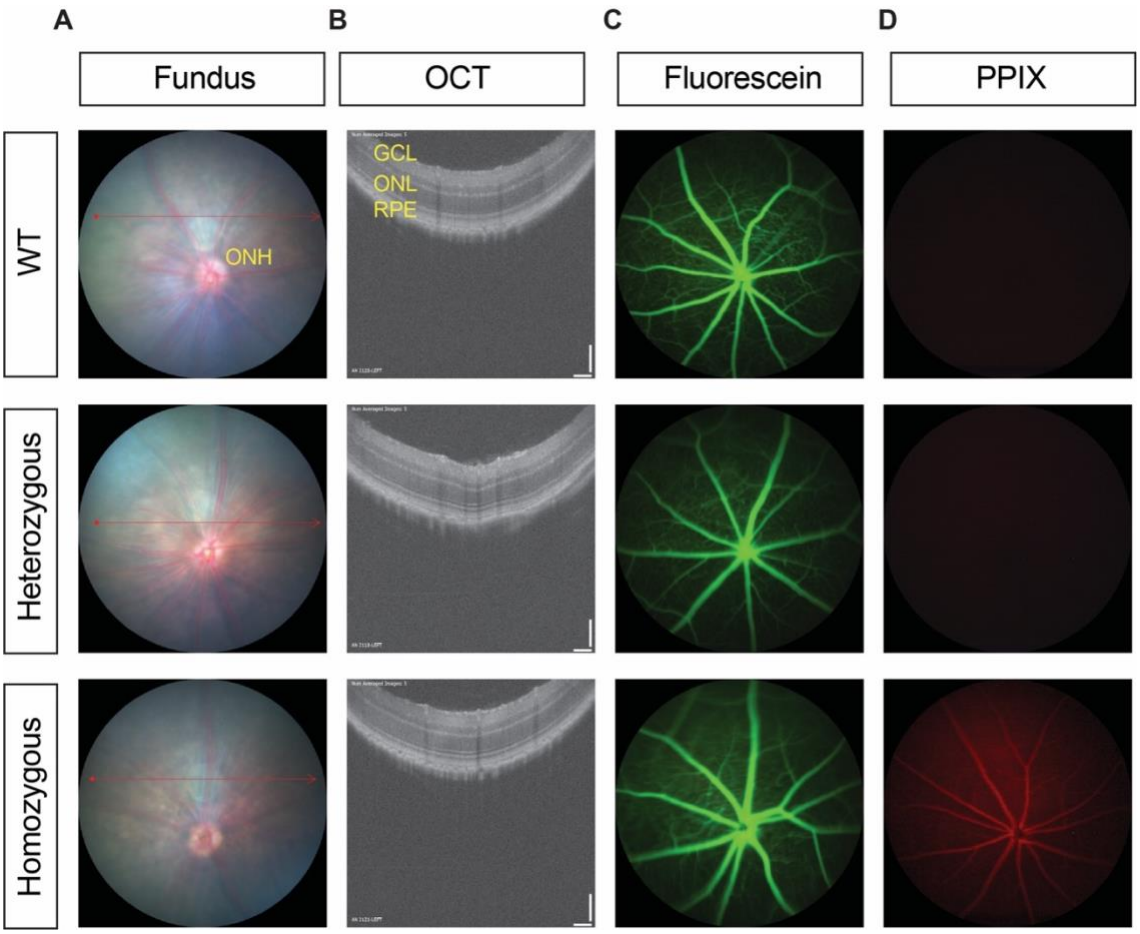

Figure 5.1. Retinal imaging of *Fech*$_{m1Pas}$ mice shows PPIX buildup. (A) Retinal fundus showing retinal vessels emerging from the optic disc. (B) Representative OCT images of sections in red arrows in the adjacent fundus images. (C) Representative images of fluorescein angiography. (D) Representative images of PPIX fluorescence. ONH = optic nerve head, GCL = ganglion cell layer, ONL = outer nuclear layer, RPE = retinal pigment epithelium. Figures A-D were generated with the assistance of Sheik Pran Babu Sardar Pasha.

5.3.2 *Fech*$_{m1Pas}$ mice Show No Abnormalities in Individual Retinal Layers

In order to assess damage to retinal tissue and individual retinal layers, I investigated hematoxylin and eosin (H&E) stained retinal sections of littermates from WT, heterozygous and homozygous *Fech*$_{m1Pas}$ mice. Qualitative analysis showed no morphological changes. Quantification of retinal thickness showed no signs of retinal thinning in all three genotypes (Figure 5.2A). We also counted individual nuclei in the ganglion cell layer, inner nuclear layer and outer nuclear layer. Thickness (in nuclei) of the respective layers did not show any changes between the littermates (Figures 5.2B-E).

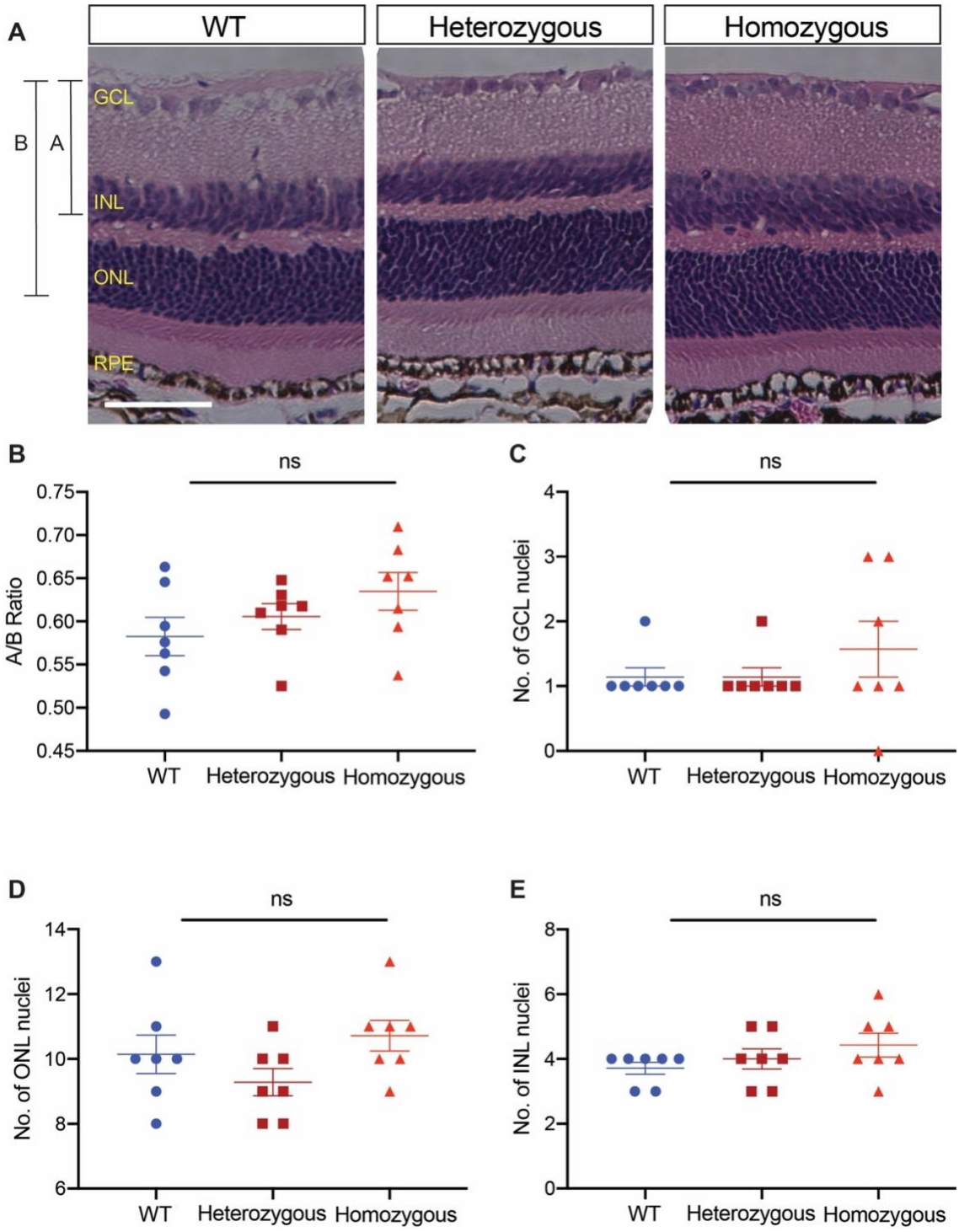

Figure 5.2. Individual retinal layers of *Fech*$_{m1Pas}$ mice are normal. (A) Representative images of H&E sections of the retina. (B) Quantification of the

A/B ratio as indicated. Quantification of the number of nuclei (thickness) in the (C) GCL (D) ONL and (E) INL. Analysis was performed with the assistance of Neeta Patwari. Mean ± SEM, n=7 eyes, one-way ANOVA, ns = not significant. Scale bar = 500 μm. GCL, ganglion cell layer; INL, inner nuclear layer; ONL, outer nuclear layer; RPE, retinal pigment epithelium. Figures B-E were generated with the assistance of Neeta Patwari.

5.3.3 Retinal Vasculature Indicates No Developmental and Physiological Changes

In order to assess any developmental defects in the retinal vasculature of *Fech*^{m1Pas} mice, I studied animals at postnatal day 3 (P3) and 8-week old retinas. Retinal vessels start growing from the optic disk at P0, spreading halfway across the inner retina by P4, and then reach the periphery by P7 (Fruttiger, 2002). Vasculature was stained at P3 and 8-weeks using isolectin B4 (Figure 5.3A) and imaged using confocal microscopy. P3 retinas from *Fech*^{m1Pas} mice did not show any signs of pathology after a qualitative assessment. Additionally, retinal flat mounts from 8-week old adult animals showed physiologically normal retinal vasculature (Figure 5.3B).

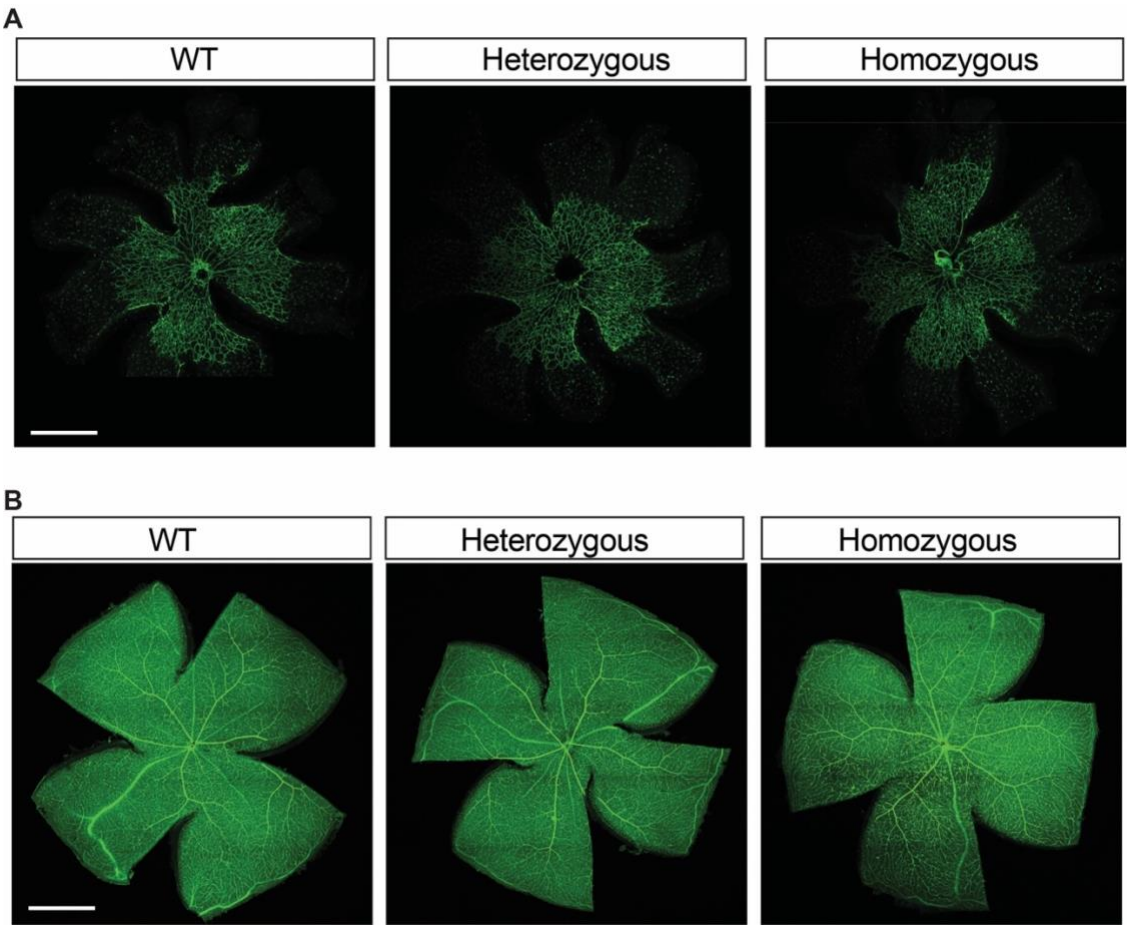

Figure 5.3. Retinal vessels indicate no developmental and physiological changes. (A) Representative images of retinal flatmounts from P3 mice and stained with isolectin B4 for vasculature in green. (B) Representative images of retinal flatmounts from 8-week old mice stained with isolectin B4. Scale bar = 1 mm. Figures A and B generated with the assistance of Sheik Pran Babu Sardar Pasha.

5.3.4 *Fech*^{m1Pas} Mice Had Comparable Visual Activity

Next, I evaluated the visual function of neural retina in *Fech*^{m1Pas} mice using electroretinogram. Dark-adapted mice were stimulated with light flashes and scotopic (rod) and photopic (cone) responses were recorded (Figure 5.4A). Scotopic a-wave corresponding to the activity of rod photoreceptor cells showed no changes in the three genotypic groups. Similarly, b-waves depicting bipolar cellular activity for both scotopic and photopic vision showed no defects in the three groups (Figures 5.4C-D).

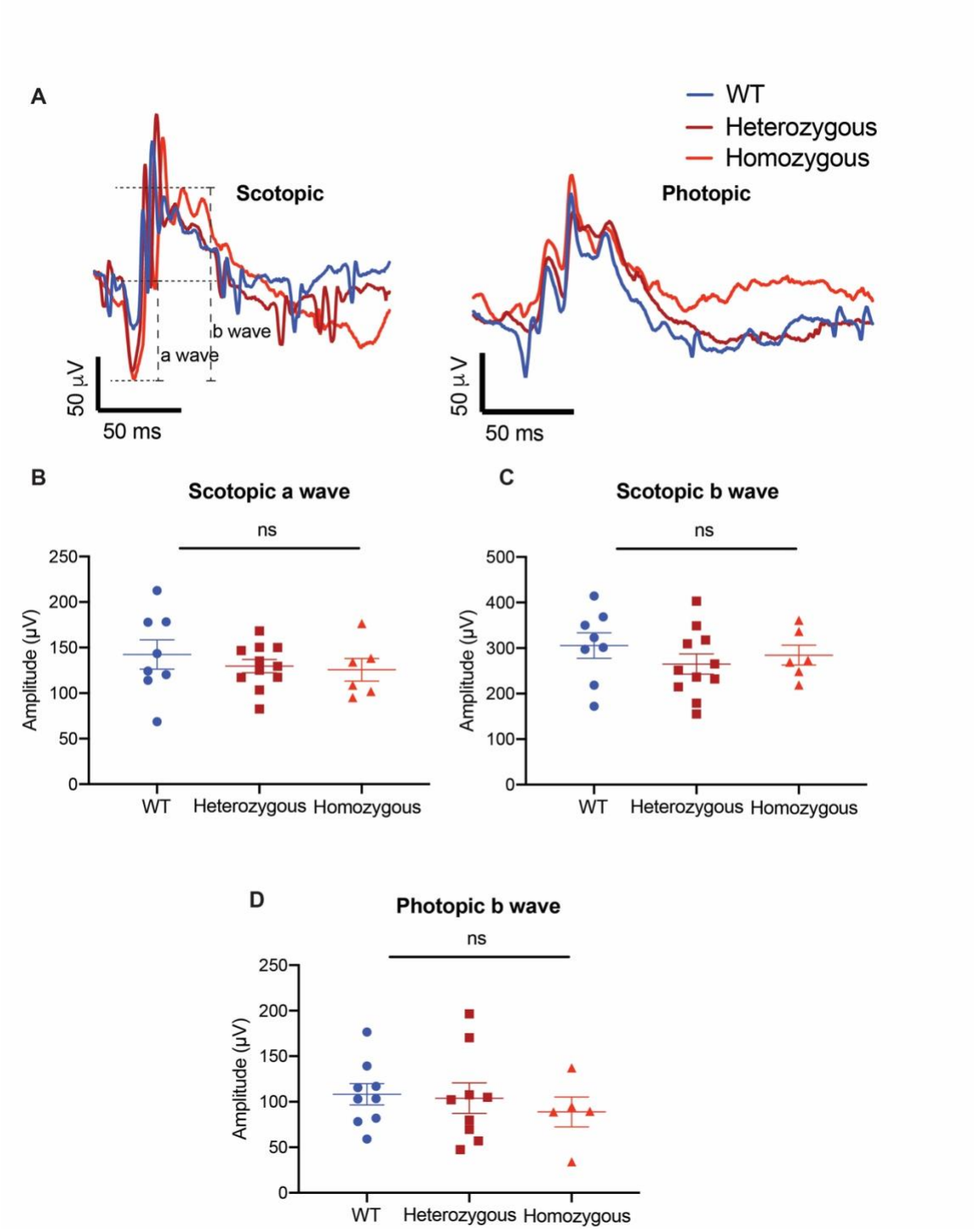

Figure 5.4. *Fech*$_{m1Pas}$ mice had comparable visual activity. (A) Representative mean ERG traces of dark-adapted mice. Quantification of (B) scotopic a wave (C) scotopic b wave and (D) Photopic b wave (stimulus: scotopic = 2.5, photopic

= 25 cd·s/m_2). Mean ± SEM, n=6-11 animals, each data point corresponds to mean of left and right eye, one-way ANOVA, ns = not significant.

5.3.5 Retinal Bioenergetics of *Fech*^{m1Pas} Mice Normal Among Littermates

Given the findings in Chapter 4, I further sought to characterize mitochondrial bioenergetics of retinal tissue punches from *Fech*^{m1Pas} mice and establish a baseline OCR of oxidative phosphorylation (Figure 5.5A). OCR corresponding to basal respiration showed comparable mitochondrial function in all the three genotypes (Figure 5.5B). FCCP uncoupler at 0.5 µM concentration was used to collapse the potential gradient and measure maximal activity of the ETC. There was no change observed in FCCP-induced maximal respiration in the littermates (Figure 5.5C). Similarly, OCR linked to spare respiratory capacity, as identified by rotenone and antimycin cocktail, showed no change between WT, heterozygous and homozygous *Fech*^{m1Pas} mice (Figure 5.5D).

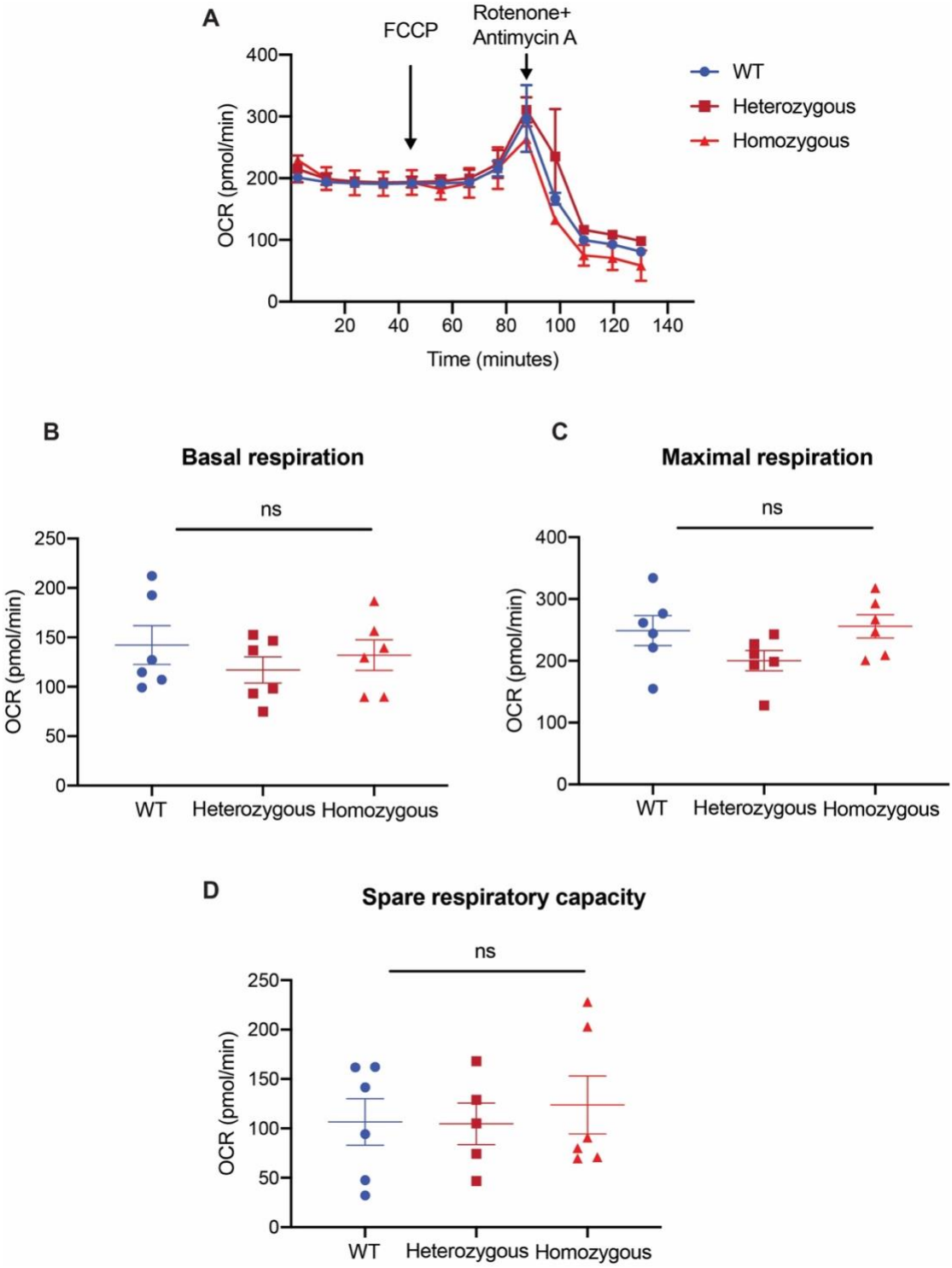

Figure 5.5. Retinal bioenergetics of *Fech*$_{m1Pas}$ mice are normal among littermates. (A) Representative OCR kinetic traces for retina from *Fech*$_{m1Pas}$

mice. (B) Basal respiration, (C) maximal respiration, and (D) spare respiratory capacity were calculated based on OCR curves for the respective treatment groups. Graphs indicate mean ± SEM for two tissue punches from each retina per group, n=6-7 per genotype, one-way ANOVA, ns = not significant. FCCP, carbonyl cyanide-4-(trifluoromethoxy)phenylhydrazone.

5.4 Discussion

Loss of FECH activity has been studied by many research groups documenting several physical abnormalities, however the role of deficient FECH activity in the ocular system remains obscure. We have strong evidence as depicted in chapter 3 and in prior publications, to suggest FECH plays an important role in ocular endothelial biology. In the first step towards providing a direct correlation between FECH and normal ocular angiogenesis in vivo, I studied the retinal phenotype of animals with loss-of-function FECH mutation. I characterized FECH substrate PPIX retinal levels, retinal morphology and structure, vasculature, visual activity and mitochondrial function.

The ENU mutagenesis approach to induce point mutations can be advantageous in identifying the gene and protein function and the downstream phenotypic effects caused due to partial or complete loss of function of the gene of interest (Justice et al., 1999). *Fech*$_{m1Pas}$ loss of function point mutation leads to deficiency in *Fech* activity, with mice homozygous for this mutation bearing less than 6% activity (Tutois et al., 1991). These *Fech*$_{m1Pas}$ display inherited EPP along with mild liver damage and photosensitivity (Boulechfar et al., 1993). Deficiency in FECH function leads to accumulation of substrate PPIX and a depletion in heme production (Brady and Lock, 1992). Using the properties of fluorescence in porphyrins I first confirmed this phenotype, by directly assessing PPIX levels in the eyes of *Fech*$_{m1Pas}$ mice. For the first time, we have demonstrated a method to assess PPIX in vivo, in live animals. This approach could potentially be scaled up clinically to assess retinas of EPP patients as

well. *Fech*$_{m1Pas}$ homozygotes show pronounced buildup of PPIX levels in the retina, with no indication of leakage from retinal vessels in 8-week old adult mice. Mice heterozygous for this mutation showed no detectable PPIX fluorescence in the retina, comparable to WT genotype. Heterozygous mutants show about 65% *Fech* activity, which possibly does not result in a significant PPIX buildup (Tutois et al., 1991). I have reported visual function of mice with a loss-of-function *Fech* mutation, that was previously undocumented. I did not find any abnormalities in the neural retinal activity, suggesting no defect in the physiological response to light stimuli and conduction of action potentials through the inner retina. Evaluation of the developing retina is limited for these parameters, as murine neonatal eyes only open in the second week after birth – rendering much live imaging unworkable.

Constitutive reduction of FECH activity did not result in an aberration to retinal mitochondrial oxidative phosphorylation, as seen with my results of mitochondrial bioenergetics. *Fech*$_{m1Pas}$ mice from BALB/cJ background show increased activity of respiratory ETC enzymes of complex I, III and IV in the liver. Additionally, no change was seen in the activity of mitochondrial complexes of the *Fech*$_{m1Pas}$ mice bred in the C57Bl/6J background (Navarro et al., 2005), supporting our finding in the retina. *Fech*$_{m1Pas}$ mice were backcrossed in the C57Bl/6J strain in my study, which may explain lack of any change in ETC function.

It is evident from the bioenergetic results described in Chapter 4, that acute inhibition of FECH results in a significant reduction of mitochondrial

respiration and COX IV levels. Thus, a constitutive decrease in *Fech* possibly masks a mitochondrial respiratory defect. Thus, I have validated and characterized mitochondrial respiration of *Fech*$_{m1Pas}$ murine retina, under normal physiological conditions and in the absence of angiogenic stimuli.

In order to study whether *Fech* deficiency led to changes in the development of retinal vessels in mice, I studied retinal vasculature from neonates at day 3. I observed no signs of aberrant vascularization in the developing retina. Adult retinas showed no signs of aberration in the vessels. Histologically, retinal layers in all three genotypes maintained normal morphology and structure. Nuclei counted in GCL, INL, and ONL were similar in all three genotypes, showing no signs of retinal thinning, degeneration or detachment of RPE. This further confirms my observations with ERG recordings, showing healthy retinal function. Thus, despite the reported phototoxicity of PPIX in vivo observed systemically (Libbrecht et al., 2003), *Fech*$_{m1Pas}$ mice showed normal retinal physiology, but with PPIX accumulation in the retinal vessels. Interestingly, a case report of an EPP patient showed development of idiopathic optic nerve atrophy caused due to vascular obstruction, and vision loss (Tsuboi et al., 2007). It is interesting to speculate whether PPIX buildup coincides with the atrophy in the fundus in this patient.

It is important to note however, that an inherent point mutation and further backcrossed breeding, may have contributed to metabolic compensation in the *Fech*$_{m1Pas}$ mice. Mouse models of metabolic disorders generated from spontaneous mutations, as in the case of *Fech*$_{m1Pas}$ mice, often make up for

reduced cellular activity in subsequent generations (Kennedy et al., 2010). The retinal structure, activity and vasculature were largely normal, even with the buildup of PPIX. Developmental angiogenesis is normal, as the adult animals show no abnormality in the vessels. However, pathological angiogenesis appears to be defective in *Fech*$_{m1Pas}$ heterozygotes and homozygotes (Basavarajappa et al., 2017). This raises an important question of whether the effect of FECH loss is exclusive to pathologically growing ECs in the vessels. In the absence of an angiogenesis stimulus, FECH deficiency does not seem to affect existing vasculature, which could be an advantage from a therapeutic perspective. These animals can be used as models of pathological angiogenesis – as preexisting vessels were found to be physiologically normal. In conclusion, while some hepatic and porphyrin-related defects are evident in this mouse model, it is still suitable for studies of retinal and choroidal neovascularization.

CHAPTER 6. DISCUSSION

6.1 Summary and Discussion

In the present chapter, I will highlight key results from Chapters 3, 4, and 5 and their significance in endothelial function and retinal physiology. To determine the mechanism of how heme synthesis is important for the process of angiogenesis, I first studied the metabolic energetics of ECs lining the retina and choroid. I **hypothesized that FECH is a mediator of pathological angiogenesis via altering mitochondrial function of endothelial cells.** In the first step towards addressing this hypothesis, I characterized mitochondrial respiration, ATP production, glycolysis, and thus, cellular energy phenotype of retinal and choroidal ECs – under normal culture conditions and under conditions of metabolic stress. Chapter 3 established for the first time the baseline bioenergetic profile of retinal and choroidal ECs and detailed optimized parameters that was used for designing all bioenergetic experiments of the thesis. Chapter 4 covered how FECH inhibition affected EC metabolic energetics and elaborated how key mitochondrial physiological processes were affected (Figure 6.1). Heme depletion due to FECH blockade directly affected the ETC by decreasing COX IV function. Finally, in chapter 5, I studied *Fech*-deficient mutant mice (*Fech*$_{m1Pas}$) and characterized their retinal physiology. This helped in understanding the contribution of *Fech* in vivo to developmental and adult vessel structure. *Fech*$_{m1Pas}$ mice had pronounced PPIX buildup with normal visual function, mitochondrial respiration and histology of retinal layers. Despite some limitations, my results identify a novel role of heme in the process of ocular angiogenesis and provide an exciting avenue to pursue future studies.

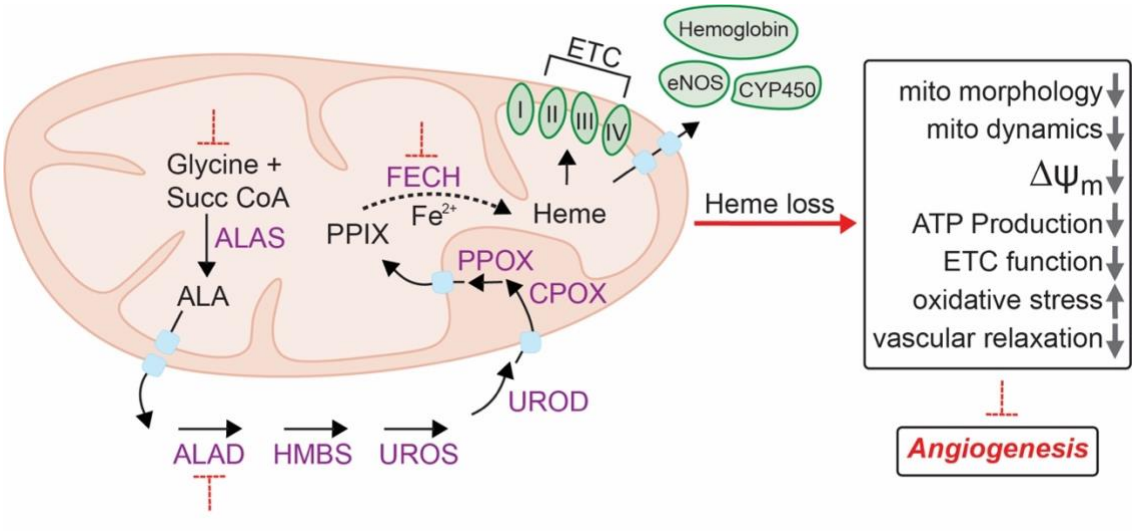

Figure 6.1. Schematic diagram of the heme synthesis pathway in the mitochondrion and effect of heme inhibition through intermediate enzymes. (Figure adapted from the following submitted manuscript: Shetty, T., and Corson, T.W. Mitochondrial heme synthesis enzymes as therapeutic targets in vascular diseases)

6.1.1 Heme and Endothelial Cells

Over five decades of heme discovery, and subsequent studies uncovering the synthesis pathway, has highlighted the contribution of heme to physiological cellular processes. However, our studies were the first to link heme directly to neovascularization in 2017. The Corson Lab first screened the effects of an anti-angiogenic small molecule derivative called cremastranone against retinal ECs (Lee et al., 2014). One of the cellular targets of cremastranone was identified as FECH. FECH is a mitochondrial enzyme responsible for inserting ferrous iron into PPIX in the final step of the heme biosynthesis pathway to produce heme (Figure 1). Our studies validating FECH inhibition, through chemical inhibition

and genetic knockdown approaches, found that heme depletion through blockade of the terminal catalyzing enzyme FECH, was anti-angiogenic to ECs in vitro and in animal models of neovascularization. Retinal and choroidal ECs showed significant reduction in angiogenesis-like properties like proliferation, migration, and tube formation. ECs showed reduced expressions of activated VEGFR-2 and heme-containing eNOS. These effects were exclusive to ocular endothelial cells and were not observed in ocular non-ECs like retinoblastoma Y-79, retinal pigment epithelium ARPE-19 and uveal melanoma 92-1 cells.

Fech inhibition in vivo in models of retinal and choroidal neovascularization resulted in fewer neovascular blood vessels compared to vehicle. *Fech*$_{m1Pas}$ homozygous mutants had reduced pathological angiogenesis compared to heterozygous mutants, and both genotypes had lower neovascular proliferation in comparison to wild-type animals. Significant overexpression of FECH was observed in neovascular tufts and regions of angiogenic vessels in the retina and choroid. A similar FECH overexpression was observed in human patient samples of wet-AMD when compared to age-matched healthy individuals (Basavarajappa et al., 2017). These results suggest that heme synthesis is crucial to the mechanism of pathological angiogenesis, however prior to the current work, the exact mechanism of how heme is essential to neovascularization in the eye remained unestablished.

6.1.2 Mitochondrial Physiology of Ocular Endothelial Cells

During mitochondrial respiration, oxidation of substrates is coupled to phosphorylation of ADP to ATP, termed as coupling efficiency (Toyabe et al., 2011). A leak in protons across the inner mitochondrial membrane can lower this coupling efficiency, resulting in incomplete utilization of oxygen and an overall reduced ATP production by ATP synthase. Under normal culture conditions, both retinal and choroidal ECs showed nearly 80% coupling efficiency, indicating a healthy state of the proton gradient maintained by the ETC complexes (Figure 5, Chapter 3). However, FECH inhibition resulted in depolarized membrane potential and reduced oxygen coupled ATP synthesis, indicating proton leak, a collapsed potential gradient and suggesting a dip in coupling efficiency. Thus, a sufficient supply of heme is needed for maintaining optimal coupling efficiency and healthy membrane potential for energy production. The loss of potential gradient of the ETC could also contribute to production of reactive oxygen radicals that can lead to oxidative stress (Zorov et al., 2014).

Retinal and choroidal ECs had a higher mitochondrion-coupled ATP production versus ATP produced through the glycolysis pathway (Figure 2, Chapter 3). Retinal and choroidal ECs had an ATP rate index of >1, indicating cellular ATP to be derived majorly from the mitochondria (Figure 3, Chapter 3). Nearly 70% of cellular ATP came from aerobic mitochondrial respiration, highlighting the significance of oxidative phosphorylation to EC metabolism,

even in the absence of an angiogenesis stimulus. On evaluating mitochondrial respiration after inhibition of heme synthesis, ECs had diminished mitochondrial respiration and low spare respiratory capacity. Additionally, FECH deficiency also resulted in a decline in the glycolysis pathway, leading to reduced glycolytic capacity and glycolytic reserve of ECs. During one cycle of ATP synthesis, glycolysis donates NADH to the ETC for electron transfer. It is possible that this could be due to a disrupted feedback loop between oxidative phosphorylation and glycolysis, both major sources of ATP for ECs (see below).

Loss of FECH activity decreases mitochondrial ATP production (Figure 4, Chapter 4), explaining why heme loss is anti-proliferative for microvascular ECs (Basavarajappa et al., 2017;Vandekeere et al., 2018). Reduced ATP could affect processes of proliferation and migration steps during angiogenesis. A shutdown of two major energetic pathways in the cell suggests a severe metabolic crisis. However, it would be interesting to investigate whether this results in an activation of other quiescence or stress-inducible metabolic factors and pathways like PGC1α, fatty acid oxidation, or amino acid degradation (Celotto et al., 2011). For instance, the TCA cycle donates succinyl-CoA, and heme synthesis is initiated with the condensation of succinyl-CoA and glycine. Thus, it is tempting to speculate that reduced heme synthesis can damage this system and in turn cause a decline in ETC and glycolysis mediated ATP production. However, heme depletion is not cytotoxic to ECs, and so it would be interesting to explore activation of alternative pathways like autophagy.

6.1.3 ETC Function After Heme Deficiency

In chapter 3, I documented the activity of the ETC of ECs and thus, mitochondrial function, by directly measuring oxygen consumption of ECs in real time, using an extracellular flux analyzer. Under metabolic stress, retinal ECs have an active mitochondrial respiration, while choroidal ECs are more glycolytic metabolically. I used this finding and studied ETC function in Chapter 4 under conditions of heme depletion through FECH blockade. After FECH inhibition, oxygen consumption by the ETC complexes was decreased in both retinal and choroidal ECs, and this resulted in a diminished oxidative phosphorylation of the ETC. Consistent with my results, recent work (Vandekeere et al., 2018) revealed that inhibition of the serine synthesis enzyme phosphoglycerate dehydrogenase (PHGDH) reduced glycine (substrate for the first step of the heme synthesis pathway), leading to an indirect decrease of heme enzymes and an eventual reduction in heme production in ECs. This also caused mitochondrial defects like reduced respiration, smaller mitochondria, increased fission, reduced fusion, and elevated mitophagy.

Vandekeere et al. also studied heme inhibition in macrovascular ECs by chemically blocking the second synthesis enzyme ALAD, and observed a decline in complex IV activity and ATP production coupled to oxygen consumption (Vandekeere et al., 2018). In another study performed on macrovascular ECs, it was found that endothelial tip cells are less glycolytic than non-tip cells and switch to mitochondrial activity during angiogenesis (Yetkin-Arik et al., 2019). Neonatal mice with silenced PHGDH had reduced retinal vascularization and

reduced vessel area in the brain, heart and kidney. Additionally, another group demonstrated that complex III is essential for EC proliferation (but not migration) in macrovascular ECs. Conditional knockout of EC-specific complex III led to reduced retinal, lung and tumor neovascular blood vessels (Diebold et al., 2019). The above-mentioned studies incorporate these in macrovascular ECs, in contrast to or studies in microvascular ECs of the retina and choroid. Furthermore, heme inhibition in macrovascular ECs via FECH blockade did not result in similar anti-angiogenic effects (Basavarajappa et al., 2017). The differential phenotypes of heme loss in microvasculature versus macrovasculature remain unclear and solicit further studies (Ghitescu and Robert, 2002; Sandoo et al., 2011).

Heme is an essential cofactor in the complexes of the ETC. Complexes II and III have hemes *b* and *c* respectively, whereas complex IV has two heme *a* groups (Kim et al., 2012). Subunit I of complex IV contains both groups of heme *a* and FECH inhibition in retinal ECs resulted in a decreased expression of COX IV subunit I specifically, with negligible effects on other complexes of the ETC (Figure 7, Chapter 4). This suggests that FECH loss particularly impacts heme *a* biosynthesis and thus the only heme *a* containing protein complex in aerobic organisms – complex IV. Heme *a* carries out electron transfer in the catalytic core of complex IV and also facilitates assembly of subsequent subunits into the COX IV multi-subunit complex (Hederstedt, 2012). Thus, heme depletion in ECs potentially leads to improper formation of COX IV subunits and may contribute to generation of reactive oxygen radicals due to a de-regulated ETC (Chapter 4).

RF/6A had slightly different energy needs than HRECs (Figures 5-6, Chapter 3), however RF/6A cells showed the same decrease in OCR-maximal respiration, spare respiratory capacity and loss of membrane potential on heme loss.

Fech$_{m1Pas}$ littermates have normal mitochondrial respiration, but it is possible that metabolic compensation is contributed by glycolysis or other energy pathways. Such an analysis of glycolytic capacity was not done in my study. It would be useful to examine levels of glucose uptake and serum levels of lactate, lipids and hepatic enzymes to understand metabolic factors compensating lack of *Fech* activity in the homozygous mutants. Adult *Fech*$_{m1Pas}$ cannot mount a sufficient angiogenic response (Basavarajappa et al., 2017), indicating insufficient energetic needs as one of the reasons for reduced neovascularization in the choroid. It would be interesting to profile the energetic state of ECs undergoing pathological angiogenesis, as in the Basavarajappa et al., study, by isolating microvascular ECs and assessing them in vitro. Another explanation for observing normal mitochondrial bioenergetics in *Fech*$_{m1Pas}$ mutants, is that energy demands possibly switch only after an angiogenic stimulus or insult. This explains why pre-existing vessels are normal in growth, but defective during neo-vessel formation. One way to study this would be to induce angiogenesis mimicking physiological conditions of either hypoxia, high glucose or injury to Bruch's membrane in *Fech*$_{m1Pas}$ mutants of 6-month age groups and then assess the energetics of ECs from these models.

6.1.4 Therapeutic Potential of Targeting Heme Synthesis in Neovascularization

Current therapeutic strategies targeting mitochondria involve key functions like mitochondrial division (Cassidy-Stone et al., 2008), ROS formation (Dhanasekaran et al., 2004), and metabolism (Mather et al., 2001; Csiszar et al., 2009) for age-related neurodegenerative diseases like Alzheimer's, Parkinson's, and Huntington's (Lane et al., 2015). Meanwhile, anti-VEGF therapies remain classic biologics used for neovascular diseases such as wet AMD, PDR, and multiple cancers (Jain, 2014). Until our and others' work described in this thesis, there was no rationale for targeting heme synthesis as neovascularization therapy. But given the specific antiproliferative effects of FECH blockade in microvascular ECs, FECH inhibitors like *N*-methyl protoporphyrin have demonstrated potential in targeting neovascular pathologies, both in vitro and in the OIR mouse model (Basavarajappa et al., 2017; Sardar Pasha and Corson, 2019). Novel, drug-like FECH inhibitors are also a possibility (Corson et al., 2019; Sishtla et al., 2019).

Repurposing existing drugs for pathological angiogenesis also holds promise towards this end. Griseofulvin, an FDA-approved anti-fungal drug, has a long-known off-target effect of FECH inhibition (Brady and Lock, 1992; Liu et al., 2015). It has anti-angiogenic effects in retinal ECs, blocking proliferation, migration and tube formation in vitro and reducing neovascularization in vivo comparable to intraocular anti-VEGF treatment, in both OIR and L-CNV mouse models (Basavarajappa et al., 2017; Sardar Pasha and Corson, 2019). Isoniazid,

an anti-mycobacterial drug, decreases FECH expression while upregulating ALAS1 (Brewer et al., 2019), and thus could be tested for potential anti-angiogenic activity in neovascularization models. Other inhibitors of heme synthesis used in vitro include succinylacetone and salicylic acid that block ALAD and FECH respectively (Giger and Meyer, 1983; Gupta et al., 2013), however their use in preclinical angiogenesis models remains to be investigated.

Targeting mitochondrial proteins directly involved in ETC activity has limitations as well, with a direct consequence on mitochondrial function. However, extracellular supplementation of hemin (a more stable form of heme) is able to normalize some of the mitochondrial physiology after FECH loss, like eNOS levels, complex IV activity, and ETC function (Basavarajappa et al., 2017; Vandekeere et al., 2018; Chapter 4). Effect of FECH blockade can be titrated, with a dose dependent decrease in angiogenesis features observed in animal models and ECs in culture. Homozygous *Fech*^{m1Pas} mice have significantly reduced neovascular lesions, compared to heterozygous *Fech*^{m1Pas} mice. And heterozygotes themselves have reduced lesions compared to wild-type (Basavarajappa et al., 2017), suggesting a window of FECH antiangiogenic effects without toxicity. However, complete loss of *Fech* and *Alas1* are embryonically lethal to mice (Magness et al., 2002; Chiabrando et al., 2014a), highlighting the importance of modulating heme inhibition carefully.

Oral supplementation of heme, while still achieving therapeutic antiangiogenic effects of inhibitors, could be considered (Luan et al., 2017). In order to limit systemic toxicity, it would be helpful to localize therapeutic

formulations to pathological tissue wherever possible. For example, in ocular neovascularization, therapeutic agents could be delivered through intravitreal or subretinal injection (Basavarajappa et al., 2017), or even as eyedrops if formulation allows; this is a promising area for future work. Therapeutic targeting specific to ECs could be included in drug delivery systems (Kawahara et al., 2013), since systemic deficiency in heme synthesis enzymes can lead to porphyria. For example, erythropoietic protoporphyria is caused by toxic buildup of PPIX (Gouya et al., 1999). The phototoxic PPIX can be detrimental to cells, and is manipulated in photodynamic therapy (PDT) (Krammer and Plaetzer, 2008). However, it is unlikely that PPIX itself mediates anti-angiogenic effects, as ALA-PDT relies heavily on uptake of ALA (Wachowska et al.). Moreover, as noted, hemin is able to rescue anti-angiogenic effects in ECs, even in the presence of PPIX build-up, suggesting that this mechanism is heme dependent and not due to PPIX toxicity.

6.2 Limitations

6.2.1 Cell Culture Models

Experiments in vascular endothelial cells, in vitro, are restricted by the use of primary cultures (except for RF/6A explained below). Primary cultures are beneficial to chart out phenotype closest to in vivo physiology. However, primary cultures permit use of cells only for a finite number of passages, owing to cellular senescence. Thus, design of studies involving stable knockdown using shRNA constructs are limited in retinal ECs. Furthermore, retinal ECs are hard to

transfect and transfection efficiency remains low in these primary microvascular cells. Thus, transient knockdown using siRNA approach was best suitable for my experimental set-up of FECH knockdowns. Transient expression of molecules meant optimizing knockdown levels to the same efficiency, every single time, to reproduce similar levels of heme synthesis depletion, and this introduced further technically laborious methods and potential variability in results. In addition, it is important to note that I used a universal negative control rather than a scrambled negative control of the *FECH* siRNA. Immortalization of endothelial cell lines is rare and often times, cells are found to lose key vascular molecular markers, suggesting loss of endothelial properties in culture (Stewart et al., 2011). In the case of the RF/6A choroidal endothelial cell line, these are immortalized cultures of non-human primate origin. Choroidal endothelial cells are technically challenging to isolate and characterize for experimental studies. Certain protocols require isolation directly from human donor eyes, which is an additional limiting factor. Moreover, during the course of my experimental studies in RF/6A, another research group demonstrated that RF/6A cells failed to exhibit significant distinguishing markers characteristic of ECs, and thus angiogenesis-related studies with these cells should be interpreted with caution (Makin et al., 2018). As an alternative, recently a study demonstrated immortalization of choroidal cells using an endothelial promoter driving genes required for immortalization, which could be considered for use (Giacalone et al., 2019). Additionally, choroidal cells can be isolated from bovine eyes.

FECH overexpression was not studied in the present study design, Transfection of a myc-tagged FECH construct in primary ECs were unsuccessful over several attempts during the course of my study (data not shown). Another limitation to consider is the use of ECs in isolation, and without the presence of governing factors, naturally present under physiological conditions. For instance, ECs of the neo-micro vessels are often covered by pericytes, whereas the larger macrovascular ECs contact smooth muscle cells. Studies suggest there is regulated interaction between pericytes and ECs during the steps of angiogenesis (Ribatti et al., 2011). Thus, a lack of true in vitro conditions that mimic vasculature in vivo is also a limiting factor in my studies.

6.2.2 Animal Models

As discussed in Chapter 5, complete knockout of *Fech* in mice is embryonically lethal. For this reason, I considered an acute exposure to NMPP, restricted to the eye with an intravitreal administration, for *Fech* inhibition in vivo in Chapter 4. Given the wide use of *Fech*^{m1Pas} mice as model organisms of porphyria, I employed use of *Fech*^{m1Pas} mice for later studies and sought to detail the ocular features of this model. Long-term aging studies were lacking in my studies, and additional time points of 6 months and/or 8 months, would be more correlative of aging neovascular diseases. It would be useful to generate an inducible *Fech* knockdown model. For example, transducing an endothelial-specific vector containing an shRNA *Fech* construct in a C57Bl/6 mouse, with an inducible promoter could be considered. This would address issues of metabolic

compensation and at the same time, allow studying direct consequences on retinal function in vivo. Furthermore, ex vivo approaches could be pursued using such a model, to further characterize molecular features of ECs during angiogenesis. Similarly, *Fech* overexpression plus PPIX supplementation, would also facilitate studies understanding the mitochondrial function in case of heme synthesis overdrive. Increased heme production might increase activities of ETC complexes, leading to increased ATP production and mitochondrial respiration. Mitochondrial biogenesis could also increase in response and mitochondria might potentially undergo increased fusion as a result of increased energetics. Furthermore, heme synthesis should be characterized in other models of angiogenesis currently used for neovascular studies. For example, laser-induced choroidal neovascularization and oxygen-induced retinopathy models should be studied to elucidate levels of heme, heme enzymes and ETC function.

6.2.3 Heme Blockade

Since heme is important in many different cellular processes, one important limitation of this work is introducing off target effects, due to the presence of many hemoproteins in the cell. This can interfere with the mitochondrial phenotype and becomes difficult to distinguish between effects exclusive to heme depletion versus off target effects. One way to overcome this would be to introduce small molecule inhibitors of heme enzymes (like NMPP), specifically targeting mitochondria (similar to siRNA), and thus minimizing cytosolic damage. This would also help clarify whether cytosolic hemoproteins

contribute to anti-glycolytic effects, and the regulation between mitochondrial metabolism and glycolysis due to heme. In contrast to reduced heme, excess of heme is also toxic to microvascular retinal ECs. Exposure to hemin for longer durations killed cells. Thus, experiments with hemin rescue in Chapter 4 were limited and complete rescue of COX IV activity levels was not observed, owing to hemin toxicity.

6.3 Future Directions

6.3.1 Role of Heme Metabolism in Glycolysis

Heme depletion significantly reduced glycolysis in retinal and choroidal ECs as described in Chapter 4. While it is possible that inhibition of oxidative phosphorylation resulted in a disruption of the glycolysis pathway, detailed analysis of how FECH blockade can influence glucose metabolism warrants further studies. Additional experiments characterizing glucose metabolism and glycolysis pathway after FECH inhibition or heme depletion are needed. Studies determining parameters like lactate production, C-labeled glucose uptake, GLUT-1 expression, NAD^+/NADH ratio, after FECH blockade can address this further. Furthermore, expression levels of glycolysis enzymes regulating different steps in the pathway like hexokinase, aldolase, phosphofructokinase, pyruvate dehydrogenase, directly after heme synthesis inhibition can also be examined.

Glyceraldehyde-3-phosphate (GAPDH) was recently demonstrated to be a heme-binding enzyme and acts as a chaperone for labile heme in the cytosol (Fleischhacker and Ragsdale, 2018; Sweeny et al., 2018). Disruption of this

heme-binding residue in GAPDH was found to reduce insertion of cytosolic heme into iNOS. It would be interesting to investigate whether a decrease in heme pool due to FECH blockade has a mechanistic link to glycolysis via the action of GAPDH. Is it possible that heme synthesis pathway and glycolysis pathway have an internal feedback inhibition in ECs? One way to answer this question would be to test activity of key heme enzymes like FECH, ALAS2 and heme-containing mitochondrial enzymes like complexes III and IV after introducing a heme-residue dead-GAPDH mutant construct in ECs. Additionally, GAPDH activity can be measured after blockade of heme synthesis via inhibition of FECH and ALAD. These experiments will potentially address links between heme, ETC and glycolysis and elaborate on the role of heme in cytosolic metabolism.

During angiogenesis, ECs are known to derive the majority of their ATP from glycolysis (Fitzgerald et al., 2018). However, EC tip cells have recently been reported to be less glycolytic during angiogenic cell differentiation (Yetkin-Arik et al., 2019). It would be interesting to induce angiogenesis in ECs in a 3D model, using VEGF-A as stimulus, and using $CD34_+$ as marker, and sort tip cells from non-tip cells. Additionally, energy phenotype (as described in Chapter 3) of these tip cells compared to non-tip cells should be determined. It is clear that heme contributes to both mitochondrial as well as glycolytic metabolism, hence it would be helpful to conduct these experiments under conditions of FECH knockdown or overexpression. This will directly address how heme synthesis facilitates energy generation in tip cells during the process of angiogenesis.

Another key enzyme related to heme is heme-oxygenase (HO-1 and HO-2), responsible for heme catabolism. Studies found some correlation between expression levels of HO isozymes and glycolysis enzyme phosphofructi-2-kinase (PFKFB4). Glucose deprivation in hepatocyte HepG2 and retinal pigment epithelium cells led to reduced expression of HO-1, HO-2 and PFKFB4 mRNAs (Li et al., 2012). HO-2 deficient mice were found to have reduced insulin and high glucose along with an impairment in endothelial function in the animals (Sodhi et al., 2009). It would be interesting to examine whether heme depletion negatively regulates HO-1/2 levels, and whether this in turn leads to a decrease in glycolysis through PFKFB4. Glucose metabolism in *Fech*$_{m1Pas}$ could also be studied to investigate whether *Fech* deficiency in vivo leads to defects in glycolysis and HO-1 metabolism. However, metabolic compensation in these mice, as seen in Chapter 5 for mitochondrial respiration, should be considered.

6.3.2 Heme Synthesis in Vasculogenesis

Chapters 4 and 5 provide detailed evidence of the contribution of heme in pathological angiogenesis in retinal and choroidal ECs. However, this brings in question the role of heme in tumor angiogenesis. Increased heme synthesis was found to contribute to increased tumorigenic properties of non-small cell lung carcinoma cells (Sohoni et al., 2019). However, how heme functions in postnatal vasculogenesis or in the process of tumor angiogenesis remains under-studied. Endothelial progenitor cells (EPCs) have been demonstrated to contribute to endothelium in tumors, and areas of revascularization in ischemia (Aghi and

Chiocca, 2005). Bone marrow-derived EPCs, the adult version of embryonic angioblasts, have been found to be mobilized by VEGF. Experimental studies show that bone marrow-derived EPCs are capable of forming blood vessels in vivo, to some extent. In a laser induced choroidal neovascularization model, GFP+ bone marrow cells were transplanted, before introducing laser injury. This led to contribution of nearly 50% of blood vessels by the bone marrow derived-EPCs in the choroidal vessels (Espinosa-Heidmann et al., 2005). Similarly, in a lung carcinoma tumor model, bone marrow transplant contributed to more than 80% of blood vessels in the tumors (Lyden et al., 2001). This raises an important question, does heme synthesis play a similar role, metabolically, in the functioning of EPCs similar to microvascular and macrovascular ECs?

HO-1 was found to induce an increase in the plasma levels of circulating EPCs in a mouse model of atherosclerosis (Wu et al., 2009). HO-1 knockout in diabetic mice caused a decline in EPCs and reduced the angiogenic potential of EPCs derived from these mice (Grochot-Przeczek et al., 2014). Interestingly, hemin induced neovascularization in vivo and was found to promote proliferation and endothelial gene expression in EPCs in culture (Wang et al., 2009). Considering these links between heme and EPCs, it would be interesting to study heme synthesis and elaborate on EPC metabolism. Studies on mitochondrial respiration and glycolytic pathway can be performed in EPCs after FECH knockdown, chemical inhibition, or in EPCs derived from bone marrow of *Fech*^{m1Pas} mice. Additional inhibitors like succinyl acetone can also be included, to create conditions of heme depletion. VEGFR2 expression along with

expression of angiogenesis signaling proteins can be measured. Furthermore, overexpression of FECH or ALAS2 in EPCs can be tested to investigate whether increased heme synthesis elevates angiogenic potential of EPCs in vitro or in vivo. Hemin can be formulated for delivery intraocularly, and injected in an oxygen-induced retinopathy model, to determine whether hemin induces revascularization of avascular regions commonly found in this model.

Similarly, tumorigenic cells can be examined for activity of heme and ETC enzymes. Additionally, FECH loss or mutation can be tested in tumor models like retinoblastoma, and mitochondrial function can be further examined.

6.3.3 Heme in Degradation Pathways

Another aspect, that studies detailed in this thesis do not cover, is the contribution of heme depletion to the activation of autophagy related pathways and damage to proteasomal degradation. While FECH inhibition in retinal ECs did not cause apoptosis (Basavarajappa et al., 2017), examination of autophagy was not done in the study. Severe damage to mitochondrial function including morphology, ETC activity, membrane potential can disrupt mitochondrial homeostasis leading to induction of autophagy. Heme depletion due to blockade of serine synthesis in ECs increased mitophagy by increasing expression of Parkin in the mitochondrial fractions (Vandekeere et al., 2018). Similar studies, after loss of heme in retinal ECs, and determining expression of proteins like LC3 and Parkin, will help address activation of the autophagy pathway (Mizushima, 2007).

Increased intracellular heme can lead to toxicity, and it has been demonstrated that acute heme levels, in the absence of HO-1, can activate the ubiquitin-proteasome system (UPS), to sequester heme into vacuoles for elimination (Vallelian et al., 2015). Interestingly, recent studies have found that both autophagy and proteasomal degradation systems are potentially linked, owing to crosstalk mechanisms (Lilienbaum, 2013). Thus, it would be interesting to explore, in case of reduced heme synthesis, whether there is an increase in autophagy-related proteins, and whether this leads to a shutdown of the UPS, in response. Furthermore, if reduced heme decreases HO-1 expression in the cells, this could also alter cues to the degradation systems and raise the question of how autophagy and UPS contribute to EC dysfunction.

6.3.4 Heme and Neurodegeneration

Heme may have some implications in neurodegenerative diseases and studies have shown a correlation between heme and mitochondrial damage in neurons. Deficiency of heme synthesis impairs neurite growth, and increases cell death of neuroblastoma cells, astrocytoma cells, and rat primary hippocampal neurons (Atamna et al., 2002; Zhu et al., 2002). Apart from reduced heme, excess heme is also toxic to neuronal health. After intracerebral hemorrhaging, hemoglobin and free-heme are exposed to surrounding tissues and cause activation of inflammation, lipid peroxidation, and neuronal apoptosis (Ma et al., 2016; Righy et al., 2016). Furthermore, a defect in heme sequestration damages myelination in mice, and defective heme export also decreases survival of

SHSY5Y neuronal cells (Chiabrando et al., 2016). Mitochondrial dysfunction in neurodegeneration includes defective calcium homeostasis, mtDNA transcription, mitophagy, apoptosis, dynamics and metabolism. For example, in case of Alzheimer's disease (AD), reduced heme synthesis was observed in temporal lobes of patients, as a result of amyloid-β binding to heme (Atamna and Frey, 2004; Atamna and Boyle, 2006).

Studies on heme and mitochondrial dysfunction in neuronal cells need to be done, as this remains an under-studied area. Does FECH blockade lead to reduced respiration, defective glycolysis and disruption of mitochondrial potential, dynamics and deformity in hippocampal and basal ganglia neurons? It would be beneficial to look for indicators of mitochondrial distress in Alzheimer's patient tissue sections using electron microscopy or immunohistochemistry. One critical challenge would be to evaluate whether heme synthesis inhibition drives AD pathogenesis. This could be examined by using small molecule heme inhibitors and by specifically targeting dopaminergic or hippocampal neurons. Neuroinflammatory markers like IBA-1 and GFAP can be determined in retinal sections of heme-deficient animal models.

In conclusion, my studies on heme and mitochondria inches one step closer to bridging the gap in heme and mitochondrial vascular biology. Implication of heme in the pathogenesis of neovascular and aging degenerative diseases is a novelty, that I hope will be explored in future studies to come. More importantly, my work has led to new and fetching questions, beyond the eye.

REFERENCES

Abitbol, M., Bernex, F., Puy, H., Jouault, H., Deybach, J.C., Guenet, J.L., and Montagutelli, X. (2005). A mouse model provides evidence that genetic background modulates anemia and liver injury in erythropoietic protoporphyria. *Am J Physiol Gastrointest Liver Physiol* 288**,** G1208-1216.

Aghi, M., and Chiocca, E.A. (2005). Contribution of bone marrow-derived cells to blood vessels in ischemic tissues and tumors. *Mol Ther* 12**,** 994-1005.

Aiello, L.P., Avery, R.L., Arrigg, P.G., Keyt, B.A., Jampel, H.D., Shah, S.T., Pasquale, L.R., Thieme, H., Iwamoto, M.A., Park, J.E., and Et Al. (1994). Vascular endothelial growth factor in ocular fluid of patients with diabetic retinopathy and other retinal disorders. *N Engl J Med* 331**,** 1480-1487.

Alizadeh, E., Mammadzada, P., and Andre, H. (2018). The Different Facades of Retinal and Choroidal Endothelial Cells in Response to Hypoxia. *Int J Mol Sci* 19.

Alonso, J.R., Cardellach, F., Lopez, S., Casademont, J., and Miro, O. (2003). Carbon monoxide specifically inhibits cytochrome c oxidase of human mitochondrial respiratory chain. *Pharmacol Toxicol* 93**,** 142-146.

Apte, R.S., Chen, D.S., and Ferrara, N. (2019). VEGF in Signaling and Disease: Beyond discovery and development. *Cell* 176**,** 1248-1264.

Atamna, H., and Boyle, K. (2006). Amyloid-beta peptide binds with heme to form a peroxidase: relationship to the cytopathologies of Alzheimer's disease. *Proc Natl Acad Sci U S A* 103**,** 3381-3386.

Atamna, H., and Frey, W.H., 2nd (2004). A role for heme in Alzheimer's disease: heme binds amyloid beta and has altered metabolism. *Proc Natl Acad Sci U S A* 101**,** 11153-11158.

Atamna, H., Killilea, D.W., Killilea, A.N., and Ames, B.N. (2002). Heme deficiency may be a factor in the mitochondrial and neuronal decay of aging. *Proc Natl Acad Sci U S A* 99**,** 14807-14812.

Atamna, H., Liu, J., and Ames, B.N. (2001). Heme deficiency selectively interrupts assembly of mitochondrial complex IV in human fibroblasts: revelance to aging. *J Biol Chem* 276**,** 48410-48416.

Austin, S., and St-Pierre, J. (2012). PGC1alpha and mitochondrial metabolism--emerging concepts and relevance in ageing and neurodegenerative disorders. *J Cell Sci* 125**,** 4963-4971.

Balogh, E., Veale, D.J., Mcgarry, T., Orr, C., Szekanecz, Z., Ng, C.T., Fearon, U., and Biniecka, M. (2018). Oxidative stress impairs energy metabolism in primary cells and synovial tissue of patients with rheumatoid arthritis. *Arthritis Res Ther* 20**,** 95.

Barot, M., Gokulgandhi, M.R., and Mitra, A.K. (2011). Mitochondrial dysfunction in retinal diseases. *Curr Eye Res* 36**,** 1069-1077.

Basavarajappa, H.D., Sulaiman, R.S., Qi, X., Shetty, T., Sheik Pran Babu, S., Sishtla, K.L., Lee, B., Quigley, J., Alkhairy, S., Briggs, C.M., Gupta, K., Tang, B., Shadmand, M., Grant, M.B., Boulton, M.E., Seo, S.Y., and Corson, T.W. (2017). Ferrochelatase is a therapeutic target for ocular neovascularization. *EMBO Mol Med* 9**,** 786-801.

Benchorin, G., Calton, M.A., Beaulieu, M.O., and Vollrath, D. (2017). Assessment of murine retinal function by electroretinography. *Bio Protoc* 7.

Bharadwaj, A.S., Appukuttan, B., Wilmarth, P.A., Pan, Y., Stempel, A.J., Chipps, T.J., Benedetti, E.E., Zamora, D.O., Choi, D., David, L.L., and Smith, J.R. (2013). Role of the retinal vascular endothelial cell in ocular disease. *Prog Retin Eye Res* 32**,** 102-180.

Bonkovsky, H.L., Guo, J.T., Hou, W., Li, T., Narang, T., and Thapar, M. (2013). Porphyrin and heme metabolism and the porphyrias. *Compr Physiol* 3**,** 365-401.

Bourque, S.L., Benjamin, C.D., Adams, M.A., and Nakatsu, K. (2010). Lack of hemodynamic effects after extended heme synthesis inhibition by succinylacetone in rats. *J Pharmacol Exp Ther* 333**,** 290-296.

Brady, A.M., and Lock, E.A. (1992). Inhibition of ferrochelatase and accumulation of porphyrins in mouse hepatocyte cultures exposed to porphyrinogenic chemicals. *Arch Toxicol* 66**,** 175-181.

Brewer, C.T., Yang, L., Edwards, A., Lu, Y., Low, J., Wu, J., Lee, R.E., and Chen, T. (2019). The Isoniazid metabolites hydrazine and pyridoxal isonicotinoyl hydrazone modulate heme biosynthesis. *Toxicol Sci* 168**,** 209-224.

Cabrera, A.P., Bhaskaran, A., Xu, J., Yang, X., Scott, H.A., Mohideen, U., and Ghosh, K. (2016). Senescence increases choroidal endothelial stiffness and susceptibility to complement injury: Implications for choriocapillaris loss in AMD. *Invest Ophthalmol Vis Sci* 57**,** 5910-5918.

Cai, J., Jiang, W.G., Grant, M.B., and Boulton, M. (2006). Pigment epithelium-derived factor inhibits angiogenesis via regulated intracellular proteolysis of vascular endothelial growth factor receptor 1. *J Biol Chem* 281**,** 3604-3613.

Campochiaro, P.A. (1999). The pathogenesis of age-related macular degeneration. *Mol Vis* 5**,** 24.

Campochiaro, P.A. (2000). Retinal and choroidal neovascularization. *J Cell Physiol* 184**,** 301-310.

Campochiaro, P.A. (2013). Ocular neovascularization. *J Mol Med (Berl)* 91**,** 311-321.

Carmeliet, P. (2003). Angiogenesis in health and disease. *Nat Med* 9**,** 653-660.

Carmeliet, P., and Jain, R.K. (2011). Molecular mechanisms and clinical applications of angiogenesis. *Nature* 473**,** 298-307.

Cassidy-Stone, A., Chipuk, J.E., Ingerman, E., Song, C., Yoo, C., Kuwana, T., Kurth, M.J., Shaw, J.T., Hinshaw, J.E., Green, D.R., and Nunnari, J. (2008). Chemical inhibition of the mitochondrial division dynamin reveals its role in Bax/Bak-dependent mitochondrial outer membrane permeabilization. *Dev Cell* 14**,** 193-204.

Cebe-Suarez, S., Zehnder-Fjallman, A., and Ballmer-Hofer, K. (2006). The role of VEGF receptors in angiogenesis; complex partnerships. *Cell Mol Life Sci* 63**,** 601-615.

Celotto, A.M., Chiu, W.K., Van Voorhies, W., and Palladino, M.J. (2011). Modes of metabolic compensation during mitochondrial disease using the Drosophila model of ATP6 dysfunction. *PLoS One* 6**,** e25823.

Cheng, X., Siow, R.C., and Mann, G.E. (2011). Impaired redox signaling and antioxidant gene expression in endothelial cells in diabetes: a role for mitochondria and the nuclear factor-E2-related factor 2-Kelch-like ECH-associated protein 1 defense pathway. *Antioxid Redox Signal* 14**,** 469-487.

Chiabrando, D., Castori, M., Di Rocco, M., Ungelenk, M., Giesselmann, S., Di Capua, M., Madeo, A., Grammatico, P., Bartsch, S., Hubner, C.A., Altruda, F., Silengo, L., Tolosano, E., and Kurth, I. (2016). Mutations in the heme exporter FLVCR1 cause sensory neurodegeneration with loss of pain perception. *PLoS Genet* 12**,** e1006461.

Chiabrando, D., Mercurio, S., and Tolosano, E. (2014a). Heme and erythropoieis: more than a structural role. *Haematologica* 99**,** 973-983.

Chiabrando, D., Vinchi, F., Fiorito, V., Mercurio, S., and Tolosano, E. (2014b). Heme in pathophysiology: a matter of scavenging, metabolism and trafficking across cell membranes. *Front Pharmacol* 5**,** 61.

Chung, A.S., and Ferrara, N. (2011). Developmental and pathological angiogenesis. *Annu Rev Cell Dev Biol* 27**,** 563-584.

Correia, M.A., Sinclair, P.R., and De Matteis, F. (2011). Cytochrome P450 regulation: the interplay between its heme and apoprotein moieties in synthesis, assembly, repair, and disposal. *Drug Metab Rev* 43**,** 1-26.

Corson, T.W., Seo, S.Y., Lee, B., and Sishtla, K. (2019). Ferrochelatase inhibitors and methods of use. PCT/US19/29909.

Crooks, D.R., Ghosh, M.C., Haller, R.G., Tong, W.H., and Rouault, T.A. (2010). Posttranslational stability of the heme biosynthetic enzyme ferrochelatase is dependent on iron availability and intact iron-sulfur cluster assembly machinery. *Blood* 115**,** 860-869.

Cryotherapy for Retinopathy of Prematurity Cooperative, G. (2001). Multicenter trial of cryotherapy for Retinopathy of Prematurity: Ophthalmological outcomes at 10 years. *Arch Ophthalmol* 119**,** 1110-1118.

Csiszar, A., Labinskyy, N., Pinto, J.T., Ballabh, P., Zhang, H., Losonczy, G., Pearson, K., De Cabo, R., Pacher, P., Zhang, C., and Ungvari, Z. (2009). Resveratrol induces mitochondrial biogenesis in endothelial cells. *Am J Physiol Heart Circ Physiol* 297**,** H13-20.

Dailey, H.A., Dailey, T.A., Gerdes, S., Jahn, D., Jahn, M., O'brian, M.R., and Warren, M.J. (2017). Prokaryotic heme biosynthesis: Multiple pathways to a common essential product. *Microbiol Mol Biol Rev* 81.

Dailey, H.A., Dailey, T.A., Wu, C.K., Medlock, A.E., Wang, K.F., Rose, J.P., and Wang, B.C. (2000). Ferrochelatase at the millennium: structures, mechanisms and [2Fe-2S] clusters. *Cell Mol Life Sci* 57**,** 1909-1926.

Dailey, H.A., and Meissner, P.N. (2013). Erythroid heme biosynthesis and its disorders. *Cold Spring Harb Perspect Med* 3**,** a011676.

De Bock, K., Georgiadou, M., Schoors, S., Kuchnio, A., Wong, B.W., Cantelmo, A.R., Quaegebeur, A., Ghesquiere, B., Cauwenberghs, S., Eelen, G.,

Phng, L.K., Betz, I., Tembuyser, B., Brepoels, K., Welti, J., Geudens, I., Segura, I., Cruys, B., Bifari, F., Decimo, I., Blanco, R., Wyns, S., Vangindertael, J., Rocha, S., Collins, R.T., Munck, S., Daelemans, D., Imamura, H., Devlieger, R., Rider, M., Van Veldhoven, P.P., Schuit, F., Bartrons, R., Hofkens, J., Fraisl, P., Telang, S., Deberardinis, R.J., Schoonjans, L., Vinckier, S., Chesney, J., Gerhardt, H., Dewerchin, M., and Carmeliet, P. (2013). Role of PFKFB3-driven glycolysis in vessel sprouting. *Cell* 154**,** 651-663.

De Cilla, S., Farruggio, S., Vujosevic, S., Raina, G., Filippini, D., Gatti, V., Clemente, N., Mary, D., Vezzola, D., Casini, G., Rossetti, L., and Grossini, E. (2017). Anti-vascular endothelial growth factors protect retinal pigment epithelium cells against oxidation by modulating nitric oxide release and autophagy. *Cell Physiol Biochem* 42**,** 1725-1738.

Deberardinis, R.J., Mancuso, A., Daikhin, E., Nissim, I., Yudkoff, M., Wehrli, S., and Thompson, C.B. (2007). Beyond aerobic glycolysis: transformed cells can engage in glutamine metabolism that exceeds the requirement for protein and nucleotide synthesis. *Proc Natl Acad Sci U S A* 104**,** 19345-19350.

Dhanasekaran, A., Kotamraju, S., Kalivendi, S.V., Matsunaga, T., Shang, T., Keszler, A., Joseph, J., and Kalyanaraman, B. (2004). Supplementation of endothelial cells with mitochondria-targeted antioxidants inhibit peroxide-induced mitochondrial iron uptake, oxidative damage, and apoptosis. *J Biol Chem* 279**,** 37575-37587.

Diebold, L.P., Gil, H.J., Gao, P., Martinez, C.A., Weinberg, S.E., and Chandel, N.S. (2019). Mitochondrial complex III is necessary for endothelial cell proliferation during angiogenesis. *Nat Metab* 1**,** 158-171.

Divakaruni, A.S., Paradyse, A., Ferrick, D.A., Murphy, A.N., and Jastroch, M. (2014). Analysis and interpretation of microplate-based oxygen consumption and pH data. *Methods Enzymol* 547**,** 309-354.

Doddaballapur, A., Michalik, K.M., Manavski, Y., Lucas, T., Houtkooper, R.H., You, X., Chen, W., Zeiher, A.M., Potente, M., Dimmeler, S., and Boon, R.A. (2015). Laminar shear stress inhibits endothelial cell metabolism via KLF2-mediated repression of PFKFB3. *Arterioscler Thromb Vasc Biol* 35**,** 137-145.

Doherty, E., and Perl, A. (2017). Measurement of Mitochondrial Mass by Flow Cytometry during Oxidative Stress. *React Oxyg Species (Apex)* 4**,** 275-283.

Dranka, B.P., Benavides, G.A., Diers, A.R., Giordano, S., Zelickson, B.R., Reily, C., Zou, L., Chatham, J.C., Hill, B.G., Zhang, J., Landar, A., and Darley-Usmar, V.M. (2011). Assessing bioenergetic function in response to oxidative stress by metabolic profiling. *Free Radic Biol Med* 51**,** 1621-1635.

Duraisamy, A.J., Mohammad, G., and Kowluru, R.A. (2019). Mitochondrial fusion and maintenance of mitochondrial homeostasis in diabetic retinopathy. *Biochim Biophys Acta Mol Basis Dis* 1865**,** 1617-1626.

Eelen, G., Dubois, C., Cantelmo, A.R., Goveia, J., Bruning, U., Deran, M., Jarugumilli, G., Van Rijssel, J., Saladino, G., Comitani, F., Zecchin, A., Rocha, S., Chen, R., Huang, H., Vandekeere, S., Kalucka, J., Lange, C., Morales-Rodriguez, F., Cruys, B., Treps, L., Ramer, L., Vinckier, S., Brepoels, K., Wyns, S., Souffreau, J., Schoonjans, L., Lamers, W.H., Wu, Y., Haustraete, J., Hofkens, J., Liekens, S., Cubbon, R., Ghesquiere, B., Dewerchin, M., Gervasio, F.L., Li, X., Van Buul, J.D., Wu, X., and Carmeliet, P. (2018). Role of glutamine synthetase in angiogenesis beyond glutamine synthesis. *Nature* 561**,** 63-69.

Ellis, L.M. (2006). Mechanisms of action of bevacizumab as a component of therapy for metastatic colorectal cancer. *Semin Oncol* 33**,** S1-7.

Engerman, R.L., Pfaffenbach, D., and Davis, M.D. (1967). Cell turnover of capillaries. *Lab Invest* 17**,** 738-743.

Espinosa-Heidmann, D.G., Reinoso, M.A., Pina, Y., Csaky, K.G., Caicedo, A., and Cousins, S.W. (2005). Quantitative enumeration of vascular smooth muscle cells and endothelial cells derived from bone marrow precursors in experimental choroidal neovascularization. *Exp Eye Res* 80**,** 369-378.

Evans, J.R., Michelessi, M., and Virgili, G. (2014). Laser photocoagulation for proliferative diabetic retinopathy. *Cochrane Database Syst Rev***,** CD011234.

Eyetech Study, G. (2002). Preclinical and phase 1A clinical evaluation of an anti-VEGF pegylated aptamer (EYE001) for the treatment of exudative age-related macular degeneration. *Retina* 22**,** 143-152.

Feng, C. (2012). Mechanism of Nitric Oxide Synthase Regulation: Electron Transfer and Interdomain Interactions. *Coord Chem Rev* 256**,** 393-411.

Ferrara, N. (1999). Vascular endothelial growth factor: molecular and biological aspects. *Curr Top Microbiol Immunol* 237**,** 1-30.

Ferrara, N., Gerber, H.P., and Lecouter, J. (2003). The biology of VEGF and its receptors. *Nat Med* 9**,** 669-676.

Ferrari, G., Cook, B.D., Terushkin, V., Pintucci, G., and Mignatti, P. (2009). Transforming growth factor-beta 1 (TGF-beta1) induces angiogenesis through vascular endothelial growth factor (VEGF)-mediated apoptosis. *J Cell Physiol* 219**,** 449-458.

Fitzgerald, G., Soro-Arnaiz, I., and De Bock, K. (2018). The Warburg Effect in Endothelial Cells and its Potential as an Anti-angiogenic Target in Cancer. *Front Cell Dev Biol* 6**,** 100.

Fleischhacker, A.S., and Ragsdale, S.W. (2018). An unlikely heme chaperone confirmed at last. *J Biol Chem* 293**,** 14569-14570.

Fong, D.S., Aiello, L., Gardner, T.W., King, G.L., Blankenship, G., Cavallerano, J.D., Ferris, F.L., 3rd, Klein, R., and American Diabetes, A. (2004). Retinopathy in diabetes. *Diabetes Care* 27 Suppl 1**,** S84-87.

Friedman, D.S., O'colmain, B.J., Munoz, B., Tomany, S.C., Mccarty, C., De Jong, P.T., Nemesure, B., Mitchell, P., Kempen, J., and Eye Diseases Prevalence Research, G. (2004). Prevalence of age-related macular degeneration in the United States. *Arch Ophthalmol* 122**,** 564-572.

Fruttiger, M. (2002). Development of the mouse retinal vasculature: angiogenesis versus vasculogenesis. *Invest Ophthalmol Vis Sci* 43**,** 522-527.

Ghitescu, L., and Robert, M. (2002). Diversity in unity: the biochemical composition of the endothelial cell surface varies between the vascular beds. *Microsc Res Tech* 57**,** 381-389.

Giacalone, J.C., Miller, M.J., Workalemahu, G., Reutzel, A.J., Ochoa, D., Whitmore, S.S., Stone, E.M., Tucker, B.A., and Mullins, R.F. (2019). Generation of an immortalized human choroid endothelial cell line (iChEC-1) using an endothelial cell specific promoter. *Microvasc Res* 123**,** 50-57.

Giger, U., and Meyer, U.A. (1983). Effect of succinylacetone on heme and cytochrome P450 synthesis in hepatocyte culture. *FEBS Lett* 153**,** 335-338.

Gouya, L., Puy, H., Lamoril, J., Da Silva, V., Grandchamp, B., Nordmann, Y., and Deybach, J.C. (1999). Inheritance in erythropoietic protoporphyria: a common wild-type ferrochelatase allelic variant with low expression accounts for clinical manifestation. *Blood* 93**,** 2105-2110.

Goveia, J., Stapor, P., and Carmeliet, P. (2014). Principles of targeting endothelial cell metabolism to treat angiogenesis and endothelial cell dysfunction in disease. *EMBO Mol Med* 6**,** 1105-1120.

Grant, M.B., Tarnuzzer, R.W., Caballero, S., Ozeck, M.J., Davis, M.I., Spoerri, P.E., Feoktistov, I., Biaggioni, I., Shryock, J.C., and Belardinelli, L. (1999). Adenosine receptor activation induces vascular endothelial growth factor in human retinal endothelial cells. *Circ Res* 85**,** 699-706.

Grochot-Przeczek, A., Kotlinowski, J., Kozakowska, M., Starowicz, K., Jagodzinska, J., Stachurska, A., Volger, O.L., Bukowska-Strakova, K., Florczyk, U., Tertil, M., Jazwa, A., Szade, K., Stepniewski, J., Loboda, A., Horrevoets, A.J., Dulak, J., and Jozkowicz, A. (2014). Heme oxygenase-1 is required for angiogenic function of bone marrow-derived progenitor cells: role in therapeutic revascularization. *Antioxid Redox Signal* 20**,** 1677-1692.

Gupta, P., Jordan, C.T., Mitov, M.I., Butterfield, D.A., Hilt, J.Z., and Dziubla, T.D. (2016). Controlled curcumin release via conjugation into PBAE nanogels enhances mitochondrial protection against oxidative stress. *Int J Pharm* 511**,** 1012-1021.

Gupta, V., Liu, S., Ando, H., Ishii, R., Tateno, S., Kaneko, Y., Yugami, M., Sakamoto, S., Yamaguchi, Y., Nureki, O., and Handa, H. (2013). Salicylic acid induces mitochondrial injury by inhibiting ferrochelatase heme biosynthesis activity. *Mol Pharmacol* 84**,** 824-833.

Hamza, I., and Dailey, H.A. (2012). One ring to rule them all: trafficking of heme and heme synthesis intermediates in the metazoans. *Biochim Biophys Acta* 1823**,** 1617-1632.

Handschin, C., Lin, J., Rhee, J., Peyer, A.K., Chin, S., Wu, P.H., Meyer, U.A., and Spiegelman, B.M. (2005). Nutritional regulation of hepatic heme biosynthesis and porphyria through PGC-1alpha. *Cell* 122**,** 505-515.

Havlickova Karbanova, V., Cizkova Vrbacka, A., Hejzlarova, K., Nuskova, H., Stranecky, V., Potocka, A., Kmoch, S., and Houstek, J. (2012).

Compensatory upregulation of respiratory chain complexes III and IV in isolated deficiency of ATP synthase due to TMEM70 mutation. *Biochim Biophys Acta* 1817**,** 1037-1043.

Hederstedt, L. (2012). Heme A biosynthesis. *Biochim Biophys Acta* 1817**,** 920-927.

Heidary, G., Vanderveen, D., and Smith, L.E. (2009). Retinopathy of prematurity: current concepts in molecular pathogenesis. *Semin Ophthalmol* 24**,** 77-81.

Hellstrom, A., Smith, L.E., and Dammann, O. (2013). Retinopathy of prematurity. *Lancet* 382**,** 1445-1457.

Hollborn, M., Stathopoulos, C., Steffen, A., Wiedemann, P., Kohen, L., and Bringmann, A. (2007). Positive feedback regulation between MMP-9 and VEGF in human RPE cells. *Invest Ophthalmol Vis Sci* 48**,** 4360-4367.

Holz, F.G., Sheraidah, G., Pauleikhoff, D., and Bird, A.C. (1994). Analysis of lipid deposits extracted from human macular and peripheral Bruch's membrane. *Arch Ophthalmol* 112**,** 402-406.

Iacovelli, J., Rowe, G.C., Khadka, A., Diaz-Aguilar, D., Spencer, C., Arany, Z., and Saint-Geniez, M. (2016). PGC-1alpha induces human RPE oxidative metabolism and antioxidant capacity. *Invest Ophthalmol Vis Sci* 57**,** 1038-1051.

Jackson, C.J., and Nguyen, M. (1997). Human microvascular endothelial cells differ from macrovascular endothelial cells in their expression of matrix metalloproteinases. *Int J Biochem Cell Biol* 29**,** 1167-1177.

Jager, R.D., Mieler, W.F., and Miller, J.W. (2008). Age-related macular degeneration. *N Engl J Med* 358**,** 2606-2617.

Jain, R.K. (2014). Antiangiogenesis strategies revisited: from starving tumors to alleviating hypoxia. *Cancer Cell* 26**,** 605-622.

Jefferies, W.A., Price, K.A., Biron, K.E., Fenninger, F., Pfeifer, C.G., and Dickstein, D.L. (2013). Adjusting the compass: new insights into the role of angiogenesis in Alzheimer's disease. *Alzheimers Res Ther* 5**,** 64.

Jezek, J., Cooper, K.F., and Strich, R. (2018). Reactive Oxygen Species and Mitochondrial dynamics: The yin and yang of mitochondrial dysfunction and cancer progression. *Antioxidants (Basel)* 7.

Joyal, J.S., Sun, Y., Gantner, M.L., Shao, Z., Evans, L.P., Saba, N., Fredrick, T., Burnim, S., Kim, J.S., Patel, G., Juan, A.M., Hurst, C.G., Hatton, C.J., Cui, Z., Pierce, K.A., Bherer, P., Aguilar, E., Powner, M.B., Vevis, K., Boisvert, M., Fu, Z., Levy, E., Fruttiger, M., Packard, A., Rezende, F.A., Maranda, B., Sapieha, P., Chen, J., Friedlander, M., Clish, C.B., and Smith, L.E. (2016). Retinal lipid and glucose metabolism dictates angiogenesis through the lipid sensor Ffar1. *Nat Med* 22**,** 439-445.

Jozkowicz, A., Huk, I., Nigisch, A., Weigel, G., Dietrich, W., Motterlini, R., and Dulak, J. (2003). Heme oxygenase and angiogenic activity of endothelial cells: stimulation by carbon monoxide and inhibition by tin protoporphyrin-IX. *Antioxid Redox Signal* 5**,** 155-162.

Justice, M.J., Noveroske, J.K., Weber, J.S., Zheng, B., and Bradley, A. (1999). Mouse ENU mutagenesis. *Hum Mol Genet* 8**,** 1955-1963.

Kauffman, M.E., Kauffman, M.K., Traore, K., Zhu, H., Trush, M.A., Jia, Z., and Li, Y.R. (2016). MitoSOX-based flow cytometry for detecting mitochondrial ROS. *React Oxyg Species (Apex)* 2**,** 361-370.

Kawahara, H., Naito, H., Takara, K., Wakabayashi, T., Kidoya, H., and Takakura, N. (2013). Tumor endothelial cell-specific drug delivery system using apelin-conjugated liposomes. *PLoS One* 8**,** e65499.

Keane, P.A., Liakopoulos, S., Ongchin, S.C., Heussen, F.M., Msutta, S., Chang, K.T., Walsh, A.C., and Sadda, S.R. (2008). Quantitative subanalysis of optical coherence tomography after treatment with ranibizumab for neovascular age-related macular degeneration. *Invest Ophthalmol Vis Sci* 49**,** 3115-3120.

Kempen, J.H., O'colmain, B.J., Leske, M.C., Haffner, S.M., Klein, R., Moss, S.E., Taylor, H.R., Hamman, R.F., and Eye Diseases Prevalence Research, G. (2004). The prevalence of diabetic retinopathy among adults in the United States. *Arch Ophthalmol* 122**,** 552-563.

Kennedy, A.J., Ellacott, K.L., King, V.L., and Hasty, A.H. (2010). Mouse models of the metabolic syndrome. *Dis Model Mech* 3**,** 156-166.

Kim, H.J., Khalimonchuk, O., Smith, P.M., and Winge, D.R. (2012). Structure, function, and assembly of heme centers in mitochondrial respiratory complexes. *Biochim Biophys Acta* 1823**,** 1604-1616.

Kim, Y.M., Youn, S.W., Sudhahar, V., Das, A., Chandhri, R., Cuervo Grajal, H., Kweon, J., Leanhart, S., He, L., Toth, P.T., Kitajewski, J., Rehman, J., Yoon, Y., Cho, J., Fukai, T., and Ushio-Fukai, M. (2018). Redox

Regulation of mitochondrial fission protein Drp1 by protein disulfide isomerase limits endothelial senescence. *Cell Rep* 23**,** 3565-3578.

Kizhakekuttu, T.J., Wang, J., Dharmashankar, K., Ying, R., Gutterman, D.D., Vita, J.A., and Widlansky, M.E. (2012). Adverse alterations in mitochondrial function contribute to type 2 diabetes mellitus-related endothelial dysfunction in humans. *Arterioscler Thromb Vasc Biol* 32**,** 2531-2539.

Kluge, M.A., Fetterman, J.L., and Vita, J.A. (2013). Mitochondria and endothelial function. *Circ Res* 112**,** 1171-1188.

Koopman, M., Michels, H., Dancy, B.M., Kamble, R., Mouchiroud, L., Auwerx, J., Nollen, E.A., and Houtkooper, R.H. (2016). A screening-based platform for the assessment of cellular respiration in Caenorhabditis elegans. *Nat Protoc* 11**,** 1798-1816.

Kooragayala, K., Gotoh, N., Cogliati, T., Nellissery, J., Kaden, T.R., French, S., Balaban, R., Li, W., Covian, R., and Swaroop, A. (2015). Quantification of oxygen consumption in retina ex vivo demonstrates limited reserve capacity of photoreceptor mitochondria. *Invest Ophthalmol Vis Sci* 56**,** 8428-8436.

Korolnek, T., and Hamza, I. (2014). Like iron in the blood of the people: the requirement for heme trafficking in iron metabolism. *Front Pharmacol* 5**,** 126.

Kowluru, R.A., and Mishra, M. (2015). Oxidative stress, mitochondrial damage and diabetic retinopathy. *Biochim Biophys Acta* 1852**,** 2474-2483.

Krammer, B., and Plaetzer, K. (2008). ALA and its clinical impact, from bench to bedside. *Photochem Photobiol Sci* 7**,** 283-289.

Krupinski, J., Kaluza, J., Kumar, P., Kumar, S., and Wang, J.M. (1994). Role of angiogenesis in patients with cerebral ischemic stroke. *Stroke* 25**,** 1794-1798.

Kurihara, T., Westenskow, P.D., Gantner, M.L., Usui, Y., Schultz, A., Bravo, S., Aguilar, E., Wittgrove, C., Friedlander, M., Paris, L.P., Chew, E., Siuzdak, G., and Friedlander, M. (2016). Hypoxia-induced metabolic stress in retinal pigment epithelial cells is sufficient to induce photoreceptor degeneration. *Elife* 5.

Lad, E.M., Hernandez-Boussard, T., Morton, J.M., and Moshfeghi, D.M. (2009). Incidence of retinopathy of prematurity in the United States: 1997 through 2005. *Am J Ophthalmol* 148**,** 451-458.

Lane, R.K., Hilsabeck, T., and Rea, S.L. (2015). The role of mitochondrial dysfunction in age-related diseases. *Biochim Biophys Acta* 1847**,** 1387-1400.

Lee, B., Basavarajappa, H.D., Sulaiman, R.S., Fei, X., Seo, S.Y., and Corson, T.W. (2014). The first synthesis of the antiangiogenic homoisoflavanone, cremastranone. *Org Biomol Chem* 12**,** 7673-7677.

Lee, I., Huttemann, M., Liu, J., Grossman, L.I., and Malek, M.H. (2012). Deletion of heart-type cytochrome c oxidase subunit 7a1 impairs skeletal muscle angiogenesis and oxidative phosphorylation. *J Physiol* 590**,** 5231-5243.

Lefevere, E., Toft-Kehler, A.K., Vohra, R., Kolko, M., Moons, L., and Van Hove, I. (2017). Mitochondrial dysfunction underlying outer retinal diseases. *Mitochondrion* 36**,** 66-76.

Li, A., Dubey, S., Varney, M.L., Dave, B.J., and Singh, R.K. (2003). IL-8 directly enhanced endothelial cell survival, proliferation, and matrix metalloproteinases production and regulated angiogenesis. *J Immunol* 170**,** 3369-3376.

Li, B., Takeda, K., Ishikawa, K., Yoshizawa, M., Sato, M., Shibahara, S., and Furuyama, K. (2012). Coordinated expression of 6-phosphofructo-2-kinase/fructose-2,6-bisphosphatase 4 and heme oxygenase 2: evidence for a regulatory link between glycolysis and heme catabolism. *Tohoku J Exp Med* 228**,** 27-41.

Libbrecht, L., Meerman, L., Kuipers, F., Roskams, T., Desmet, V., and Jansen, P. (2003). Liver pathology and hepatocarcinogenesis in a long-term mouse model of erythropoietic protoporphyria. *J Pathol* 199**,** 191-200.

Lilienbaum, A. (2013). Relationship between the proteasomal system and autophagy. *Int J Biochem Mol Biol* 4**,** 1-26.

Lin, K.H., Xie, A., Rutter, J.C., Ahn, Y.R., Lloyd-Cowden, J.M., Nichols, A.G., Soderquist, R.S., Koves, T.R., Muoio, D.M., Maciver, N.J., Lamba, J.K., Pardee, T.S., Mccall, C.M., Rizzieri, D.A., and Wood, K.C. (2019). Systematic dissection of the metabolic-apoptotic interface in AML reveals heme biosynthesis to be a regulator of drug sensitivity. *Cell Metab* 29**,** 1217-1231 e1217.

Lin, M.T., and Beal, M.F. (2006). Mitochondrial dysfunction and oxidative stress in neurodegenerative diseases. *Nature* 443**,** 787-795.

Liu, K., Yan, J., Sachar, M., Zhang, X., Guan, M., Xie, W., and Ma, X. (2015). A metabolomic perspective of griseofulvin-induced liver injury in mice. *Biochem Pharmacol* 98**,** 493-501.

Liu, Y.J., Mcintyre, R.L., Janssens, G.E., and Houtkooper, R.H. (2020). Mitochondrial fission and fusion: A dynamic role in aging and potential target for age-related disease. *Mech Ageing Dev* 186**,** 111212.

Liu, Z., Yan, S., Wang, J., Xu, Y., Wang, Y., Zhang, S., Xu, X., Yang, Q., Zeng, X., Zhou, Y., Gu, X., Lu, S., Fu, Z., Fulton, D.J., Weintraub, N.L., Caldwell, R.B., Zhang, W., Wu, C., Liu, X.L., Chen, J.F., Ahmad, A., Kaddour-Djebbar, I., Al-Shabrawey, M., Li, Q., Jiang, X., Sun, Y., Sodhi, A., Smith, L., Hong, M., and Huo, Y. (2017). Endothelial adenosine A2a receptor-mediated glycolysis is essential for pathological retinal angiogenesis. *Nat Commun* 8**,** 584.

Lohela, M., Bry, M., Tammela, T., and Alitalo, K. (2009). VEGFs and receptors involved in angiogenesis versus lymphangiogenesis. *Curr Opin Cell Biol* 21**,** 154-165.

Lou, D.A., and Hu, F.N. (1987). Specific antigen and organelle expression of a long-term rhesus endothelial cell line. *In Vitro Cell Dev Biol* 23**,** 75-85.

Lowe, J., Araujo, J., Yang, J., Reich, M., Oldendorp, A., Shiu, V., Quarmby, V., Lowman, H., Lien, S., Gaudreault, J., and Maia, M. (2007). Ranibizumab

inhibits multiple forms of biologically active vascular endothelial growth factor in vitro and in vivo. *Exp Eye Res* 85**,** 425-430.

Luan, Y., Zhang, F., Cheng, Y., Liu, J., Huang, R., Yan, M., Wang, Y., He, Z., Lai, H., Wang, H., Ying, H., Guo, F., and Zhai, Q. (2017). Hemin improves insulin sensitivity and lipid metabolism in cultured hepatocytes and mice fed a high-fat diet. *Nutrients* 9.

Lyden, D., Hattori, K., Dias, S., Costa, C., Blaikie, P., Butros, L., Chadburn, A., Heissig, B., Marks, W., Witte, L., Wu, Y., Hicklin, D., Zhu, Z., Hackett, N.R., Crystal, R.G., Moore, M.A., Hajjar, K.A., Manova, K., Benezra, R., and Rafii, S. (2001). Impaired recruitment of bone-marrow-derived endothelial and hematopoietic precursor cells blocks tumor angiogenesis and growth. *Nat Med* 7**,** 1194-1201.

Ma, B., Day, J.P., Phillips, H., Slootsky, B., Tolosano, E., and Dore, S. (2016). Deletion of the hemopexin or heme oxygenase-2 gene aggravates brain injury following stroma-free hemoglobin-induced intracerebral hemorrhage. *J Neuroinflammation* 13**,** 26.

Magness, S.T., Maeda, N., and Brenner, D.A. (2002). An exon 10 deletion in the mouse ferrochelatase gene has a dominant-negative effect and causes mild protoporphyria. *Blood* 100**,** 1470-1477.

Makin, R.D., Apicella, I., Nagasaka, Y., Kaneko, H., Turner, S.D., Kerur, N., Ambati, J., and Gelfand, B.D. (2018). RF/6A chorioretinal cells do not display key endothelial phenotypes. *Invest Ophthalmol Vis Sci* 59**,** 5795-5802.

Makino, A., Scott, B.T., and Dillmann, W.H. (2010). Mitochondrial fragmentation and superoxide anion production in coronary endothelial cells from a mouse model of type 1 diabetes. *Diabetologia* 53**,** 1783-1794.

Martinez, P., Esbrit, P., Rodrigo, A., Alvarez-Arroyo, M.V., and Martinez, M.E. (2002). Age-related changes in parathyroid hormone-related protein and vascular endothelial growth factor in human osteoblastic cells. *Osteoporos Int* 13**,** 874-881.

Masland, R.H. (2012). The neuronal organization of the retina. *Neuron* 76**,** 266-280.

Mather, K.J., Verma, S., and Anderson, T.J. (2001). Improved endothelial function with metformin in type 2 diabetes mellitus. *J Am Coll Cardiol* 37**,** 1344-1350.

Mavria, G., Vercoulen, Y., Yeo, M., Paterson, H., Karasarides, M., Marais, R., Bird, D., and Marshall, C.J. (2006). ERK-MAPK signaling opposes Rho-kinase to promote endothelial cell survival and sprouting during angiogenesis. *Cancer Cell* 9**,** 33-44.

Melincovici, C.S., Bosca, A.B., Susman, S., Marginean, M., Mihu, C., Istrate, M., Moldovan, I.M., Roman, A.L., and Mihu, C.M. (2018). Vascular endothelial growth factor (VEGF) - key factor in normal and pathological angiogenesis. *Rom J Morphol Embryol* 59**,** 455-467.

Meyer, M., Clauss, M., Lepple-Wienhues, A., Waltenberger, J., Augustin, H.G., Ziche, M., Lanz, C., Buttner, M., Rziha, H.J., and Dehio, C. (1999). A novel vascular endothelial growth factor encoded by Orf virus, VEGF-E,

mediates angiogenesis via signalling through VEGFR-2 (KDR) but not VEGFR-1 (Flt-1) receptor tyrosine kinases. *EMBO J* 18**,** 363-374.

Mishra, M., and Kowluru, R.A. (2015). Epigenetic modification of mitochondrial dna in the development of diabetic retinopathy. *Invest Ophthalmol Vis Sci* 56**,** 5133-5142.

Mishra, M., and Kowluru, R.A. (2018). DNA methylation-A potential source of mitochondria dna base mismatch in the development of Diabetic Retinopathy. *Mol Neurobiol*.

Mizushima, N. (2007). Autophagy: Process and function. *Genes Dev* 21**,** 2861-2873.

Mohamed Al-Sayed Al-Shabrawey, H.M.S., Khaled Elmasry, Ismail Kaddour-Dejebbar, Amany Tawfik, Ahmed Ibrahim (2017). Hypoxia is essential for hyperglycemia to induce permeability and angiogenesis in retinal endothelial cells via GLUT1. *Invest. Ophthalmol. Vis. Sci.*

Moser, T.L., Stack, M.S., Asplin, I., Enghild, J.J., Hojrup, P., Everitt, L., Hubchak, S., Schnaper, H.W., and Pizzo, S.V. (1999). Angiostatin binds ATP synthase on the surface of human endothelial cells. *Proc Natl Acad Sci U S A* 96**,** 2811-2816.

Motterlini, R., Foresti, R., Bassi, R., Calabrese, V., Clark, J.E., and Green, C.J. (2000). Endothelial heme oxygenase-1 induction by hypoxia. Modulation by inducible nitric-oxide synthase and S-nitrosothiols. *J Biol Chem* 275**,** 13613-13620.

Navarro, S., Del Hoyo, P., Campos, Y., Abitbol, M., Moran-Jimenez, M.J., Garcia-Bravo, M., Ochoa, P., Grau, M., Montagutelli, X., Frank, J., Garesse, R., Arenas, J., De Salamanca, R.E., and Fontanellas, A. (2005). Increased mitochondrial respiratory chain enzyme activities correlate with minor extent of liver damage in mice suffering from erythropoietic protoporphyria. *Exp Dermatol* 14**,** 26-33.

Nepomuceno, A.B., Takaki, E., Paes De Almeida, F.P., Peroni, R., Cardillo, J.A., Siqueira, R.C., Scott, I.U., Messias, A., and Jorge, R. (2013). A prospective randomized trial of intravitreal bevacizumab versus ranibizumab for the management of diabetic macular edema. *Am J Ophthalmol* 156**,** 502-510 e502.

Neufeld, G., Cohen, T., Gengrinovitch, S., and Poltorak, Z. (1999). Vascular endothelial growth factor (VEGF) and its receptors. *FASEB J* 13**,** 9-22.

Nilsson, R., Schultz, I.J., Pierce, E.L., Soltis, K.A., Naranuntarat, A., Ward, D.M., Baughman, J.M., Paradkar, P.N., Kingsley, P.D., Culotta, V.C., Kaplan, J., Palis, J., Paw, B.H., and Mootha, V.K. (2009). Discovery of genes essential for heme biosynthesis through large-scale gene expression analysis. *Cell Metab* 10**,** 119-130.

Olofsson, B., Korpelainen, E., Pepper, M.S., Mandriota, S.J., Aase, K., Kumar, V., Gunji, Y., Jeltsch, M.M., Shibuya, M., Alitalo, K., and Eriksson, U. (1998). Vascular endothelial growth factor B (VEGF-B) binds to VEGF receptor-1 and regulates plasminogen activator activity in endothelial cells. *Proc Natl Acad Sci U S A* 95**,** 11709-11714.

Pangare, M., and Makino, A. (2012). Mitochondrial function in vascular endothelial cell in diabetes. *J Smooth Muscle Res* 48**,** 1-26.

Park, H.Y., Shin, H.Y., Yoon, J.Y., Jung, Y., and Park, C.K. (2014). Intereye comparison of cirrus OCT in early glaucoma diagnosis and detecting photographic retinal nerve fiber layer abnormalities. *Invest Ophthalmol Vis Sci* 56**,** 1733-1742.

Pearlstein, D.P., Ali, M.H., Mungai, P.T., Hynes, K.L., Gewertz, B.L., and Schumacker, P.T. (2002). Role of mitochondrial oxidant generation in endothelial cell responses to hypoxia. *Arterioscler Thromb Vasc Biol* 22**,** 566-573.

Perelman, A., Wachtel, C., Cohen, M., Haupt, S., Shapiro, H., and Tzur, A. (2012). JC-1: Alternative excitation wavelengths facilitate mitochondrial membrane potential cytometry. *Cell Death Dis* 3**,** e430.

Perron, N.R., Beeson, C., and Rohrer, B. (2013). Early alterations in mitochondrial reserve capacity; a means to predict subsequent photoreceptor cell death. *J Bioenerg Biomembr* 45**,** 101-109.

Persico, M.G., Vincenti, V., and Dipalma, T. (1999). Structure, expression and receptor-binding properties of placenta growth factor (PlGF). *Curr Top Microbiol Immunol* 237**,** 31-40.

Petrillo, S., Chiabrando, D., Genova, T., Fiorito, V., Ingoglia, G., Vinchi, F., Mussano, F., Carossa, S., Silengo, L., Altruda, F., Merlo, G.R., Munaron, L., and Tolosano, E. (2018). Heme accumulation in endothelial cells

impairs angiogenesis by triggering paraptosis. *Cell Death Differ* 25**,** 573-588.

Picard, M., White, K., and Turnbull, D.M. (2013). Mitochondrial morphology, topology, and membrane interactions in skeletal muscle: A quantitative three-dimensional electron microscopy study. *J Appl Physiol (1985)* 114**,** 161-171.

Poulos, T.L. (2014). Heme enzyme structure and function. *Chem Rev* 114**,** 3919-3962.

Rafikov, R., Sun, X., Rafikova, O., Louise Meadows, M., Desai, A.A., Khalpey, Z., Yuan, J.X., Fineman, J.R., and Black, S.M. (2015). Complex I dysfunction underlies the glycolytic switch in pulmonary hypertensive smooth muscle cells. *Redox Biol* 6**,** 278-286.

Raman, C.S., Li, H., Martasek, P., Kral, V., Masters, B.S., and Poulos, T.L. (1998). Crystal structure of constitutive endothelial nitric oxide synthase: A paradigm for pterin function involving a novel metal center. *Cell* 95**,** 939-950.

Ribatti, D., Nico, B., and Crivellato, E. (2011). The role of pericytes in angiogenesis. *Int J Dev Biol* 55**,** 261-268.

Righy, C., Bozza, M.T., Oliveira, M.F., and Bozza, F.A. (2016). Molecular, cellular and clinical aspects of intracerebral hemorrhage: Are the enemies within? *Curr Neuropharmacol* 14**,** 392-402.

Rolland, S.G., Motori, E., Memar, N., Hench, J., Frank, S., Winklhofer, K.F., and Conradt, B. (2013). Impaired complex IV activity in response to loss of

LRPPRC function can be compensated by mitochondrial hyperfusion. *Proc Natl Acad Sci U S A* 110**,** E2967-2976.

Ruckman, J., Green, L.S., Beeson, J., Waugh, S., Gillette, W.L., Henninger, D.D., Claesson-Welsh, L., and Janjic, N. (1998). 2'-Fluoropyrimidine RNA-based aptamers to the 165-amino acid form of vascular endothelial growth factor (VEGF165). Inhibition of receptor binding and VEGF-induced vascular permeability through interactions requiring the exon 7-encoded domain. *J Biol Chem* 273**,** 20556-20567.

Rufenacht, U.B., Gouya, L., Schneider-Yin, X., Puy, H., Schafer, B.W., Aquaron, R., Nordmann, Y., Minder, E.I., and Deybach, J.C. (1998). Systematic analysis of molecular defects in the ferrochelatase gene from patients with erythropoietic protoporphyria. *Am J Hum Genet* 62**,** 1341-1352.

Rusovici, R., Patel, C.J., and Chalam, K.V. (2013). Bevacizumab inhibits proliferation of choroidal endothelial cells by regulation of the cell cycle. *Clin Ophthalmol* 7**,** 321-327.

Ryter, S.W., and Tyrrell, R.M. (2000). The heme synthesis and degradation pathways: role in oxidant sensitivity. Heme oxygenase has both pro- and antioxidant properties. *Free Radic Biol Med* 28**,** 289-309.

Saaddine, J.B., Honeycutt, A.A., Narayan, K.M., Zhang, X., Klein, R., and Boyle, J.P. (2008). Projection of Diabetic Retinopathy and other major eye diseases among people with Diabetes Mellitus: United States, 2005-2050. *Arch Ophthalmol* 126**,** 1740-1747.

Saint-Geniez, M., Jiang, A., Abend, S., Liu, L., Sweigard, H., Connor, K.M., and Arany, Z. (2013). PGC-1alpha regulates normal and pathological angiogenesis in the retina. *Am J Pathol* 182**,** 255-265.

Sandoo, A., Carroll, D., Metsios, G.S., Kitas, G.D., and Veldhuijzen Van Zanten, J.J. (2011). The association between microvascular and macrovascular endothelial function in patients with rheumatoid arthritis: A cross-sectional study. *Arthritis Res Ther* 13**,** R99.

Santos, J.M., Mishra, M., and Kowluru, R.A. (2014). Posttranslational modification of mitochondrial transcription factor A in impaired mitochondria biogenesis: Implications in diabetic retinopathy and metabolic memory phenomenon. *Exp Eye Res* 121**,** 168-177.

Sapieha, P., Joyal, J.S., Rivera, J.C., Kermorvant-Duchemin, E., Sennlaub, F., Hardy, P., Lachapelle, P., and Chemtob, S. (2010). Retinopathy of Prematurity: Understanding ischemic retinal vasculopathies at an extreme of life. *J Clin Invest* 120**,** 3022-3032.

Sapieha, P., Sirinyan, M., Hamel, D., Zaniolo, K., Joyal, J.S., Cho, J.H., Honore, J.C., Kermorvant-Duchemin, E., Varma, D.R., Tremblay, S., Leduc, M., Rihakova, L., Hardy, P., Klein, W.H., Mu, X., Mamer, O., Lachapelle, P., Di Polo, A., Beausejour, C., Andelfinger, G., Mitchell, G., Sennlaub, F., and Chemtob, S. (2008). The succinate receptor GPR91 in neurons has a major role in retinal angiogenesis. *Nat Med* 14**,** 1067-1076.

Sardar Pasha Spb, C.T. (2019). Targeting ferrochelatase for treating of retinal neovascularization. . *FASEB J* 33**,** 679.678.

Schaal, S., Kaplan, H.J., and Tezel, T.H. (2008). Is there tachyphylaxis to intravitreal anti-vascular endothelial growth factor pharmacotherapy in age-related macular degeneration? *Ophthalmology* 115**,** 2199-2205.

Schmucker, C., Antes, G., and Lelgemann, M. (2009). Position paper: The need for head-to-head studies comparing Avastin versus Lucentis. *Surv Ophthalmol* 54**,** 705-707.

Schoors, S., Bruning, U., Missiaen, R., Queiroz, K.C., Borgers, G., Elia, I., Zecchin, A., Cantelmo, A.R., Christen, S., Goveia, J., Heggermont, W., Godde, L., Vinckier, S., Van Veldhoven, P.P., Eelen, G., Schoonjans, L., Gerhardt, H., Dewerchin, M., Baes, M., De Bock, K., Ghesquiere, B., Lunt, S.Y., Fendt, S.M., and Carmeliet, P. (2015). Fatty acid carbon is essential for dNTP synthesis in endothelial cells. *Nature* 520**,** 192-197.

Schoors, S., De Bock, K., Cantelmo, A.R., Georgiadou, M., Ghesquiere, B., Cauwenberghs, S., Kuchnio, A., Wong, B.W., Quaegebeur, A., Goveia, J., Bifari, F., Wang, X., Blanco, R., Tembuyser, B., Cornelissen, I., Bouche, A., Vinckier, S., Diaz-Moralli, S., Gerhardt, H., Telang, S., Cascante, M., Chesney, J., Dewerchin, M., and Carmeliet, P. (2014). Partial and transient reduction of glycolysis by PFKFB3 blockade reduces pathological angiogenesis. *Cell Metab* 19**,** 37-48.

Semeraro, F., Morescalchi, F., Duse, S., Parmeggiani, F., Gambicorti, E., and Costagliola, C. (2013). Aflibercept in Wet AMD: Specific role and optimal use. *Drug Des Devel Ther* 7**,** 711-722.

Shi, Z., and Ferreira, G.C. (2006). Modulation of inhibition of ferrochelatase by *N*-methylprotoporphyrin. *Biochem J* 399**,** 21-28.

Shinoda, K., Ishida, S., Kawashima, S., Wakabayashi, T., Uchita, M., Matsuzaki, T., Takayama, M., Shinmura, K., and Yamada, M. (2000). Clinical factors related to the aqueous levels of vascular endothelial growth factor and hepatocyte growth factor in proliferative diabetic retinopathy. *Curr Eye Res* 21**,** 655-661.

Shiojima, I., and Walsh, K. (2002). Role of Akt signaling in vascular homeostasis and angiogenesis. *Circ Res* 90**,** 1243-1250.

Silver, J. (2014). Drugs for macular degeneration, price discrimination, and medicare's responsibility not to overpay. *JAMA* 312**,** 23-24.

Sinkler, C.A., Kalpage, H., Shay, J., Lee, I., Malek, M.H., Grossman, L.I., and Huttemann, M. (2017). Tissue- and condition-specific isoforms of Mammalian cytochrome c oxidase subunits: From function to human disease. *Oxid Med Cell Longev* 2017**,** 1534056.

Sishtla, K., Lee, S., Lee, J., E., Seo, S.Y., and Corson, T.W. (2019). Discovery of ferrochelatase inhibitors as antiangiogenic agents. *Invest. Ophthalmol. Vis. Sci* 2019;60(9):5405.

Smith, J.R., Choi, D., Chipps, T.J., Pan, Y., Zamora, D.O., Davies, M.H., Babra, B., Powers, M.R., Planck, S.R., and Rosenbaum, J.T. (2007). Unique gene expression profiles of donor-matched human retinal and choroidal vascular endothelial cells. *Invest Ophthalmol Vis Sci* 48**,** 2676-2684.

Smith, L.E., Kopchick, J.J., Chen, W., Knapp, J., Kinose, F., Daley, D., Foley, E., Smith, R.G., and Schaeffer, J.M. (1997). Essential role of growth hormone in ischemia-induced retinal neovascularization. *Science* 276**,** 1706-1709.

Sodhi, K., Inoue, K., Gotlinger, K.H., Canestraro, M., Vanella, L., Kim, D.H., Manthati, V.L., Koduru, S.R., Falck, J.R., Schwartzman, M.L., and Abraham, N.G. (2009). Epoxyeicosatrienoic acid agonist rescues the metabolic syndrome phenotype of HO-2-null mice. *J Pharmacol Exp Ther* 331**,** 906-916.

Sohoni, S., Ghosh, P., Wang, T., Kalainayakan, S.P., Vidal, C., Dey, S., Konduri, P.C., and Zhang, L. (2019). Elevated heme synthesis and uptake underpin intensified oxidative metabolism and tumorigenic functions in non-small cell lung cancer cells. *Cancer Res* 79**,** 2511-2525.

Sone, H., Deo, B.K., and Kumagai, A.K. (2000). Enhancement of glucose transport by vascular endothelial growth factor in retinal endothelial cells. *Invest Ophthalmol Vis Sci* 41**,** 1876-1884.

Stewart, E.A., Samaranayake, G.J., Browning, A.C., Hopkinson, A., and Amoaku, W.M. (2011). Comparison of choroidal and retinal endothelial cells: characteristics and response to VEGF isoforms and anti-VEGF treatments. *Exp Eye Res* 93**,** 761-766.

Stitt, A.W., Mcgoldrick, C., Rice-Mccaldin, A., Mccance, D.R., Glenn, J.V., Hsu, D.K., Liu, F.T., Thorpe, S.R., and Gardiner, T.A. (2005). Impaired retinal angiogenesis in diabetes: role of advanced glycation end products and galectin-3. *Diabetes* 54**,** 785-794.

Stone, J., Chan-Ling, T., Pe'er, J., Itin, A., Gnessin, H., and Keshet, E. (1996). Roles of vascular endothelial growth factor and astrocyte degeneration in the genesis of retinopathy of prematurity. *Invest Ophthalmol Vis Sci* 37**,** 290-299.

Sulaiman, R.S., Merrigan, S., Quigley, J., Qi, X., Lee, B., Boulton, M.E., Kennedy, B., Seo, S.Y., and Corson, T.W. (2016). A novel small molecule ameliorates ocular neovascularisation and synergises with anti-VEGF therapy. *Sci Rep* 6**,** 25509.

Sun, Y., and Smith, L.E.H. (2018). Retinal vasculature in development and diseases. *Annu Rev Vis Sci* 4**,** 101-122.

Sweeny, E.A., Singh, A.B., Chakravarti, R., Martinez-Guzman, O., Saini, A., Haque, M.M., Garee, G., Dans, P.D., Hannibal, L., Reddi, A.R., and Stuehr, D.J. (2018). Glyceraldehyde-3-phosphate dehydrogenase is a chaperone that allocates labile heme in cells. *J Biol Chem* 293**,** 14557-14568.

Talks, K.L., and Harris, A.L. (2000). Current status of antiangiogenic factors. *Br J Haematol* 109**,** 477-489.

Tang, X., Luo, Y.X., Chen, H.Z., and Liu, D.P. (2014). Mitochondria, endothelial cell function, and vascular diseases. *Front Physiol* 5**,** 175.

Tien, T., Zhang, J., Muto, T., Kim, D., Sarthy, V.P., and Roy, S. (2017). High glucose induces mitochondrial dysfunction in retinal muller cells: Implications for Diabetic Retinopathy. *Invest Ophthalmol Vis Sci* 58**,** 2915-2921.

The CATT Research Group, Martin, D.F., Maguire, M.G., Ying, G.S., Grunwald, J.E., Fine, S.L., and Jaffe, G.J. (2011). Ranibizumab and bevacizumab for neovascular age-related macular degeneration. *N Engl J Med* 364**,** 1897-1908.

Timar, J., Dome, B., Fazekas, K., Janovics, A., and Paku, S. (2001). Angiogenesis-dependent diseases and angiogenesis therapy. *Pathol Oncol Res* 7**,** 85-94.

Tong, L., Vernon, S.A., Kiel, W., Sung, V., and Orr, G.M. (2001). Association of macular involvement with proliferative retinopathy in Type 2 diabetes. *Diabet Med* 18**,** 388-394.

Toyabe, S., Watanabe-Nakayama, T., Okamoto, T., Kudo, S., and Muneyuki, E. (2011). Thermodynamic efficiency and mechanochemical coupling of F1-ATPase. *Proc Natl Acad Sci U S A* 108**,** 17951-17956.

Trudeau, K., Molina, A.J., Guo, W., and Roy, S. (2010). High glucose disrupts mitochondrial morphology in retinal endothelial cells: Implications for Diabetic Retinopathy. *Am J Pathol* 177**,** 447-455.

Trudeau, K., Molina, A.J., and Roy, S. (2011). High glucose induces mitochondrial morphology and metabolic changes in retinal pericytes. *Invest Ophthalmol Vis Sci* 52**,** 8657-8664.

Tsuboi, H., Yonemoto, K., and Katsuoka, K. (2007). Erythropoietic protoporphyria with eye complications. *J Dermatol* 34**,** 790-794.

Tutois, S., Montagutelli, X., Da Silva, V., Jouault, H., Rouyer-Fessard, P., Leroy-Viard, K., Guenet, J.L., Nordmann, Y., Beuzard, Y., and Deybach, J.C.

(1991). Erythropoietic protoporphyria in the house mouse. A recessive inherited ferrochelatase deficiency with anemia, photosensitivity, and liver disease. *J Clin Invest* 88**,** 1730-1736.

Ucuzian, A.A., Gassman, A.A., East, A.T., and Greisler, H.P. (2010). Molecular mediators of angiogenesis. *J Burn Care Res* 31**,** 158-175.

Vallelian, F., Deuel, J.W., Opitz, L., Schaer, C.A., Puglia, M., Lonn, M., Engelsberger, W., Schauer, S., Karnaukhova, E., Spahn, D.R., Stocker, R., Buehler, P.W., and Schaer, D.J. (2015). Proteasome inhibition and oxidative reactions disrupt cellular homeostasis during heme stress. *Cell Death Differ* 22**,** 597-611.

Vandekeere, S., Dewerchin, M., and Carmeliet, P. (2015). Angiogenesis revisited: An overlooked role of endothelial cell metabolism in vessel sprouting. *Microcirculation* 22**,** 509-517.

Vandekeere, S., Dubois, C., Kalucka, J., Sullivan, M.R., Garcia-Caballero, M., Goveia, J., Chen, R., Diehl, F.F., Bar-Lev, L., Souffreau, J., Pircher, A., Kumar, S., Vinckier, S., Hirabayashi, Y., Furuya, S., Schoonjans, L., Eelen, G., Ghesquiere, B., Keshet, E., Li, X., Vander Heiden, M.G., Dewerchin, M., and Carmeliet, P. (2018). Serine synthesis via PHGDH Is essential for heme production in endothelial cells. *Cell Metab* 28**,** 573-587 e513.

Varma, R. (2008). From a population to patients: the Wisconsin epidemiologic study of diabetic retinopathy. *Ophthalmology* 115**,** 1857-1858.

Veikkola, T., and Alitalo, K. (1999). VEGFs, receptors and angiogenesis. *Semin Cancer Biol* 9**,** 211-220.

Vijayasarathy, C., Damle, S., Lenka, N., and Avadhani, N.G. (1999). Tissue variant effects of heme inhibitors on the mouse cytochrome c oxidase gene expression and catalytic activity of the enzyme complex. *Eur J Biochem* 266**,** 191-200.

Vinchi, F., De Franceschi, L., Ghigo, A., Townes, T., Cimino, J., Silengo, L., Hirsch, E., Altruda, F., and Tolosano, E. (2013). Hemopexin therapy improves cardiovascular function by preventing heme-induced endothelial toxicity in mouse models of hemolytic diseases. *Circulation* 127**,** 1317-1329.

Wachowska, M., Muchowicz, A., Firczuk, M., Gabrysiak, M., Winiarska, M., Wańczyk, M., Bojarczuk, K., and Golab, J. Aminolevulinic acid (ALA) as a prodrug in photodynamic therapy of cancer. *Molecules* 2011 May 19;16(5):4140–4164.

Waheed, S.M., Ghosh, A., Chakravarti, R., Biswas, A., Haque, M.M., Panda, K., and Stuehr, D.J. (2010). Nitric oxide blocks cellular heme insertion into a broad range of heme proteins. *Free Radic Biol Med* 48**,** 1548-1558.

Wang, J.Y., Lee, Y.T., Chang, P.F., and Chau, L.Y. (2009). Hemin promotes proliferation and differentiation of endothelial progenitor cells via activation of AKT and ERK. *J Cell Physiol* 219**,** 617-625.

Wang, Y., Zang, Q.S., Liu, Z., Wu, Q., Maass, D., Dulan, G., Shaul, P.W., Melito, L., Frantz, D.E., Kilgore, J.A., Williams, N.S., Terada, L.S., and Nwariaku,

F.E. (2011). Regulation of VEGF-induced endothelial cell migration by mitochondrial reactive oxygen species. *Am J Physiol Cell Physiol* 301**,** C695-704.

Wang, Z., Zhao, H., Guan, W., Kang, X., Tai, X., and Shen, Y. (2018). Metabolic memory in mitochondrial oxidative damage triggers diabetic retinopathy. *BMC Ophthalmol* 18**,** 258.

Warren, C.M., Ziyad, S., Briot, A., Der, A., and Iruela-Arispe, M.L. (2014). A ligand-independent VEGFR2 signaling pathway limits angiogenic responses in diabetes. *Sci Signal* 7**,** ra1.

Wellen, K.E., and Thompson, C.B. (2010). Cellular metabolic stress: considering how cells respond to nutrient excess. *Mol Cell* 40**,** 323-332.

Wenzel, A.A., O'hare, M.N., Shadmand, M., and Corson, T.W. (2015). Optical coherence tomography enables imaging of tumor initiation in the TAg-RB mouse model of retinoblastoma. *Mol Vis* 21**,** 515-522.

Westermann, B. (2010). Mitochondrial fusion and fission in cell life and death. *Nat Rev Mol Cell Biol* 11**,** 872-884.

Wickstrom, S.A., Alitalo, K., and Keski-Oja, J. (2005). Endostatin signaling and regulation of endothelial cell-matrix interactions. *Adv Cancer Res* 94**,** 197-229.

Williamson, J.R., Chang, K., Frangos, M., Hasan, K.S., Ido, Y., Kawamura, T., Nyengaard, J.R., Van Den Enden, M., Kilo, C., and Tilton, R.G. (1993). Hyperglycemic pseudohypoxia and diabetic complications. *Diabetes* 42**,** 801-813.

Wolfbeis, O.S. (2015). Luminescent sensing and imaging of oxygen: fierce competition to the Clark electrode. *Bioessays* 37**,** 921-928.

Wu, B.J., Midwinter, R.G., Cassano, C., Beck, K., Wang, Y., Changsiri, D., Gamble, J.R., and Stocker, R. (2009). Heme oxygenase-1 increases endothelial progenitor cells. *Arterioscler Thromb Vasc Biol* 29**,** 1537-1542.

Wyld, L., Burn, J.L., Reed, M.W., and Brown, N.J. (1997). Factors affecting aminolaevulinic acid-induced generation of protoporphyrin IX. *Br J Cancer* 76**,** 705-712.

Xie, L., Zhu, X., Hu, Y., Li, T., Gao, Y., Shi, Y., and Tang, S. (2008). Mitochondrial DNA oxidative damage triggering mitochondrial dysfunction and apoptosis in high glucose-induced HRECs. *Invest Ophthalmol Vis Sci* 49**,** 4203-4209.

Xiong, Y., Liu, W., Huang, Q., Wang, J., Wang, Y., Li, H., and Fu, X. (2018). Tigecycline as a dual inhibitor of retinoblastoma and angiogenesis via inducing mitochondrial dysfunctions and oxidative damage. *Sci Rep* 8**,** 11747.

Yang, S., Zhao, J., and Sun, X. (2016). Resistance to anti-VEGF therapy in neovascular Age-Related Macular Degeneration: A comprehensive review. *Drug Des Devel Ther* 10**,** 1857-1867.

Yano, K., Brown, L.F., and Detmar, M. (2001). Control of hair growth and follicle size by VEGF-mediated angiogenesis. *J Clin Invest* 107**,** 409-417.

Yetkin-Arik, B., Vogels, I.M.C., Neyazi, N., Van Duinen, V., Houtkooper, R.H., Van Noorden, C.J.F., Klaassen, I., and Schlingemann, R.O. (2019).

Endothelial tip cells in vitro are less glycolytic and have a more flexible response to metabolic stress than non-tip cells. *Sci Rep* 9**,** 10414.

Youle, R.J., and Van Der Bliek, A.M. (2012). Mitochondrial fission, fusion, and stress. *Science* 337**,** 1062-1065.

Zhang, B., Alruwaili, N., Kandhi, S., Deng, W., Huang, A., Wolin, M.S., and Sun, D. (2018). Inhibition of ferrochelatase impairs vascular eNOS/NO and sGC/cGMP signaling. *PLoS One* 13**,** e0200307.

Zhu, Y., Hon, T., Ye, W., and Zhang, L. (2002). Heme deficiency interferes with the Ras-mitogen-activated protein kinase signaling pathway and expression of a subset of neuronal genes. *Cell Growth Differ* 13**,** 431-439.

Zielinski, L.P., Smith, A.C., Smith, A.G., and Robinson, A.J. (2016). Metabolic flexibility of mitochondrial respiratory chain disorders predicted by computer modelling. *Mitochondrion* 31**,** 45-55.

Zorov, D.B., Juhaszova, M., and Sollott, S.J. (2014). Mitochondrial reactive oxygen species (ROS) and ROS-induced ROS release. *Physiol Rev* 94**,** 909-950.

CURRICULUM VITAE

Trupti Shetty

Education

Ph.D. Major: Pharmacology and Toxicology, GPA: 3.8/4.0 2015 – 2020

Minor: Communicating Science

Indiana University, Indianapolis, USA

M.Sc. Biological Sciences, GPA: 3.83/4.0 2012 – 2014

NMIMS University, Mumbai, India

B.Sc. Biotechnology, GPA: 3.23/4.0 2009 – 2012

University of Mumbai

Professional Experience

Graduate Research Assistant Aug 2015 – Aug 2020

Department of Pharmacology and Toxicology

Indiana University School of Medicine, Indianapolis, USA

Project Trainee Jun 2014 – Dec 2014

Tata Institute of Fundamental Sciences, Mumbai, India

Graduate Research Trainee Nov 2013 – Apr 2014

Advanced Centre for Treatment, Research and Education

in Cancer (ACTREC), Navi Mumbai, India

Summer Intern Apr 2013 – Jun 2013

Reliance Life Sciences, Mumbai, India

Summer Trainee Apr 2010 – May 2010

Sreedhar Bhat's Laboratory, Bangalore, India

Publications

1. **Shetty T**, Sishtla K, Park B, Repass MJ, Corson TW. Heme synthesis inhibition blocks angiogenesis via mitochondrial dysfunction. iScience. http://dx.doi.org/10.2139/ssrn.3494377 *(Accepted)* July 2020.
2. **Shetty T**, Corson TW. Mitochondrial heme synthesis mediators as therapeutic targets in vascular diseases. Frontiers in Pharmacology. July 2020.
3. Schwikkard S, Whitmore H, Sishtla K, Sulaiman R, **Shetty T,** Basavarajappa HD, Waller C…, Mulholland, Dulcie; Corson TW. The Antiangiogenic Activity of Naturally-occurring and synthetic Homoisoflavonoids from the Hyacinthaceae (sensu APGII). Journal of Natural Products. April 2019.
4. Maniyadath B, Chattopadhyay T, Verma S, Kumari S, Kulkarni P, Banerjee K, Lazarus A, Kokane S, **Shetty T**, Krishnapal A, Kolthur-Seetharam U. Loss of hepatic oscillatory fed-miRs abrogates refed transition and causes liver dysfunctions. Cell Reports. Jan 2019.
5. Pran Babu SS, Sishtla K, Sulaiman RS, Park B, **Shetty T**, Shah F, Fishel ML, Wikel JH, Kelly MR, Corson TW. Ref-1/APE1 inhibition with novel small

molecules blocks ocular neovascularization. The Journal of Pharmacology and Experimental Therapeutics. Jun 2018.

6. Gurjar M, Raychaudhuri K, Mahadik S, Reddy D, Atak A, **Shetty T**, Rao K, Karkhanis MS, Gosavi P, Sehgal L, Gupta S, Dalal SN. Plakophlin2 increases desmosome assembly, size and stability by increasing expression of desmocollin2. Biochemical and Biophysical Research Communications. Nov 2017.

7. Basavarajappa HD, Sulaiman RS, Qi X, **Shetty T**, Pran Babu SS, Sishtla K, Lee B, Quigley J, Alkhairy S, Briggs CM, Gupta K, Tang B, Shadmand M, Grant MB, Boulton ME, Seo SY, Corson TW. Ferrochelatase is a therapeutic target for ocular neovascularization. EMBO Molecular Medicine. Apr 2017.

Presentations and Abstracts

1. **Shetty T**, Corson TW. Inhibition of heme synthesis enzyme blocks ocular angiogenesis by causing mitochondrial dysfunction. Poster Presentation. Association of Research in Vision and Ophthalmology Annual Meeting, Vancouver, Canada, Apr 2019.

2. **Shetty T,** Hughes K, Hoffman-Longtin K, Organ J, Wininger M, Corson TW. Using game simulation to disseminate vision research and connect with the community. Paper presentation. Science Communicators' Association of New Zealand (SCANZ) Annual Meeting, Wellington, New Zealand, Nov 2018.

3. **Shetty T**, Pran Babu SS Corson TW. Role of heme biosynthetic enzyme ferrochelatase in mitochondrial function of ocular endothelial cells underlying

proliferative diabetic retinopathy. Poster Presentation. 4th Annual Diabetes Symposium, Indianapolis, IN, USA Aug 2018.

4. **Shetty T**, Corson TW. Ferrochelatase: How a heme biosynthetic enzyme could be significant in ocular neovascularization. Paper presentation. Resident's Day, Dept of Ophthalmology, Indiana University School of Medicine, Indianapolis, IN, USA June 2018.

5. Hoffman-Longtin K, Organ J, Wininger M, Hughes K, **Shetty T**. Making Science Make Sense: Using Applied Improvisational Theater to Teach Science Communication. Paper presentation. Teach Play Learn Conference 1st Annual Conference, Indiana University South Bend, IN, USA June 2018.

6. **Shetty T**, Corson TW. Role of Ferrochelatase in Ocular Angiogenesis. Student Seminar Series. Dept. of Pharmacology and Toxicology. Indiana University School of Medicine, Indianapolis, IN, USA Jan 2019 and March 2018.

7. **Shetty T**, Pran Babu SS, Corson TW. Role of Ferrochelatase in Mitochondrial Bioenergetics of Ocular Endothelial Cells. Poster Competition. American Society for Pharmacology and Experimental Therapeutics Annual Meeting, San Diego, CA, USA. Apr 2018.

8. Corson TW, Pran Babu SS, White D, **Shetty T**. Ferrochelatase inhibitor griseofulvin prevents retinal angiogenesis without ocular toxicity. Paper presentation. Association of Research in Vision and Ophthalmology Annual Meeting, Honolulu, HI, USA. Apr 2018.

9. **Shetty T**, Pran Babu SS, Sulaiman RS, Basavarajappa HD, Sishtla K, Briggs CM, Corson TW. Poster presentation. Association of Research in Vision and Ophthalmology Annual Meeting, Baltimore, MD, USA. May 2017.

Academic and Professional Honors

Graduate Student Speaker, IUSM Commencement Ceremony	2020
American Heart Association (AHA) Early Career Blogger	2018 – 2019
Paradise Travel Award, Dept of Pharmacology and Toxicology, Indiana University School of Medicine,	2018, 2017
Indiana University School of Medicine Diversity Travel Award	2018
Indianapolis University - Purdue University Indianapolis Travel Fellowship	2018 – 2019
Graduate-Professional Education Grant Travel Award	2018
Akira E. Takemori Commemorative Travel Award, American Society for Pharmacology and Experimental Therapeutics (ASPET)	2018
Communicator Ribbon, poster presentation, Annual Meeting of Association for research in Vision and Ophthalmology (ARVO)	2017
First Rank Holder, Class of ’14 M.Sc., NMIMS University, Felicitation by Former President of India Dr. APJ Abdul Kalam	2014

Teaching and Mentoring

Mentor of undergraduate students from LHSI program, IUPUI	2016, 2019
Mentor of summer undergraduate students, IUSM	2017, 2018

Mentor, Graduate Student Mentoring Group for students, Indiana University School of Medicine Biomedical Gateway program 2017

Mentor of high school Project SEED student IUSM 2016

Service

Volunteer, Taste of Science, Central Indiana Science Outreach (CINSO), Indianapolis 2016 – 2019

Member and Volunteer, IUSM Science Outreach Community Engagement 2018 – 2019

Member and Volunteer, 314 Action@IUSM, STEM Advocacy Group 2018

Presentation for high school students of Shortridge High School, Indianapolis 2017

Team Leader, National Service Scheme Unit, K.C College, University of Mumbai 2009 – 2012